UNIVERSITY OF CALIFORNIA
RIVERSIDE

Structural and Kinetic Studies of Xanthine Oxidase and the Xanthine Oxidase Family of Enzymes

A Dissertation submitted in partial satisfaction
of the requirements for the degree of

Doctor of Philosophy

in

Biochemistry and Molecular Biology

by

James Hall

June 2014

Dissertation Committee:
Dr. Russ Hille, Chairperson
Dr. Michael Dunn
Dr. Li Fan

The Dissertation of James Hall is approved:

_____

_____

_____

Committee Chairperson

University of California, Riverside

ACKNOWLEDGMENT

I would like to thank Dr. Russ Hille for his mentorship and support during my graduate studies. I have learned much about how to be a thoughtful and effective professional researcher. The fostering of independent thinking and freedom to investigate the available projects through a diverse variety of methods was greatly appreciated. His knowledge, patience and advice were always a valuable resource. The friendly atmosphere and open cooperation among colleagues of various backgrounds in the laboratory prevented stagnation and encouraged the development of problem solving skills and collaboration. The encouragement to meet other professionals in the field and participate in international collaborations and conferences were also an unforgettable experience.

I would like to thank Chris Kieslich and Dimitrios Morikis for their guidance in learning to use the molecular dynamics software NAMD and VMD. I would also like to thank Dr. Silke Leimkühler for collaboration on cloning, mutagenesis, expression and purification of *R. capsulatus* xanthine dehydrogenase, as well as providing the plasmids for the bacterial XDH, XdhC and the hinge fragment.

Lastly, I would like to thank Dr. Michael Dunn and Li Fan for being on my thesis committee and all of the advice and knowledge they have shared along the way.

DEDICATION

To Holly, my friends, family, and all those who have supported me and fostered both my curiosity and pursuit of knowledge.

"Every one of us begins life with an open mind, a driving curiosity, a sense of wonder. The exploration of the cosmos is a voyage of self-discovery."

–Carl Sagan

ABSTRACT OF THE DISSERTATION

Structural and Kinetic Studies of Xanthine Oxidase and the Xanthine Oxidase Family of Enzymes

by

James Hall

Doctor of Philosophy, Graduate Program in Biochemistry and Molecular Biology
University of California, Riverside, June 2014
Dr. Russ Hille, Chairperson

Xanthine dehydrogenase/oxidase (XDH/XO) is a molybdenum-containing enzyme which is involved with hydroxylation a number of sp^2-hybridized centers including purines, heterocycles, and aldehydes. Its main role in the cell is to convert hypoxanthine to xanthine and xanthine to uric acid. Although xanthine oxidase has been studied for decades, details of its mechanism and how the active site allows for substrate specificity and catalysis are still not completely known.

In the present work, several methods have been used to investigate the mechanism of xanthine oxidase and the roles of the active site residues towards substrate binding and catalysis. 1.) The kinetic rates of bovine xanthine oxidase and variants of the homologous *Rhodobacter capsulatus* xanthine dehydrogenase toward various substrates have been observed. Investigation of the E232Q variant of *R. capsulatus* xanthine dehydrogenase revealed that removal of the ionizable Glutamate 232 resulted in a dramatic loss in activity at higher pH, as compared to wild-type enzyme, providing insight into the role of

Glu 232. 2.) We used X-ray crystallography to investigate interactions of the enzyme with the slow substrate indole-3-aldehyde and the non-substrate guanine. The dominant nonproductive orientations of the molecules correlate with the observed kinetic rates. 3.) The effects of active site residues on the chemical step of the reaction were investigated utilizing kinetic isotope effect studies. With the primary deuterium isotope effects, previously described by Dr. Cao, and intrinsic isotope effects ^{D}k, derived from the tritium isotope effect studies conducted for bovine xanthine oxidase and bacterial xanthine dehydrogenase, the extent that the chemical step is rate-limiting was calculated for each. Comparison of the enzymes with amino acid substitution variants allowed for insight into the role of the active site residues by the monitoring of changes (or lack of change) in the rate of the chemical step and it's comparison to changes in the overall rate of reaction.

To examine how the molybdenum cofactor matures and is incorporated into the xanthine oxidase family of enzymes, computational structural studies have been performed looking at the enzymes involved in the sulfuration of the molybdenum cofactor and incorporation of the enzyme into members of the xanthine oxidase family of enzymes. Identification of a conserved ~125 amino acid motif was identified whose connectivity to the remainder of the polypeptide makes possible a "hinge" movement to act as a target for cofactor insertion machinery. Potential open conformations have also been computationally simulated. Homologs to NifS-4, which is involved in cofactor sulfuration, and XdhC, which is involved in sulfuration and incorporation into the apo-enzyme were analyzed and docked with bacterial xanthine dehydrogenase to provide a structural basis for how the sulfuration and incorporation of cofactor occurs.

TABLE OF CONTENTS

LIST OF FIGURES

LIST OF TABLES

CHAPTER 1

INTRODUCTION

1.1 General background

1.1.1 Molybdenum and tungsten in biology

Molybdenum and tungsten are relatively scarce elements in nature. In terms of abundance on earth, they are ranked 53rd and 54th, respectively (1). Although the elemental content of most rock formations contain similar amounts of molybdenum and tungsten, molybdenum is typically found at higher concentrations in surface waters and is the most abundant transition metal in the oceans. The oxygen-rich and slightly alkaline environment of seawater results in molybdenum being exclusively present as molybdate ion (MoO_4^{2-}) and can be found at a concentration of about 10μg /L, which is roughly 10 times more concentrated than zinc and 100 times that of copper (2). Tungsten, laying just below molybdenum on the periodic table, is found at much lower concentrations in aerobic marine environments (0.1 μg/L) due to intensive sorptional precipitation (removal from solution and incorporation into soil or rocks).

When compared to sea water, hot-springs and hydrothermal vents contain much higher concentrations of tungsten. Tungsten in this environment can be found to be around 0.3mg/L, and found to be ten-fold higher in concentration than that of molybdenum. The 'black smoker' hydrothermal vents, characteristic of divergent tectonic plate boundaries, produce jets of water blackened by sulfide precipitates. Solubility of Mo and W species in hydrothermal processes is determined by the reduction potential of the mineral-forming solution, which is typically insufficient to reduce W^{VI} but adequate

oxidize Mo^{IV}. While WS_2 can be readily converted into soluble compounds like WS_4^{2-} or WO_4^{2-} in the hot and sulfur rich conditions, MoS_2 is not and precipitates, making tungsten much more bioavailable around the vents (1).

Molybdenum-containing enzymes can be found in all three kingdoms of life, while tungsten-containing enzymes are only found in prokaryotes, particularly thermophilic anaerobes. Both elements are useful to biological systems due to their ability to transition between oxidation states IV and VI under physiological conditions. In addition, the V valence state is accessible, allowing for facilitation of one- and two-electron transfers (3). It is believed that as life began, earth's biosphere was essentially anoxic, high in sulfur, and highly reducing, similar to the conditions of hydrothermal vents today (4). Tungsten, being readily available and more stable in the conditions of early earth, was likely the first of these elements to be incorporated. However, as Earth cooled and photosynthetic bacteria caused O_2 levels to increase, soluble molybdenum compounds slowly became more likely to form. Due to the similarities of both elements and the enzymes that contain them, as the abundance of soluble tungsten compounds decreased and molybdenum bioavailablity increased, life likely made the transition from utilizing tungsten to molybdenum(3,4).

1.1.2 Molybdenum and tungsten in chemistry.

Molybdenum (Mo, atomic number 42) is a period 5 element in group 6B and has an electron configuration of [Kr] $4d^5 5s^1$. Tungsten (W, atomic number 74) is found directly below molybdenum on the periodic table and is a period 6 element in group 6B

and has an electron configuration of [Xe] $4f^{14}5d^{4}6s^{2}$ (1,5). Both elements can occupy oxidation states from –II to VI and can have a maximum coordination number of eight (1,6,7). In addition, molybdenum and tungsten have similar atomic radii (1.75 Å and 1.78 Å, respectively), the same electronegativity, the same free energy of solvation (−226.8 kcal/mol and −230.1 kcal/mol, respectively) and the same covalent solution radii (2.75 Å and 2.83 Å, respectively) (4). They also exhibit similar ionic radii in the IV oxidation state (0.68 Å), and similar metal-oxygen bond lengths (M=O bond lengths are ~1.76 Å) (1). Due to these similar properties, the metals can carry out similar roles in guiding the formation of tetroses, heptoses, and pentoses(8), and in the catalysis of key steps in carbon, nitrogen and sulfur metabolism(3).

While molybdenum and tungsten contain similar size, coordination chemistry, and valence electron configurations, it is important to note that the two elements differ in, solubility, bond stability, and reduction potential. As mentioned above, the formation of tungstates rather than molybdates and of molybdenites rather than tungstenites in hydrothermal processes is determined by the reduction potential of the mineral-forming solution, which is typically much higher than that required to reduce W^{VI} but below that necessary to oxidize Mo^{IV} (1). This allows WS_2 to be readily converted into soluble compounds like WS_4^{2-} or WO_4^{2-} in the hot and sulfur rich conditions, while MoS_2 is not readily converted and precipitates. In terms of bond stability, tungsten–sulfur bonds are more stable than their molybdenum counterparts. Lastly, oxidation-reduction reactions catalyzed by tungsten typically occur at much lower potentials than those catalyzed by molybdenum(3).

1.1.3 Molybdenum and tungsten enzymes.

Molybdenum and tungsten oxyanions (primarily molybdate and tungstate) are taken up into the cell by high-affinity ABC transporters. These transporters typically contain a periplasmic oxyanion-binding protein, a transmembrane protein involved in translocation of anions, and a cytoplasmic membrane-associated protein that drives the translocation via ATP hydrolysis(2). Once in the cell, molybdenum and tungsten are incorporated into enzymes in similar ways, typically through attachment to a pyranopterin cofactor which acts as a scaffold while allowing for the metal to cycle through the catalytically relevant oxidation states(4). The pterin cofactor coordinates the metal via a dithiolene side chain(9). The pterin-based metal centers come in a number of variations, falling into three major groups: The molybdopterin (MPT) type cofactor that is equivalent to a mononucleotide, molybdopterin dinucleotide (MCD) type and the bis-molybdopterin guanine dinucleotide (bis-MGD) type cofactor (Figure 1.1). The tungsten-containing cofactors characterized so far appear to only fall into the bis-pterin category, containing two equivalents of the pterin cofactor coordinated to the metal, examples being the bis-tungstopterin guanine dinucleotide cofactor of formate dehydrogenase from *Desulfovibrio gigas*(10) and the bis-tungstopterin cofactor of aldehyde ferredoxin oxidoreductase from *Pyrococcus furinosus*(11) (Figure 1.1 E & F, respectively).

Given the similarities in atomic size and coordination chemistry and the similar ways that molybdenum and tungsten are incorporated into enzymes, it has been proposed early on that molybdenum or tungsten could be substituted for the other, or that other transition metals such as niobium and tantalum could also be substituted(1). A few

examples of incorporation of tungsten into a molybdenum-containing enzyme have been achieved. Due to the lower reduction potential of tungsten, activity and substrate specificity are significantly affected. In the case of dimethylsulfoxide reductase from *Rhodobacter capsulatus*, the tungsten-substituted enzyme exhibits lower (V/VI) and (IV/V) redox potentials and that the enzyme is able to catalyze dimethylsulfoxide reduction (the forward reaction), but not dimethylsulfide oxidation (the backward reaction) (4,12). However, in the case of sulfite oxidase, tungsten substitution produces an inactive enzyme (13). This presents a serious issue concerning Mo/W toxicity in the cell, requiring strict discrimination between the two oxyanions, but also highlights that active sites of these enzymes have evolved to modulate the oxidation-reduction properties of their respective metal ion in order to carry out the catalysis of a variety of steps in nitrogen, carbon, and sulfur metabolism (3,4).

One unique type of molybdenum-containing cofactor which does not include a pterin, is the multinuclear center of nitrogenase, where the molybdenum is incorporated into a complex cluster referred to as the iron-molybdenum cofactor (Figure 1.1 G), which is composed of seven iron ions, one molybdenum ion, nine sulfides and a central carbon (14). This multinuclear metal center allows the enzyme to catalyze the reduction of dinitrogen to ammonia, making nitrogen biologically available. Nitrogenase also been shown to catalyze the reduction of a number of non-physiological doubly and triply bonded small molecules (15).

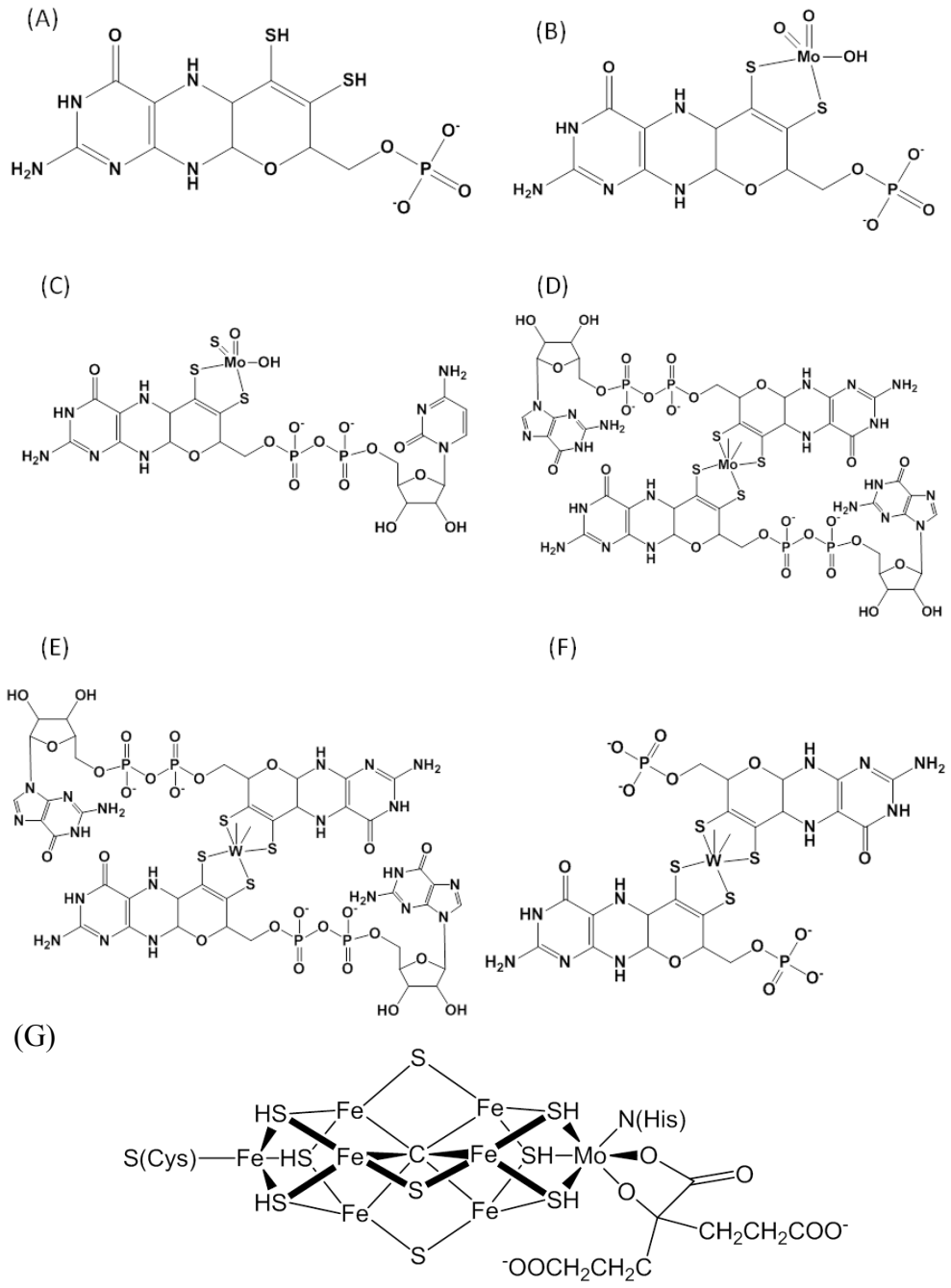

Figure 1.1 *The pyranopterin cofactor and common molybdenum and tungsten cofactors.* (A) The pyranopterin cofactor. (B) The molybdopterin cofactor (MPT). (C) The molybdopterin cytosine dinucleotide cofactor (MCD). (D) The Bis-molybdopterin guanine dinucleotide cofactor (bis-MGD). (E) The bis-tungstopterin guanine dinucleotide cofactor (bis-TGD). (F) The bis-tungstopterin cofactor (bis-TPT). (G) The iron-molybdenum cofactor (FeMoco) from nitrogenase.

The pterin-containing molybdenum and tungsten enzymes catalyze a wide variety of reactions but are most commonly grouped into five families based upon the structure of their active sites and named after a well characterized example of each family. The pterin-containing tungsten enzymes fall into two families, the formate dehydrogenase family and the aldehyde reductase family (Cofactors depicted in Figure 1.1 E and F, respectively), while the pterin-containing mononuclear molybdenum containing enzymes are most commonly grouped into three families; the xanthine oxidase family, the sulfite oxidase family, and the dimethylsulfoxide reductase family (2,16). The structures of the cofactors within each family are typically conserved, although atoms/residues ligated to the molybdenum center can vary based upon the various members within the family of enzymes (figure 1.2).

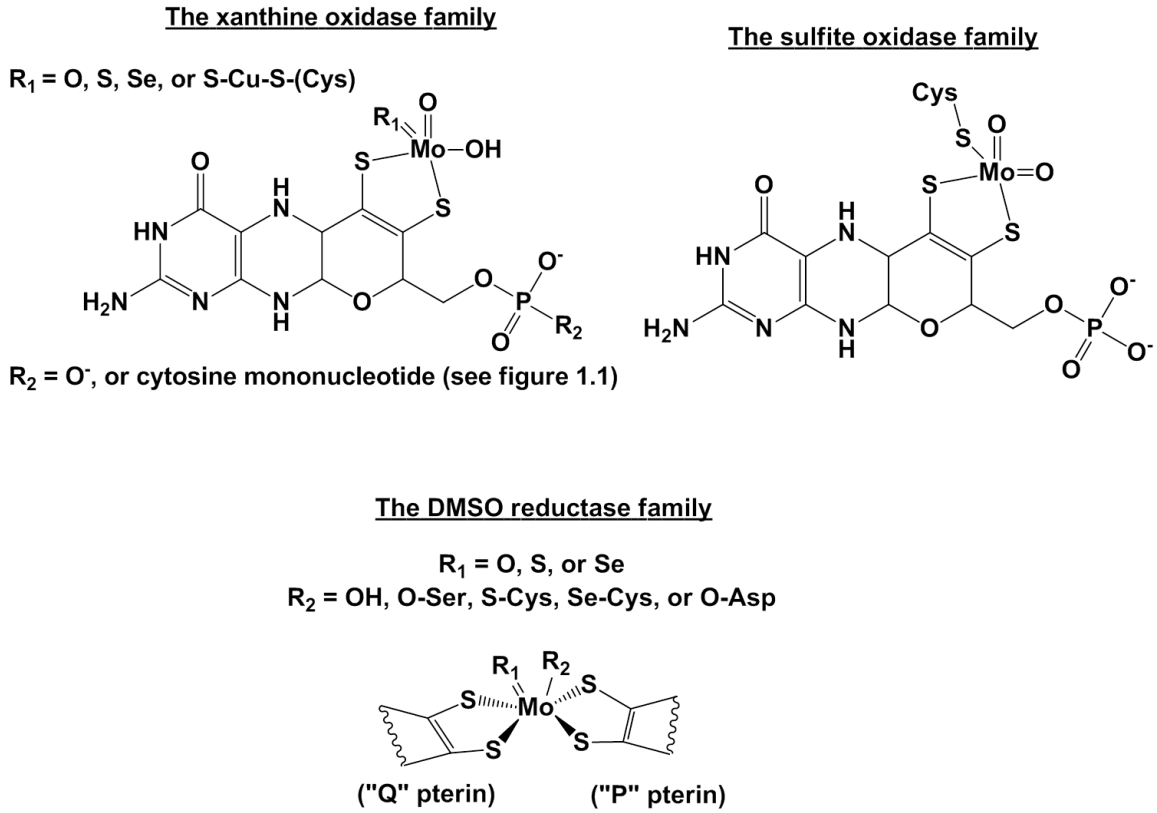

Figure 1.2 *The mononuclear molybdenum enzyme families.* The cofactor structures of the molybdenum enzyme families of the xanthine oxidase family, the sulfite oxidase family, and the dimethylsulfoxide reductase family. The possible variations of ligands to the metal and/or cofactor are also shown. The structure of the bis-MGD cofactor seen in the DMSO reductase family can also be found in figure 1.1 D.

The xanthine oxidase family of enzymes contain a molybdenum center with a single equivalent of the pyranopterin attached via dithiolene sulfur groups, an axial =O, an equatorial =S (in most cases, however this can also be an =O or =Se group), and an equatorial hydroxyl group. Most enzymes of this family are considered true hydroxylases and catalyze the hydroxylation of sp^2-hybridized centers on molecules such as purines, aldehydes and other heterocyclic molecules. Unlike monooxygenases, the molybdenum-containing hydroxylases use oxygen that is ultimately derived from water, rather than from O_2, as the source of the transferred oxygen atom and generate reducing equivalents (typically in the form of NADH), instead of consuming them. The hydroxylation is also accompanied by cleavage of a C–H bond (16). Aside from the typical members of this family, one unique member, carbon monoxide dehydrogenase from *Oligotropha carboxidovorans*, contains a binuclear Mo-S-Cu-S-Cys cluster and catalyzes carbon monoxide oxidation to carbon dioxide without cleavage of a C–H bond. Although the molybdenum center is different, the overall coordination of the molybdenum is still conserved. Most xanthine oxidase family members all share an overall conserved structure containing a molybdenum center, a pair of [2Fe-2S] clusters, and an FAD (Figure 1.3), although some (e.g. the aldehyde:ferredoxin oxidoreductase from *Desulfovibrio gigas* (17)) lack the FAD cofactor (18).

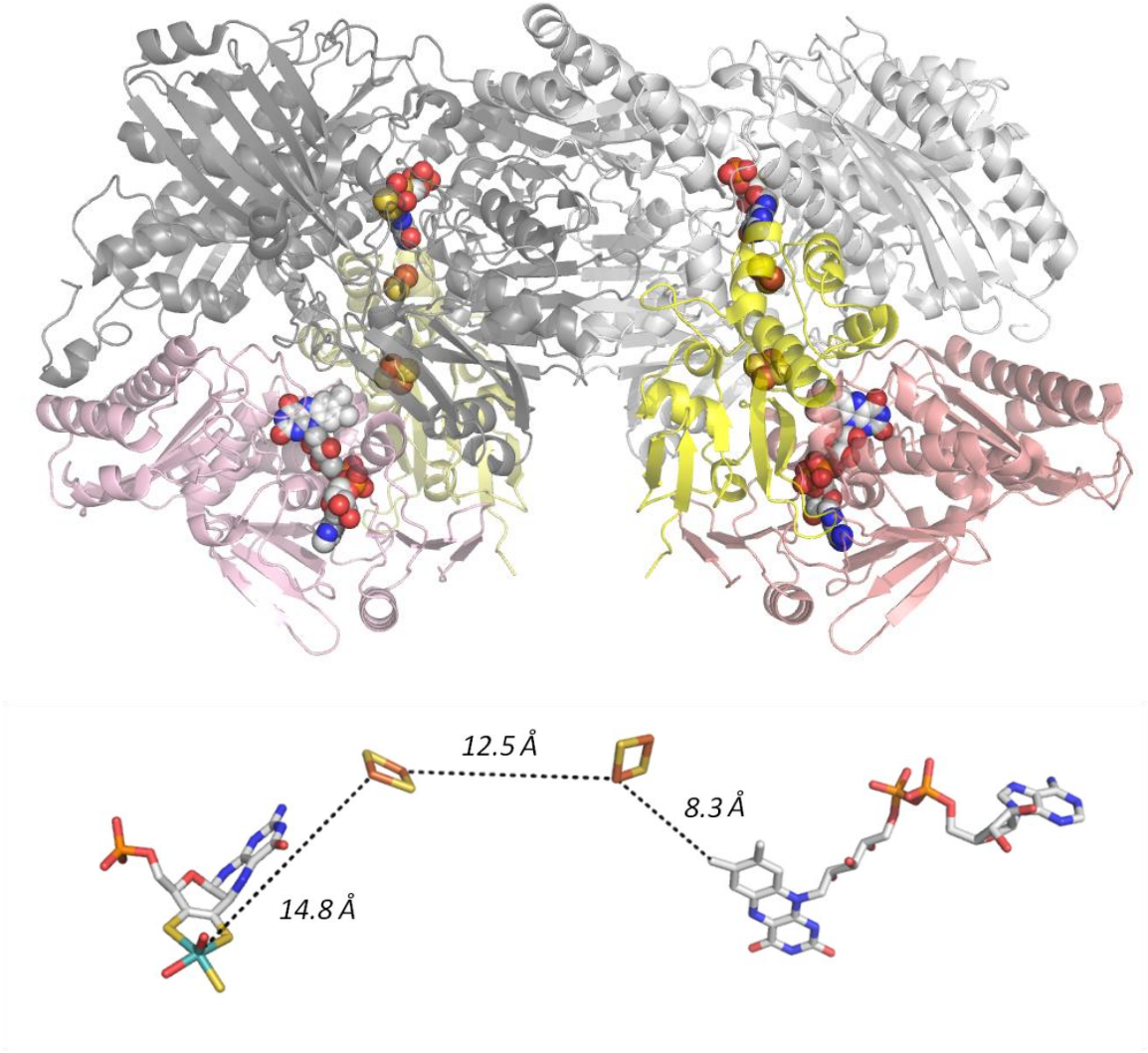

Figure 1.3 *The structure of bovine xanthine oxidase.* (Top) The overall dimeric structure of xanthine oxidase (PDB ID: 3NRZ) is shown in cartoon representation with the domains of each monomeric unit shown in different shades. The molybdenum binding domains in grey, the iron-sulfur cluster domains in yellow, and the FAD binding domain in pink. The redox active centers are shown in sphere representation and colored in CPK. (bottom) The arrangement and distances of the redox active centers of one of the monomeric units shown in stick representation and CPK color scheme. The redox active centers for one half of the holoenzyme are rotated 90^0 counterclockwise and enlarged.

The sulfite oxidase family is composed of sulfite oxidases and dehydrogenases, and the assimilatory nitrate reductases (which catalyze the first and rate-limiting step of nitrate assimilation in fungi, algae, and higher plants, the reduction of nitrate to nitrite (19)). These enzymes can be found in eukaryotes and prokaryotes and are true oxygen atom transferases. The molybdenum coordination sphere is composed a single pterin, an axial =O, an equatorial =O (or hydroxyl), and a cysteine residue contributed by the polypeptide (16). Chicken sulfite oxidase is an α_2 dimer with each subunit consisting of a small N-terminal cytochrome b domain connected via a 10-aa tether to the main body of the subunit, which consists of molybdenum-binding and dimerization domains (Figure 1.4) (20). Recently, mitochondrial Amidoxime Reducing Component (mARC) and several other enzymes of unknown function have been discovered which have been grouped with this family. The eukaryotic mARC has been shown to reductively detoxify N-hydroxylated nucleobases and nucleosides (21). Other proteins, including the YedY gene product from *Escherichia coli*, as well as YcbX and YiiM from other bacteria, share some structural homology to sulfite oxidase and while no known function has yet been found, it is suggested that these enzymes may act as chaperones for the molybdenum cofactor (16,22).

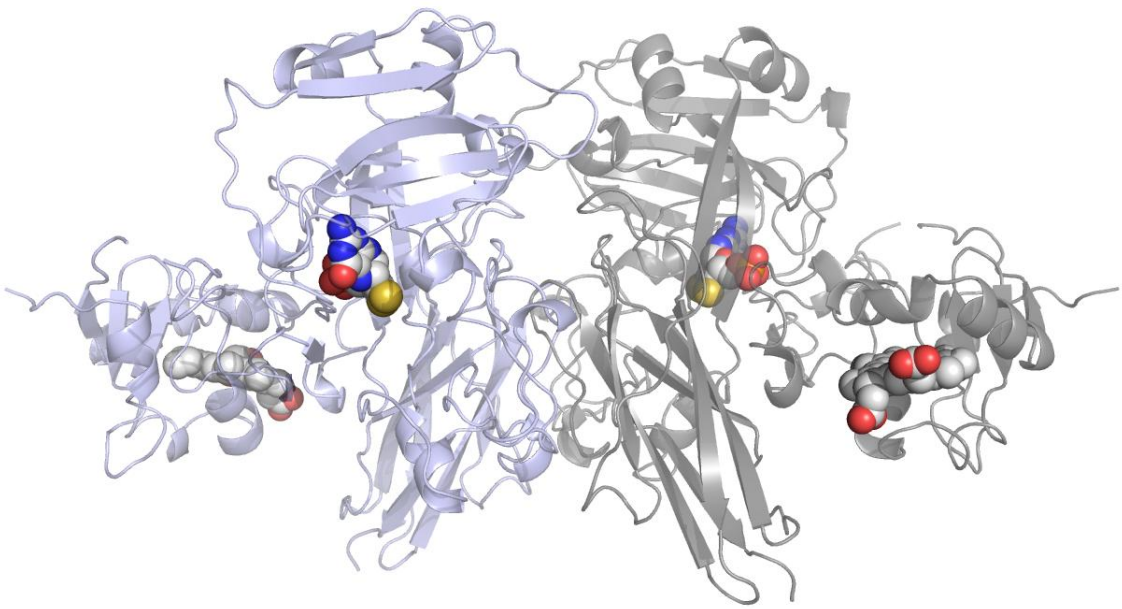

Figure 1.4 *The structure of chicken sulfite oxidase.* The overall dimeric structure of chicken sulfite oxidase (PDB ID: 1SOX) is shown in cartoon representation with each monomeric unit shown in different colors. The redox active centers are shown in sphere representation and CPK color scheme.

The DMSO reductase (DMSOR) family is the most diverse group of the three mononuclear molybdenum enzyme families, both structurally and catalytically. Enzymes of this family are found in prokaryotes and catalyze oxygen transfer reactions, oxidation/reduction or hydroxylation/hydration reactions. The molybdenum center has a trigonal prismatic coordination geometry, consisting of two equivalents of the pyranopterin cofactor ligated to the molybdenum, along with a =O (or hydroxyl, =S, or =Se), and a hydroxyl group (which can also be a covalent attachment to the enzyme via a cysteine, selenocysteine, serine, or aspartate). The enzymes of this family vary greatly in structure from the simple periplasmic DMSOR of *Rhodobacter capsulatus*, in which the molybdenum center is the only redox-active center, to complex integral membrane proteins such as formate dehydrogenase N and the dissimalatory nitrate reductase (NarGHI) from *Escherichia coli*, which contain multiple iron-sulfur clusters in addition to the molybdenum center (Figure 1.5) (16).

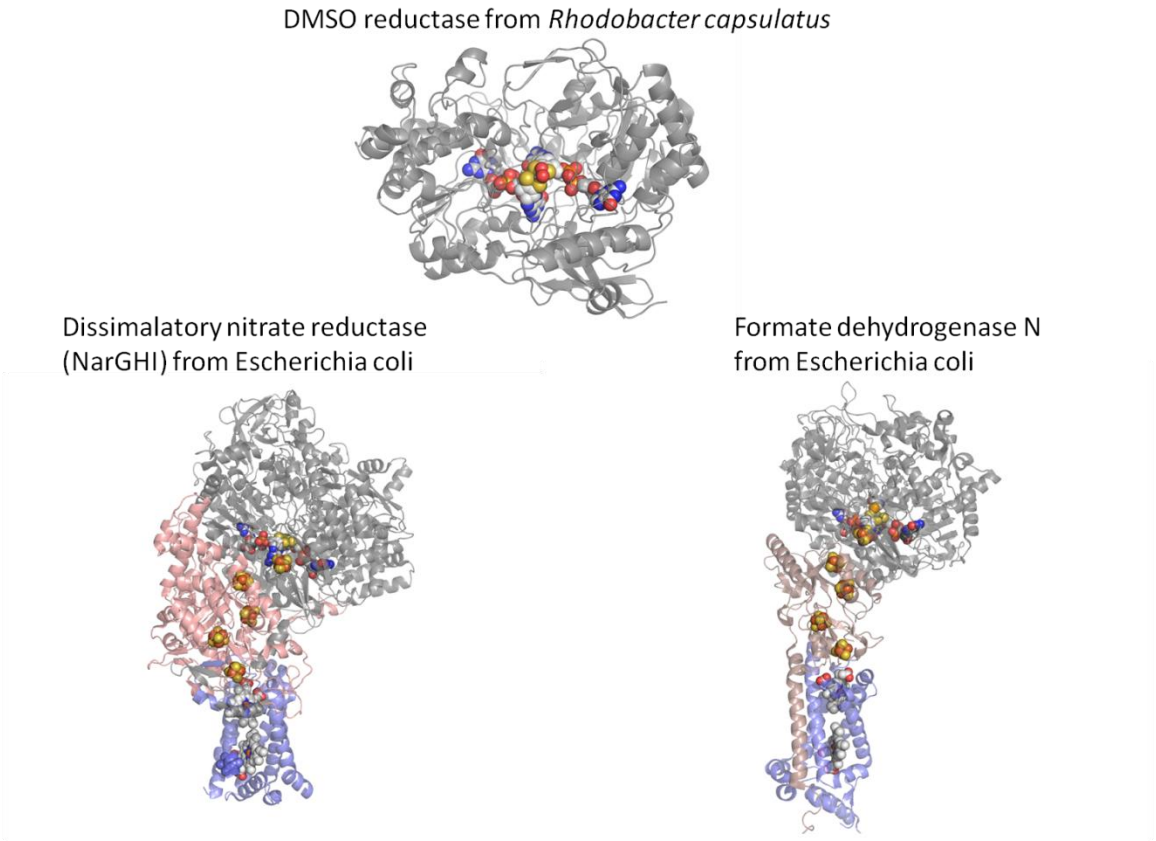

Figure 1.5 *Structures of several members of the DMSO reductase family.* (Top) The structure of DMSO reductase from *Rhodobacter capsulatus* (PDB ID: 1DMR) is shown in cartoon representation with the redox active center shown in sphere representation and CPK color scheme. (Bottom) The structure of the dissimalatory nitrate reductase (NarGHI) and the formate dehydrogenase N from *Escherichia coli*. Each subunit is represented in cartoon representation with different colors depicting each subunit, while the redox active centers are shown in sphere representation and CPK color scheme.

1.2 Xanthine oxidase and related enzymes

1.2.1 The conserved structure of the xanthine oxidase family

Xanthine oxidase has been studied for close to a century, being discovered in 1922 (23). It was initially isolated from cow's milk (24), but it is also found in the cytoplasm of cells where it catalyzes the hydroxylation of sp^2-hybridized centers on molecules such as purines, aldehydes and other heterocyclic molecules (9). The 300 kDa enzyme is characterized by an overall "butterfly" shape, consisting of an α_2 dimer (Figure 1.3). From N-terminus to C terminus, each subunit contains five domains: two iron-sulfur domains, each containing one [2Fe-2S] cluster; a flavin-binding domain, containing FAD; and two molybdenum-binding domains, which sandwich the molybdenum cofactor. (18). The enzyme is typically isolated from cow's milk as an oxidase, but is expressed in cells as a dehydrogenase, utilizing NAD^+, rather than O_2 as its final electron acceptor. In mammals, the dehydrogenase form can be converted to the oxidase form reversibly, via oxidation of thiols to disulfides, or irreversibly, via proteolytic cleavage; leading the enzyme to commonly be referred to in literature as xanthine oxidoreductase. Conversion to the oxidase form alters the final electron acceptor specificity from NAD^+ to O_2, allowing the enzyme to produce reactive oxygen species. The dehydrogenase form is the stable form in all other eukaryotes and prokaryotes (16). The enzyme is broadly distributed in nature, although a non-molybdenum containing xanthine oxidase has been discovered in fungi which lacks structural similarity to the molybdenum-containing xanthine oxidase family of enzymes and instead utilizes iron (II) and α-ketoglutarate to hydroxylate xanthine (25).

Members of the molybdenum-containing xanthine oxidase family of enzymes each share an overall similar structure to xanthine oxidase. The X-ray crystal structures of several members of this family are known, including aldehyde oxidoreductase from *Desulfovibrio gigas* (17), mouse aldehyde oxidase 3 (26), bovine xanthine dehydrogenase/oxidase (27), CO dehydrogenase from *Oligotropha carboxidovorans* (28,29), xanthine dehydrogenase from *Rhodobacter capsulatus* (30), quinoline-2-oxidoreductase from *Pseudomonas putida* (31), 4-hydroxybenzoyl-CoA reductase from *Thauera aromatica* (32,33), and nicotinate dehydrogenase from *Eubacterium barkeri* (34) (Figure 1.6). Most of these still follow the same arrangement of domains and redox-active centers as the bovine xanthine oxidase, often sharing 25-50% sequence homology (Figure 1.7). Eukaryotic members of this family typically have a α_2 dimer configuration while the bacterial enzymes of the family tend to be broken up into multiple subunits. Examples of prokaryotic family members containing more than two subunits characterized so far include xanthine dehydrogenase from *Rhodobacter capsulatus*, which is a $(\alpha\beta)_2$ tetramer (a dimer of heterodimers); CO dehydrogenase from *Oligotropha carboxidovorans*, which is an $(\alpha\beta\gamma)_2$ hexamer (a dimer of heterotrimers); and nicotinate dehydrogenase from *Eubacterium barkeri*, which has an $(\alpha\beta\gamma\delta)_2$ configuration (a dimer of heterotetramers). Two unique members of this family further vary from the typical architecture of the family, the first being aldehyde oxidoreductase from *D. gigas*, which lacks the FAD domain, and the other, 4-hydroxybenzoyl-CoA reductase from *Thauera aromatica*, which contains an additional [4Fe-4S] cluster (18).

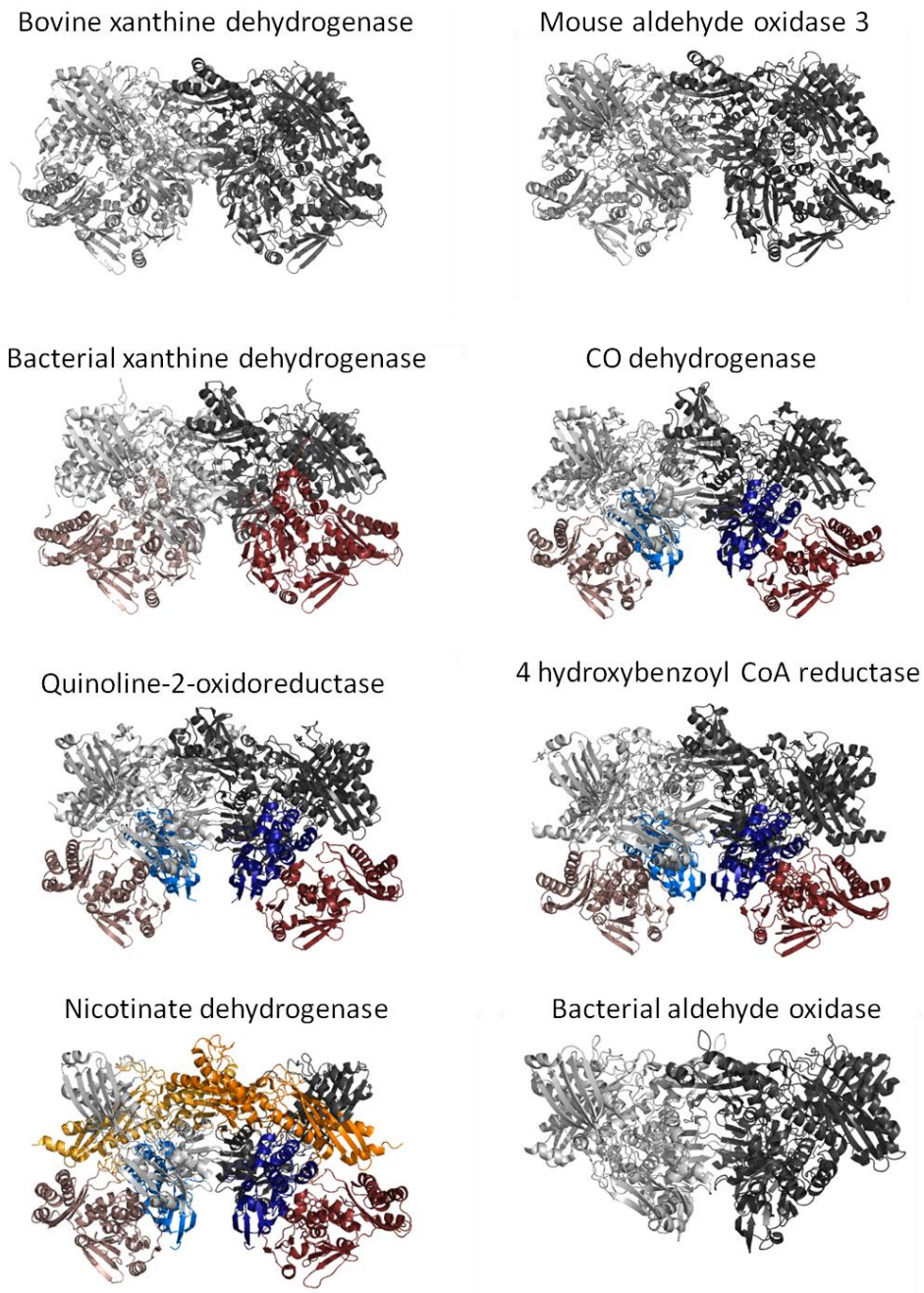

Figure 1.6 *Structures of several xanthine oxidase family members*. The structures in order above are: Bovine xanthine dehydrogenase (PDB ID: 1FO4), mouse aldehyde oxidase 3 (PDB ID: 3ZYV), xanthine dehydrogenase from *Rhodobacter capsulatus* (PDB ID: 2W3S), carbon monoxide dehydrogenase from *Oligotropha carboxidovorans* (PDB ID: 1N5W), quinoline-2-oxidoreductase from *Pseudomonas putida* (PDB ID: 1T3Q), 4-hydroxybenzoyl-CoA reductase from *Thauera aromatica* (PDB ID:1SB3), nicotinate dehydrogenase from *Eubacterium barkeri* (PDB ID: 3HRD), and aldehyde oxidoreductase from *Desulfovibrio gigas* (PDB ID: 1VLD). The enzymes are shown in cartoon representation with each subunit in different colors and with different shades of the same color given to identical subunits within the holoenzymes.

Figure 1.7 The alignment of several members of the xanthine oxidase family of enzymes

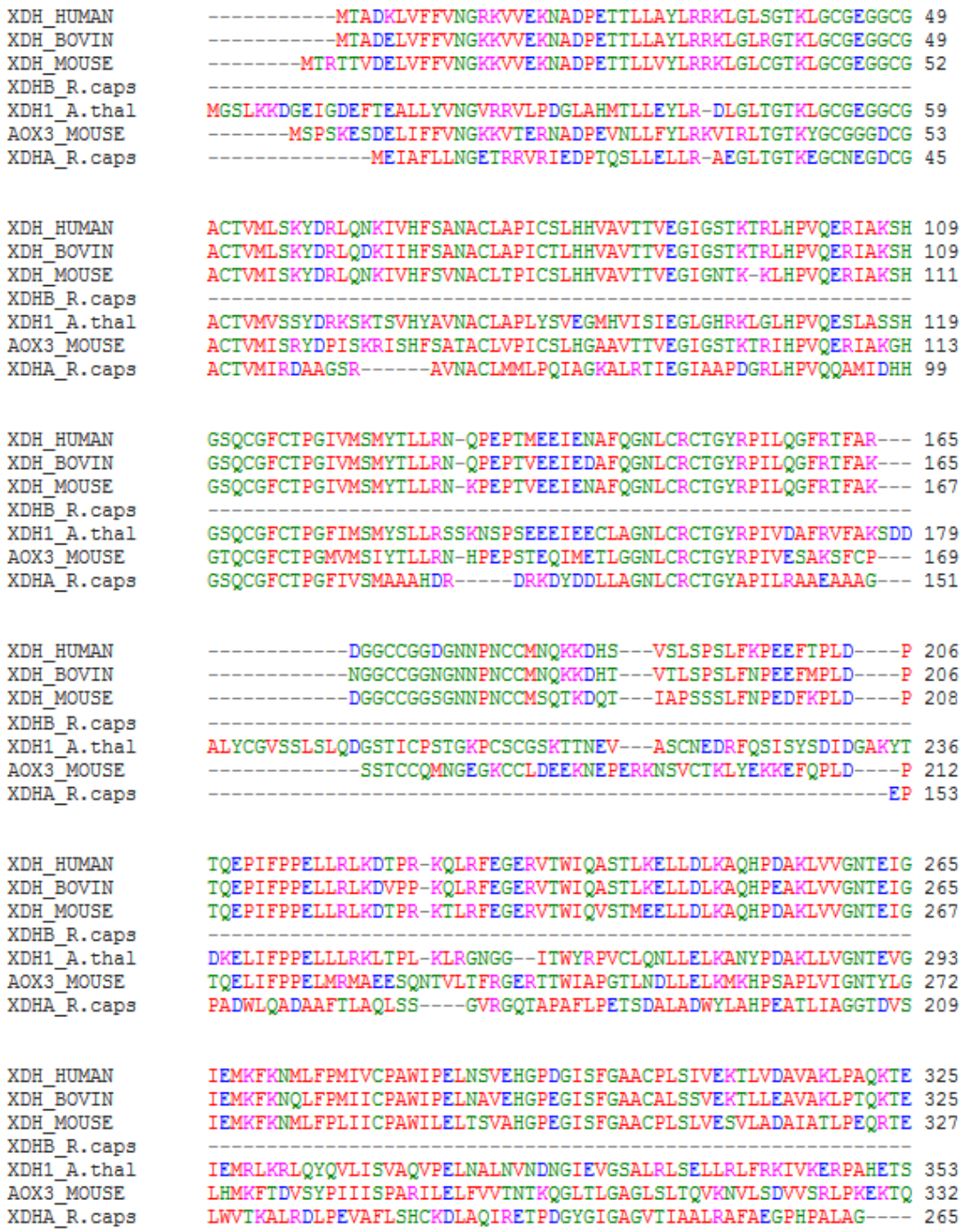

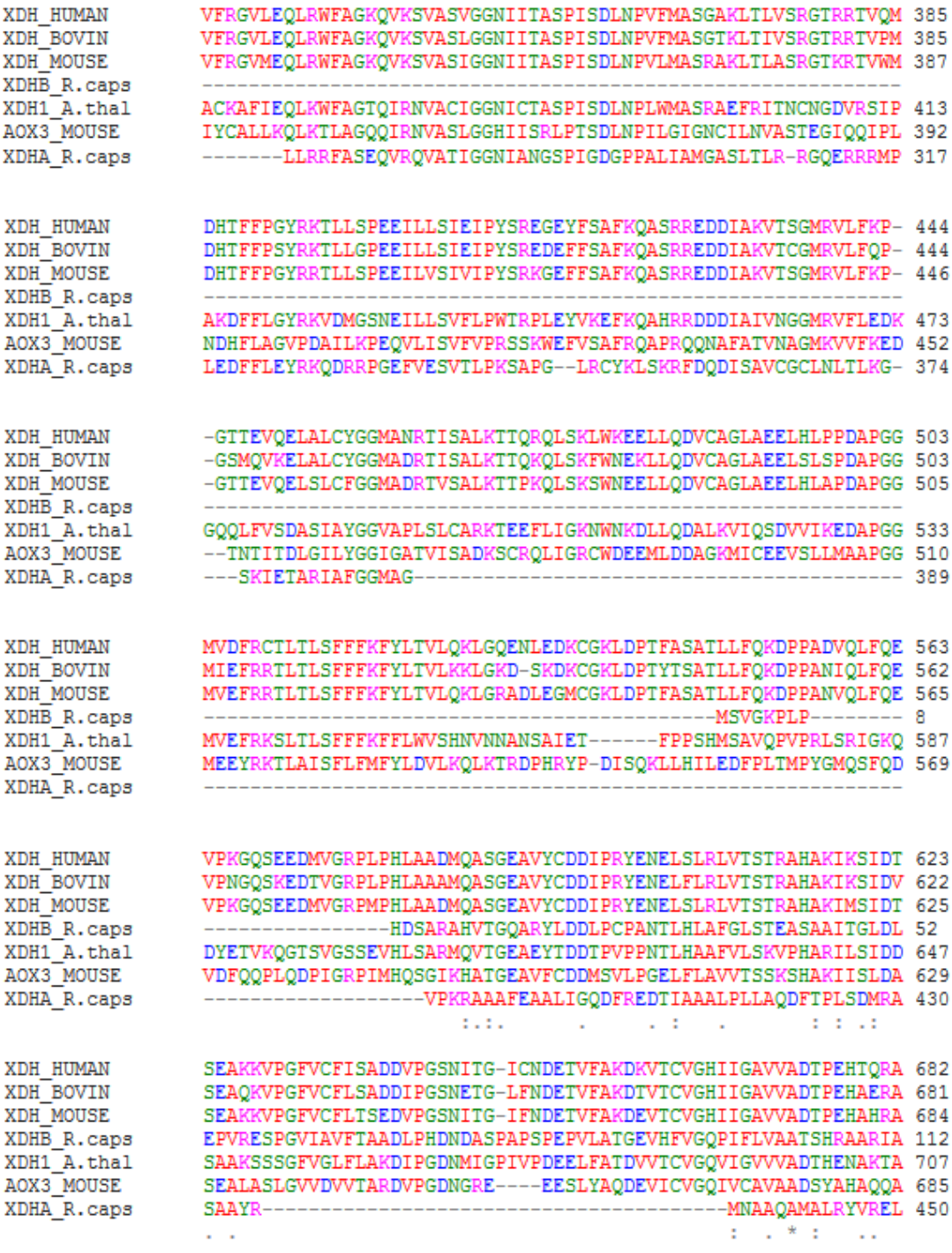
XDH_HUMAN VFRGVLEQLRWFAGKQVKSVASVGGNIITASPISDLNPVFMASGAKLTLVSRGTRRTVQM 385
XDH_BOVIN VFRGVLEQLRWFAGKQVKSVASLGGNIITASPISDLNPVFMASGTKLTIVSRGTRRTVPM 385
XDH_MOUSE VFRGVMEQLRWFAGKQVKSVASIGGNIITASPISDLNPVLMASRAKLTLASRGTKRTVWM 387
XDHB_R.caps --
XDH1_A.thal ACKAFIEQLKWFAGTQIRNVACIGGNICTASPISDLNPLWMASRAEFRITNCNGDVRSIP 413
AOX3_MOUSE IYCALLKQLKTLAGQQIRNVASLGGHIISRLPTSDLNPILGIGNCILNVASTEGIQQIPL 392
XDHA_R.caps -------LLRRFASEQVRQVATIGGNIANGSPIGDGPPALIAMGASLTLR-RGQERRRMP 317
XDH_HUMAN DHTFFPGYRKTLLSPEEILLSIEIPYSREGEYFSAFKQASRREDDIAKVTSGMRVLFKP- 444
XDH_BOVIN DHTFFPSYRKTLLGPEEILLSIEIPYSREDEFFSAFKQASRREDDIAKVTCGMRVLFQP- 444
XDH_MOUSE DHTFFPGYRRTLLSPEEILVSIVIPYSRKGEFFSAFKQASRREDDIAKVTSGMRVLFKP- 446
XDHB_R.caps --
XDH1_A.thal AKDFFLGYRKVDMGSNEILLSVFLPWIRPLEYVKEFKQAHRRDDDIAIVNGGMRVFLEDK 473
AOX3_MOUSE NDHFLAGVPDAILKPEQVLISVFVPRSSKWEFVSAFRQAPRQQNAFATVNAGMKVVFKED 452
XDHA_R.caps LEDFFLEYRKQDRRPGEFVESVTLPKSAPG--LRCYKLSKRFDQDISAVCGCLNLTLKG- 374
XDH_HUMAN -GTTEVQELALCYGGMANRTISALKTTQRQLSKLWKEELLQDVCAGLAEELHLPPDAPGG 503
XDH_BOVIN -GSMQVKELALCYGGMADRTISALKTTQKQLSKFWNEKLLQDVCAGLAEELSLSPDAPGG 503
XDH_MOUSE -GTTEVQELSLCFGGMADRTVSALKTTPKQLSKSWNEELLQDVCAGLAEELHLAPDAPGG 505
XDHB_R.caps --
XDH1_A.thal GQQLFVSDASIAYGGVAPLSLCARKTEEFLIGKNWNKDLLQDALKVIQSDVVIKEDAPGG 533
AOX3_MOUSE --TNTITDLGILYGGIGATVISADKSCRQLIGRCWDEEMLDDAGKMICEEVSLLMAAPGG 510
XDHA_R.caps ---SKIETARIAFGGMAG-- 389
XDH_HUMAN MVDFRCTLTLSFFFKFYLTVLQKLGQENLEDKCGKLDPTFASATLLFQKDPPADVQLFQE 563
XDH_BOVIN MIEFRRTLTLSFFFKFYLTVLKKLGKD-SKDKCGKLDPTYTSATLLFQKDPPANIQLFQE 562
XDH_MOUSE MVEFRRTLTLSFFFKFYLTVLQKLGRADLEGMCGKLDPTFASATLLFQKDPPANVQLFQE 565
XDHB_R.caps --MSVGKPLP-------- 8
XDH1_A.thal MVEFRKSLTLSFFFKFFLWVSHNVNNANSAIET------FPPSHMSAVQPVPRLSRIGKQ 587
AOX3_MOUSE MEEYRKTLAISFLFMFYLDVLKQLKTRDPHRYP-DISQKLLHILEDFPLTMPYGMQSFQD 569
XDHA_R.caps --
XDH_HUMAN VPKGQSEEDMVGRPLPHLAADMQASGEAVYCDDIPRYENELSLRLVTSTRAHAKIKSIDT 623
XDH_BOVIN VPNGQSKEDTVGRPLPHLAAAMQASGEAVYCDDIPRYENELFLRLVTSTRAHAKIKSIDV 622
XDH_MOUSE VPKGQSEEDMVGRPMPHLAADMQASGEAVYCDDIPRYENELSLRLVTSTRAHAKIMSIDT 625
XDHB_R.caps ---------------HDSARAHVTGQARYLDDLPCPANTLHLAFGLSTEASAAITGLDL 52
XDH1_A.thal DYETVKQGTSVGSSEVHLSARMQVTGEAEYTDDTPVPPNTLHAAFVLSKVPHARILSIDD 647
AOX3_MOUSE VDFQQPLQDPIGRPIMHQSGIKHATGEAVFCDDMSVLPGELFLAVVTSSKSHAKIISLDA 629
XDHA_R.caps ------------------VPKRAAAFEAALIGQDFREDTIAAALPLLAQDFTPLSDMRA 430
XDH_HUMAN SEAKKVPGFVCFISADDVPGSNITG-ICNDETVFAKDKVTCVGHIIGAVVADTPEHTQRA 682
XDH_BOVIN SEAQKVPGFVCFLSADDIPGSNETG-LFNDETVFAKDTVTCVGHIIGAVVADTPEHAERA 681
XDH_MOUSE SEAKKVPGFVCFLTSEDVPGSNITG-IFNDETVFAKDEVTCVGHIIGAVVADTPEHAHRA 684
XDHB_R.caps EPVRESPGVIAVFTAADLPHDNDASPAPSPEPVLATGEVHFVGQPIFLVAATSHRAARIA 112
XDH1_A.thal SAAKSSSGFVGLFLAKDIPGDNMIGPIVPDEELFATDVVTCVGQVIGVVVADTHENAKTA 707
AOX3_MOUSE SEALASLGVVDVVTARDVPGDNGRE----EESLYAQDEVICVGQIVCAVAADSYAHAQQA 685
XDHA_R.caps SAAYR--MNAAQAMALRYVREL 450

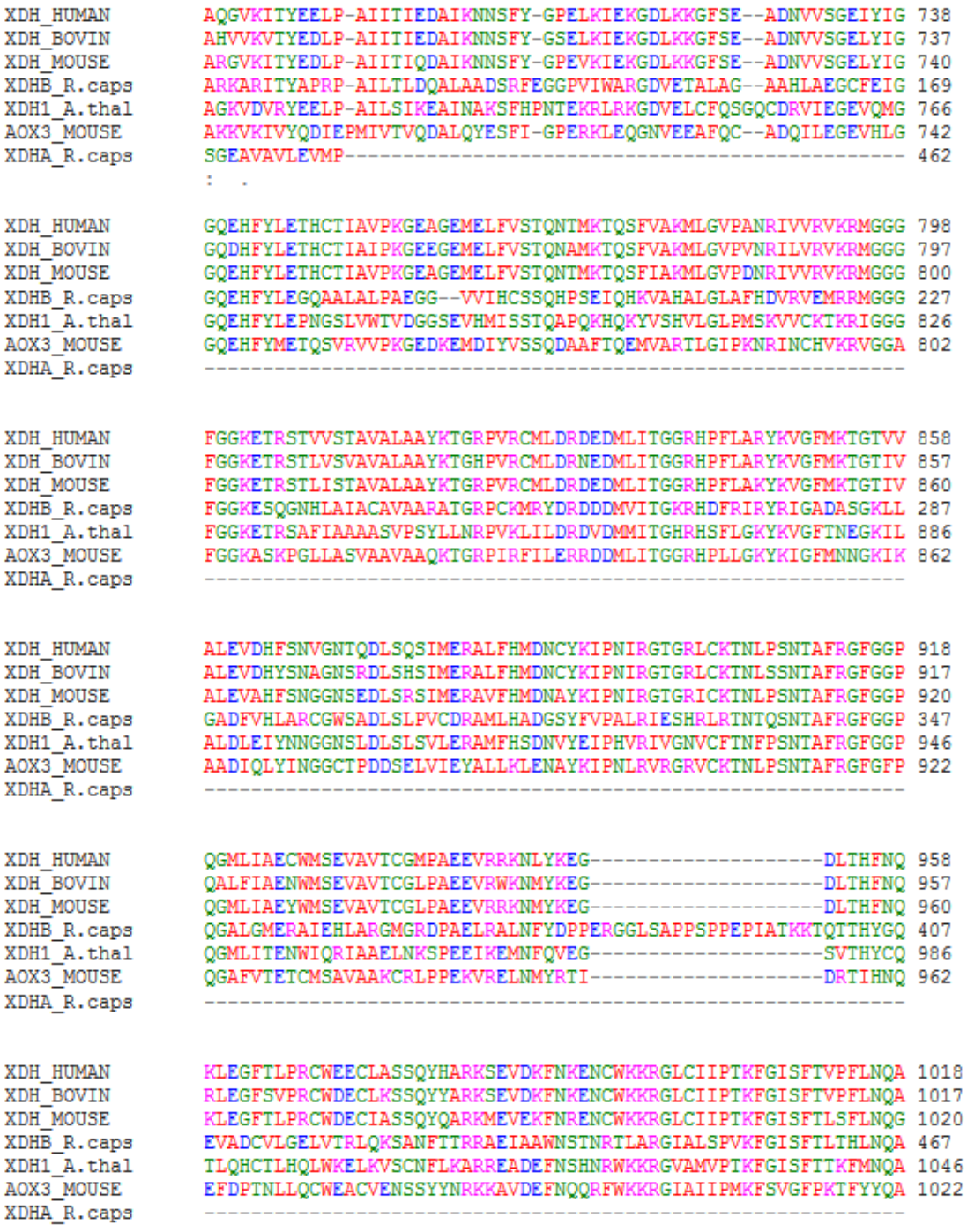
XDH_HUMAN AQGVKITYEELP-AIITIEDAIKNNSFY-GPELKIEKGDLKKGFSE--ADNVVSGEIYIG 738
XDH_BOVIN AHVVKVTYEDLP-AIITIEDAIKNNSFY-GSELKIEKGDLKKGFSE--ADNVVSGELYIG 737
XDH_MOUSE ARGVKITYEDLP-AIITIQDAIKNNSFY-GPEVKIEKGDLKKGFSE--ADNVVSGELYIG 740
XDHB_R.caps ARKARITYAPRP-AILTLDQALAADSRFEGGPVIWARGDVETALAG--AAHLAEGCFEIG 169
XDH1_A.thal AGKVDVRYEELP-AILSIKEAINAKSFHPNTEKRLRKGDVELCFQSGQCDRVIEGEVQMG 766
AOX3_MOUSE AKKVKIVYQDIEPMIVTVQDALQYESFI-GPERKLEQGNVEEAFQC--ADQILEGEVHLG 742
XDHA_R.caps SGEAVAVLEVMP---------- 462
XDH_HUMAN GQEHFYLETHCTIAVPKGEAGEMELFVSTQNTMKTQSFVAKMLGVPANRIVVRVKRMGGG 798
XDH_BOVIN GQDHFYLETHCTIAIPKGEEGEMELFVSTQNAMKTQSFVAKMLGVPVNRILVRVKRMGGG 797
XDH_MOUSE GQEHFYLETHCTIAVPKGEAGEMELFVSTQNTMKTQSFIAKMLGVPDNRIVVRVKRMGGG 800
XDHB_R.caps GQEHFYLEGQAALALPAEGG--VVIHCSSQHPSEIQHKVAHALGLAFHDVRVEMRRMGGG 227
XDH1_A.thal GQEHFYLEPNGSLVWTVDGGSEVHMISSTQAPQKHQKYVSHVLGLPMSKVVCKTKRIGGG 826
AOX3_MOUSE GQEHFYMETQSVRVVPKGEDKEMDIYVSSQDAAFTQEMVARTLGIPKNRINCHVKRVGGA 802
XDHA_R.caps ---------- 462
XDH_HUMAN FGGKETRSTVVSTAVALAAYKTGRPVRCMLDRDEDMLITGGRHPFLARYKVGFMKTGTVV 858
XDH_BOVIN FGGKETRSTLVSVAVALAAYKTGHPVRCMLDRNEDMLITGGRHPFLARYKVGFMKTGTIV 857
XDH_MOUSE FGGKETRSTLISTAVALAAYKTGRPVRCMLDRDEDMLITGGRHPFLAKYKVGFMKTGTIV 860
XDHB_R.caps FGGKESQGNHLAIACAVAARATGRPCKMRYDRDDDMVITGKRHDFRIRYRIGADASGKLL 287
XDH1_A.thal FGGKETRSAFIAAAASVPSYLLNRPVKLILDRDVDMMITGHRHSFLGKYKVGFTNEGKIL 886
AOX3_MOUSE FGGKASKPGLLASVAAVAAQKTGRPIRFILERRDDMLITGGRHPLLGKYKIGFMNNGKIK 862
XDHA_R.caps ---------- 462
XDH_HUMAN ALEVDHFSNVGNTQDLSQSIMERALFHMDNCYKIPNIRGTGRLCKTNLPSNTAFRGFGGP 918
XDH_BOVIN ALEVDHYSNAGNSRDLSHSIMERALFHMDNCYKIPNIRGTGRLCKTNLSSNTAFRGFGGP 917
XDH_MOUSE ALEVAHFSNGGNSEDLSRSIMERAVFHMDNAYKIPNIRGTGRICKTNLPSNTAFRGFGGP 920
XDHB_R.caps GADFVHLARCGWSADLSLPVCDRAMLHADGSYFVPALRIESHRLRTNTQSNTAFRGFGGP 347
XDH1_A.thal ALDLEIYNNGGNSLDLSLSVLERAMFHSDNVYEIPHVRIVGNVCFTNFPSNTAFRGFGGP 946
AOX3_MOUSE AADIQLYINGGCTPDDSELVIEYALLKLENAYKIPNLRVRGRVCKTNLPSNTAFRGFGFP 922
XDHA_R.caps ---------- 462
XDH_HUMAN QGMLIAECWMSEVAVTCGMPAEEVRRKNLYKEG----------DLTHFNQ 958
XDH_BOVIN QALFIAENWMSEVAVTCGLPAEEVRWKNMYKEG----------DLTHFNQ 957
XDH_MOUSE QGMLIAEYWMSEVAVTCGLPAEEVRRKNMYKEG----------DLTHFNQ 960
XDHB_R.caps QGALGMERAIEHLARGMGRDPAELRALNFYDPPERGGLSAPPSPPEPIATKKTQTTHYGQ 407
XDH1_A.thal QGMLITENWIQRIAAELNKSPEEIKEMNFQVEG----------SVTHYCQ 986
AOX3_MOUSE QGAFVTETCMSAVAAKCRLPPEKVRELNMYRTI----------DRTIHNQ 962
XDHA_R.caps ---------- 462
XDH_HUMAN KLEGFTLPRCWEECLASSQYHARKSEVDKFNKENCWKKRGLCIIPTKFGISFTVPFLNQA 1018
XDH_BOVIN RLEGFSVPRCWDECLKSSQYYARKSEVDKFNKENCWKKRGLCIIPTKFGISFTVPFLNQA 1017
XDH_MOUSE KLEGFTLPRCWDECIASSQYQARKMEVEKFNRENCWKKRGLCIIPTKFGISFTLSFLNQG 1020
XDHB_R.caps EVADCVLGELVTRLQKSANFTTRRAEIAAWNSTNRTLARGIALSPVKFGISFTLTHLNQA 467
XDH1_A.thal TLQHCTLHQLWKELKVSCNFLKARREADEFNSHNRWKKRGVAMVPTKFGISFTTKFMNQA 1046
AOX3_MOUSE EFDPTNLLQCWEACVENSSYYNRKKAVDEFNQQRFWKKRGIAIIPMKFSVGFPKTFYYQA 1022
XDHA_R.caps ---------- 462

Figure 1.7 *The alignment of several members of the xanthine oxidase family of enzymes***.** Sequences for several xanthine oxidase family members were obtained from the UniProt protein knowledgebase. Sequences were aligned and colored using the European Bioinformatics Institute (EMBL-EBI) ClustalW2 program. Abbreviations used are XDH_HUMAN for human xanthine dehydrogenase, XDH_BOVINE for bovine xanthine dehydrogenase, XDH_MOUSE for mouse xanthine dehydrogenase, XDHB/XDHA_R.caps for xanthine dehydrogenase from *Rhodobacter capsulatus*, AOX3_MOUSE for mouse aldehyde oxidase 3, and lastly, XDH1_A.thal for xanthine dehydrogenase 1 from *Arabidopsis thaliana*. The color scheme is red for small/hydrophobic residues (including the aromatic residue - tyrosine); blue for acidic residues; magenta for basic residues; and green for neutral residues (hydroxyls, sulfhydryls, amines and glycine).

1.2.2 The active site of the xanthine oxidase

The active site of xanthine oxidase contains several highly conserved residues: Phe 914, Phe 1009, Glu 802, Glu 1261, Gln 767, and Arg 880. In the xanthine dehydrogenase from *Rhodobacter capsulatus*, the crystal structure shows the highly conserved nature of the active site which contains the same residues as the bovine enzyme and in virtually identical positions, allowing a convenient system to conduct mutational studies. Due to the differing composition of subunits, the numbering in the bacterial enzyme is as follows: Phe 344, Phe 459, Glu 232, Glu 730, Gln 197, and Arg 310 (Figure 1.8).

Based upon crystallographic data, substrates wedge in between the phenylalanines, which serve to orient the substrate for catalysis. Glutamate 1261 (730 in the bacterial enzyme), lies beneath the molybdenum center, as shown in Figure 1.8. Being within hydrogen bonding distance of the equatorial Mo-OH, this "bottom" glutamate is universally conserved and is required for activity (35,36). As for arginine 880 and glutamate 802 (residues 310 and 232 in the bacterial enzyme, respectively), structural and kinetic data suggest that both play a role in substrate binding and orientation, as well as transition state stabilization (36,37).

The aldehyde oxidases tend to vary from xanthine oxidase in their active sites. One or both of the phenylalanines may be a tyrosine residue, although it still acts to orient the substrate in the active site. Glutamate 802 and arginine 880 are not conserved in the aldehyde oxidases, and these residues are instead typically residues which allow for altered binding specificity towards their respective substrate(s) (16). A number of

structural and mutational studies with the *R. capsulatus* xanthine dehydrogenase have frequently shown dramatic reductions in activity from xanthine oxidase activity to that of aldehyde oxidase activity, highlighting the importance of these residues in substrate binding and catalysis. Current work and further analysis on the roles of the active site residues and their contributions to binding and catalysis will be discussed in later chapters of this thesis.

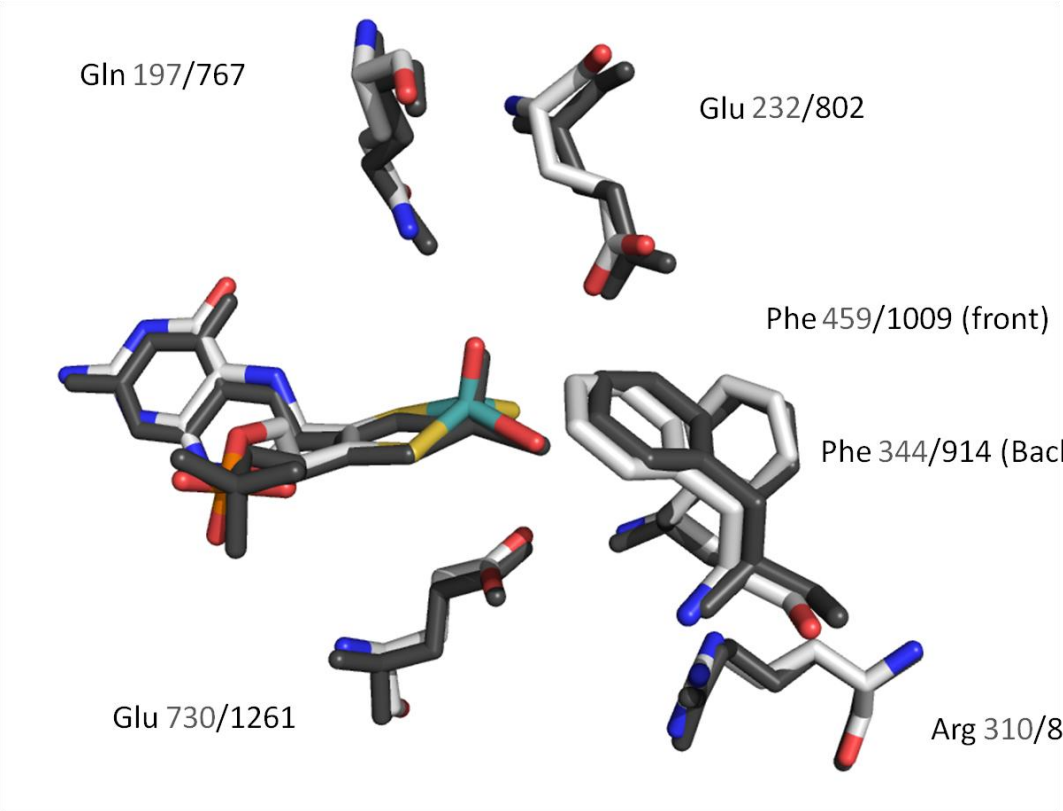

Figure 1.8 *The active sites of xanthine dehydrogenase from Rhodobacter capsulatus and bovine xanthine oxidase.* The active site of the bacterial xanthine dehydrogenase is shown in grey with the numbering of the residues also in grey. The bovine xanthine oxidase active site has been overlayed and is shown in CPK color scheme while the numbering of the residues is in black.

1.3 The catalytic mechanism of xanthine oxidase

1.3.1 The overall mechanism of xanthine oxidase

In the cell, xanthine oxidase catalyzes the conversion of hypoxanthine to xanthine, and further catalyzes the conversion of xanthine to uric acid, the final two steps in the purine degradation pathway (Figure 1.9) (38). The enzyme also has limited activity towards purine analogs and aldehydes. The reduction mechanism, shown in Figure 1.10, with xanthine as a substrate has been well agreed upon in the literature (16). The reaction begins with glutamate 1261 (Glu 730 in the bacterial enzyme), abstracting a proton from the Mo-OH, which can then undertake a nucleophilic attack on the sp^2-hybridized center of the substrate to be hydroxylated. In the case of hypoxanthine, this is C2 and in the case of xanthine, it is C8. At the same time, a hydride transfer to the Mo=S group occurs resulting in the reduction of the molybdenum center from Mo^{VI} to Mo^{IV}. The initial intermediate formed has product bound to the molybdenum center via its new hydroxyl group. The intermediate then breaks down by electron transfer out of the active site and product is displaced via hydroxide from the solvent, readying the enzyme for another round of catalysis.

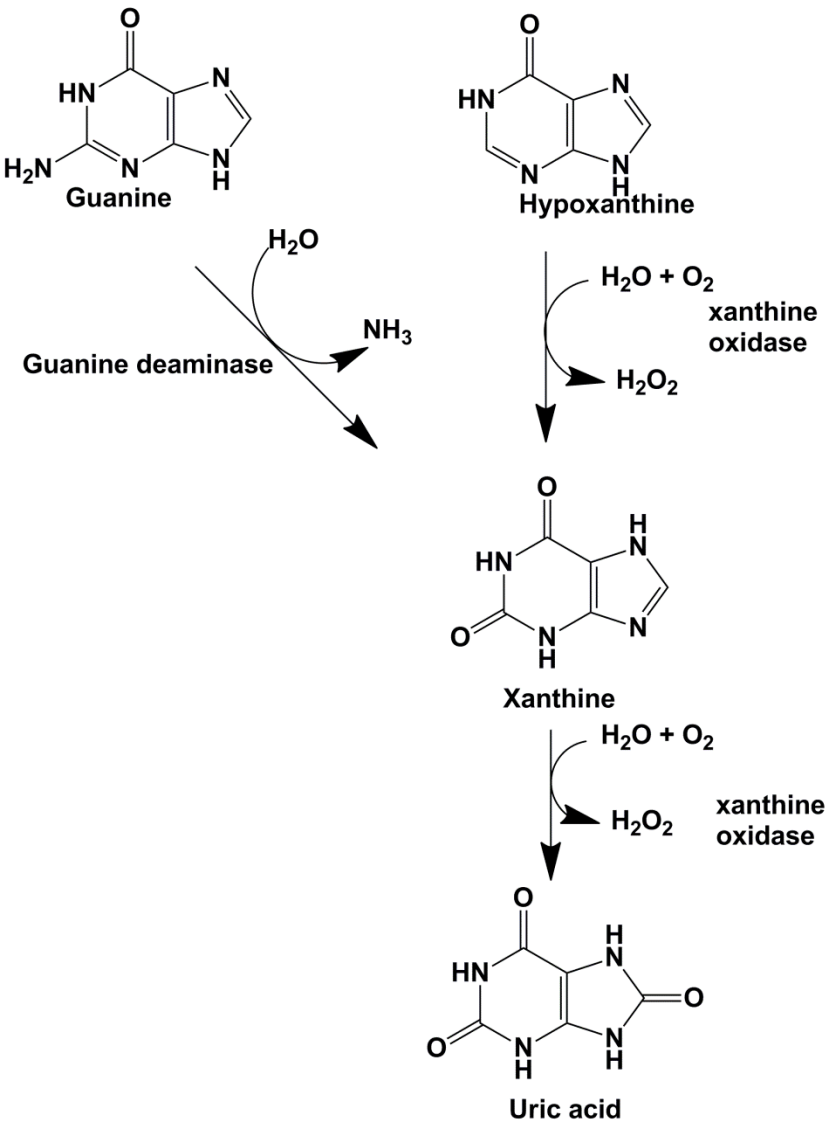

Figure 1.9 *Production of uric acid through the catabolism of hypoxanthine/guanine.* The sequential hydroxylation of hypoxanthine to xanthine and xanthine to uric acid by xanthine oxidase is shown. Hypoxanthine is hydroxylated at the C2 position, dissociates from the enzyme complex as xanthine and then can rebind to the enzyme in order for the C8 of xanthine to be hydroxylated, producing uric acid. The pathway for which guanine is converted to xanthine via guanine deaminase is also shown (38).

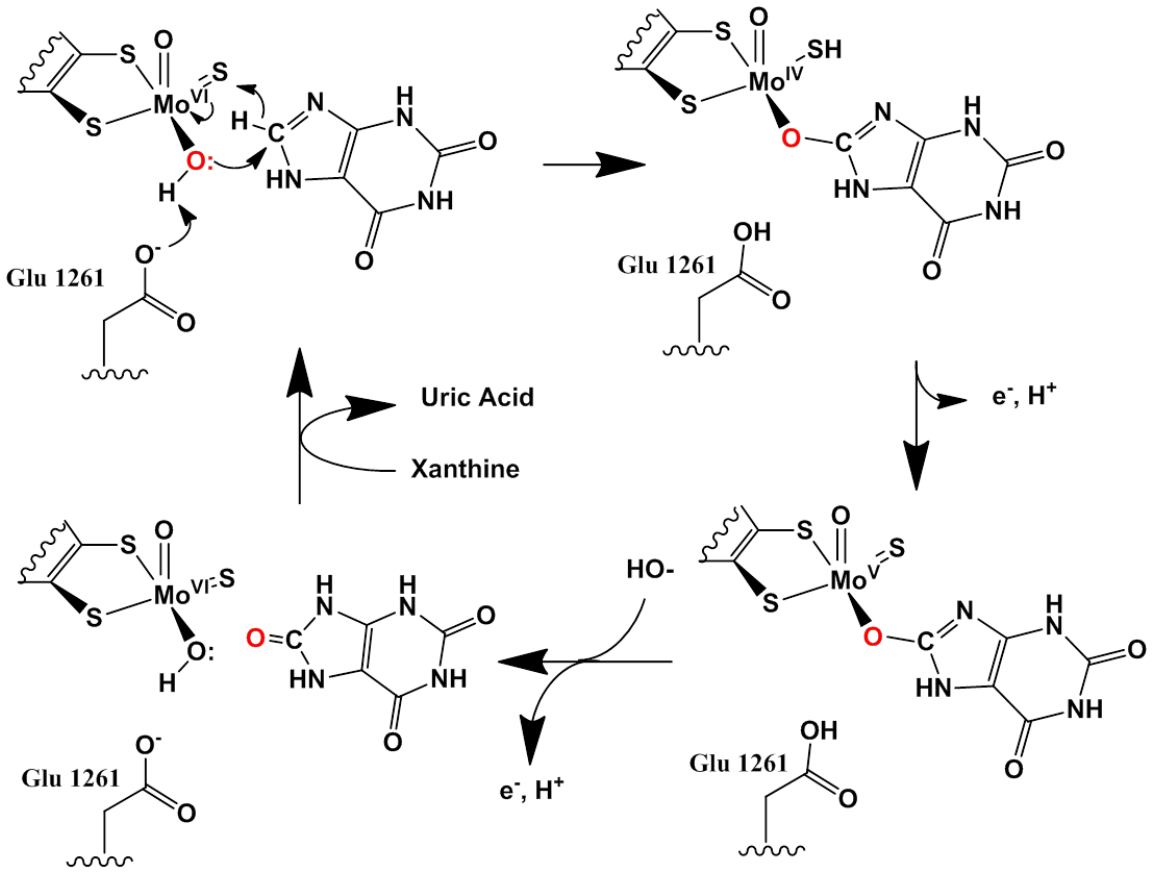

Figure 1.10 *The mechanism of xanthine oxidase*.

1.3.2 Electron transfer in xanthine oxidase

In xanthine oxidase, the overall intramolecular electron transfer is Mo→Fe/S I →Fe/S II→FAD. The reductive and oxidative half-reactions are separated with the reductive half-reaction occurring at the molybdenum center, while the oxidative half reaction occurs at the flavin. The two are linked by a pair of 2Fe-2S clusters.

In the reductive half-reaction, electrons enter the system via a hydride transfer from the substrate, reducing MoVI to Mo^{IV}. Electrons can then move into the iron sulfur clusters; each being able to hold one electron. The first of the two [2Fe-2S] clusters sits 14.8Å away from the molybdenum center with the pyranopterin intervening. The second of the [2Fe-2S] clusters sits 12.8Å away from Fe/S I and 8.3Å away from the flavin (Figure 1.3). The electrons then move to the flavin, which can donate the electrons to NAD^+ in the dehydrogenase form, producing NADH; or to O_2 in the oxidase form, producing H_2O_2 or superoxide (16,39).

The flavin donates electrons to NAD^+ via a hydride transfer; however, the reaction donating electrons to O_2 is more complex. The fully reduced enzyme contains six electrons; two associated with the flavin, one on each Fe/S cluster, and two associated with the reduced molybdenum center. In the process of reoxidation with O_2, the system moves from containing six reducing equivalents to four, with the reduction of O_2 to H_2O_2; from four reducing equivalents to two, also from the reduction of another equivalent of O_2 to H_2O_2; and the last two reducing equivalents each end up as $O_2^{\bullet -}$, for a total of two equivalents of superoxide (39).

Due to the relative reduction potentials of the redox-active centers, at pH 8.5 the electrons distribution across the centers gives ~50% of the enzyme population has $FADH_2$ and the other 50% has the Fe/S clusters reduced (Some molybdenum reduction occurs, however it is small). When the oxidase form of the enzyme has four or six reducing equivalents, an initial one electron transfer from the flavin to O_2 produces $FADH•---O_2•-$ after which, the $FADH_2$ is quickly regenerated by electron transfer from the Fe/S cluster and forms $FADH_2---O_2•-$. A second rapid electron transfer then occurs, producing $FADH•---H_2O_2$. These three steps occur once more, bringing the total reducing equivalents in the system to two. Once only two reducing equivalents are left, however, they then distribute between the flavin and the Fe/S clusters. $FADH_2$ can donate an electron to O_2 forming $O_2•-$, but absent additional reducing equivalents to quickly replenish the electron on the flavin, the $O_2•-$ can escape before reduction to H_2O_2 (39).

1.4 Cofactor maturation and incorporation

Biosynthesis of the pyranopterin cofactor occurs in three main steps: cyclization of GTP to form a cyclopterin monophosphate intermediate, sulfuration of cPMP to give the mature pyranopterin, and coordination of the molybdenum to the enedithiolate of the pyranopterin (Figure 1.11) (39,40). The first step is carried out by the proteins MoaA and MoaC in *E. coli* (MOCS1A and MOCS1B in humans). Cyclization of the GTP produces cyclopyranopterin monophosphate (cPMP; also referred to in the literature as "precursor *Z*"). The sulfuration of cPMP to produce molybdopterin is catalyzed by the enzyme MPT synthase in *E. coli*, composed of an $(\alpha\beta)_2$ heterotetramers consisting of two units of

MoaD and MoaE (MOCS2B and MOCS1B in humans). MoeB is involved in the initial sulfuration of MoaD, which then can sulfurate the cPMP. The molybdenum is attached to the molybdopterin via MogA and MoeA in *E. coli* (gephyrin in humans). MogA adenylylates the pyranopterin phosphate, preparing the molecule for insertion of the metal and then MoeA inserts the molybdate. It has been observed that copper can bind bound to the dithiolene of this cofactor intermediate, however is not required for maturation of the molybdenum cofactor *in vivo* (41). Insertion of molybdate displaces copper (if present) and promotes the molybdate-dependent hydrolysis of adenylylated cofactor, releasing AMP (39).

The mature molybdenum cofactor, which typically exists in the tri-oxo form ($LMoO_3$ or $LMoO_2(OH)$), is highly sensitive to air-oxidation (39,42). Due to the sensitivity to air oxidation, evidence has been growing that chaperones exist that protect and store the cofactor. A number of these chaperones have been shown to be able to insert this initial form of the cofactor into members of the sulfite oxidase family in *Chlamydomonas reinhardii, Neurospora crassa*, and *Arabidopsis thaliana* (39).

In prokaryotes, trafficking of the cofactor to different apoproteins is often determined by additional modifications to the cofactor, particularly the addition of a dinucleotide to the cofactor. As seen in figure 1.1, in *E. coli* the cytosine dinucleotide is targeted to xanthine oxidase family (43); while the guanine dinucleotide, which is found primarily in members of the DMSO reductase family. The MCD and MGD cofactors are produced by MocA and MobA, respectively, allowing for specific targeting of the specific forms of the cofactor into specific enzyme systems by the cell (39).

The xanthine oxidase family requires sulfuration of the molybdenum cofactor for activity (Figure 1.12), replacing the equatorial Mo=O with a Mo=S. Incorporation of the sulfur to produce the LMoO(S)(OH) form of the cofactor requires XdhC, an α_2 homodimeric protein which binds the cofactor, sulfurates it, and then inserts it into the apo-enzyme(43-45). XdhC has been shown to be able to bind MoeA, but specific interactions are yet to be known (46). XdhC also interacts with NifS4, a cysteine desulfurase that can cleave cysteine to alanine and donate the sulfur to XdhC (47). In eukaryotes, sulfuration is carried out by ABA3 (or molybdenum cofactor sulfurase in humans). It is to note that while ABA3 has homologous activity to XdhC, it contains very little similarity in structure and the two systems do not complement one another *in vivo* (39,48).

The last of the mononuclear molybdenum enzyme families depicted in Figure 1.12, the DMSO reductase family, requires the bis-molybdopterin guanine dinucleotide cofactor. MobA catalyzes the addition of the guanine dinucleotide, although much is not known of how the complete bis-MGD cofactor is assembled. It has been shown that MobA, molybdopterin cofactor, and Mg•GTP are sufficient to restore activity *in vitro* in DMSO reductase of *Rhodobacter capsulatus*, however MobB, another protein has been shown to enhance the efficiency of bis-MGD incorporation *in vivo*. MobB, along with other chaperones are likely required for incorporation into the bis-MGD containing enzymes (39). Interestingly in *Rhodobacter capsulatus,* XdhC has been shown to prevent the binding of molybdenum cofactor to MobA, thus ensuring that not all of the molybdenum cofactor is converted to the MGD form in the cell (46).

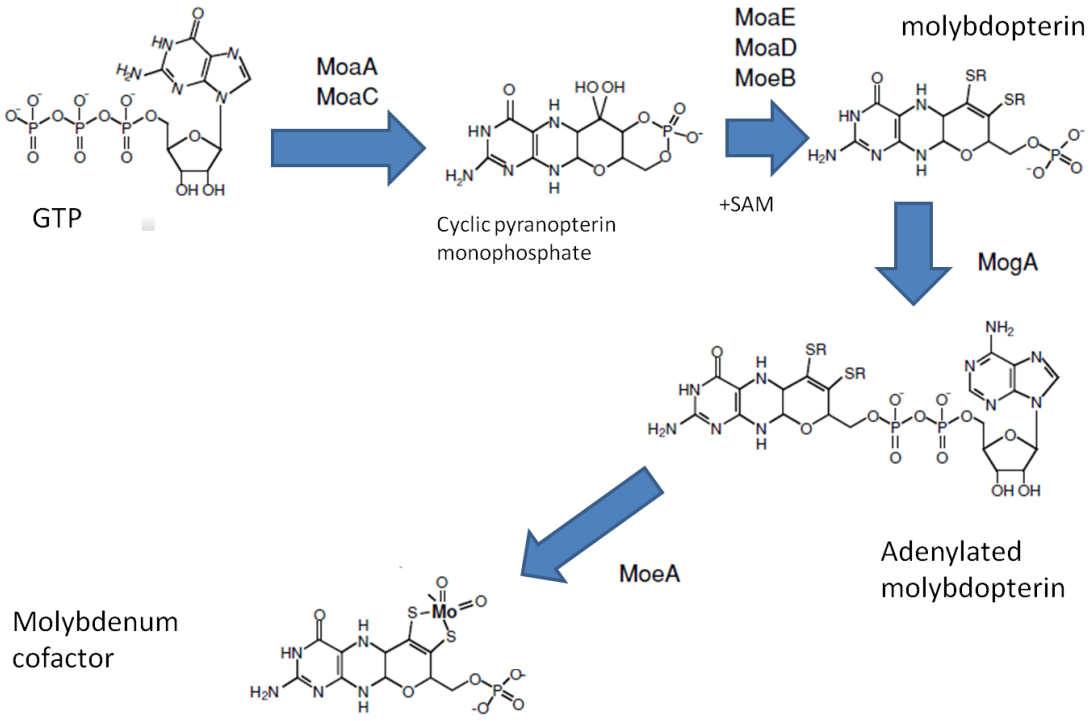

Figure 1.11 *Biosynthesis of the molybdenum cofactor.*

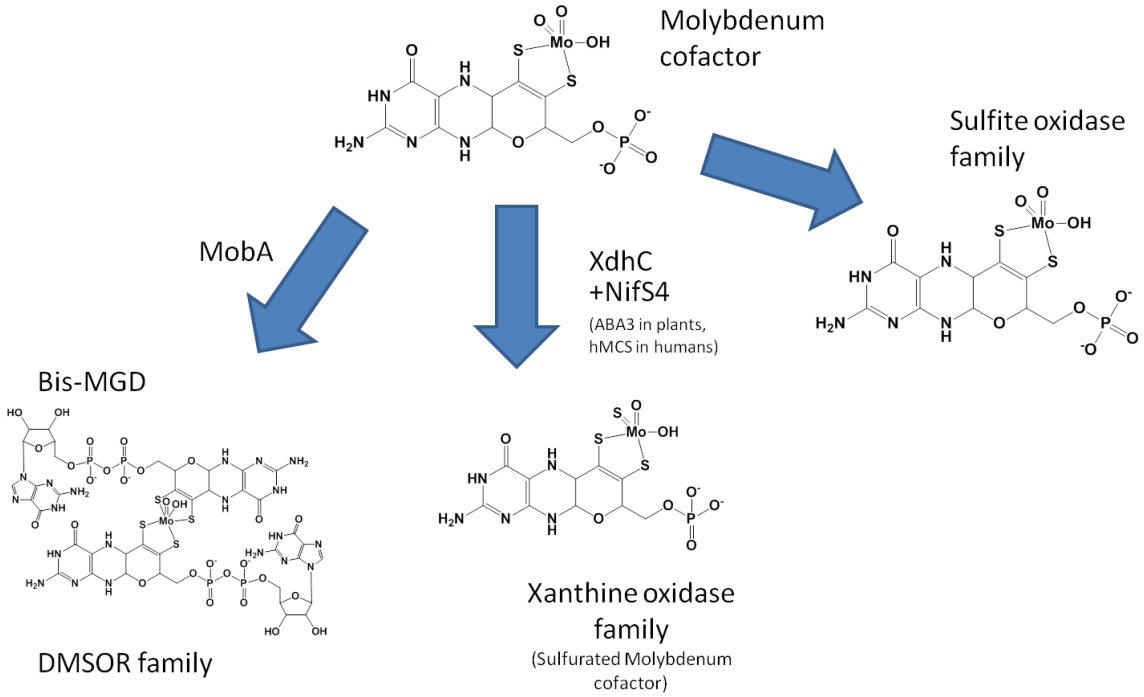

Figure 1.12 *Pathways of production of the various forms of the molybdenum cofactor.*

1.5 Brief introduction into the present work and goals

Although xanthine oxidase has been studied for decades, details of its mechanism and how the active site allows for substrate specificity and catalysis are still not completely understood. In the present work, several methods have been used to investigate the mechanism of xanthine oxidase and the roles of the active site residues in substrate binding and catalysis. Utilizing UV/Vis spectroscopy, the kinetic rates of bovine xanthine oxidase and variants of the homologous *Rhodobacter capsulatus* xanthine dehydrogenase toward various substrates have been determined. While the effects of active site amino acid substitutions on rate can be observed spectroscopically, contributions to substrate binding and/or the chemical step of the reaction must be determined utilizing other techniques such as x-ray crystallography and the measurement of kinetic isotope effects. X-ray crystallography gives a snapshot of stable configurations of the enzyme and substrate, allowing for identification of interactions between enzyme and substrate. The effects of active site residues on the chemical step of the reaction have been investigated utilizing kinetic isotope effect studies. Due to product release being the rate-limiting step in the turnover of xanthine oxidoreductase, the primary deuterium isotope effect ($^{H/D}V$), the deuterium isotope effect on (V/K), and the tritium isotope effect on (V/K) have been determined, permitting calculation of the intrinsic isotope effect ^{D}k. With the primary deuterium isotope effects, previously described by Dr. Hongnan Cao, and intrinsic isotope effects ^{D}k, derived from the tritium isotope effect studies for bovine XO and bacterial XDH, the extent to which the chemical step is rate-limiting has been calculated for each. Knowledge of the previously documented rates of

reduction of these enzymes, the calculation and comparison of k_{cat} and the rate of the chemical step provides insight into similarities differences between the three enzymes when it comes to the rate of the chemical step of the reaction and the overall rate of enzymatic turnover. Analysis of variants of the bacterial enzyme provides insight into the role of the active site residues by the monitoring of changes (or lack of change) in the rate of the chemical step and it's comparison to changes in the overall rate of reaction.

With regard to cofactor insertion, it is to note that in the xanthine oxidase family the molybdenum cofactor is deeply buried. To gain insight into how the cofactor is incorporated into the enzyme, computational structural studies have been performed looking at the sulfuration of the molybdenum cofactor and incorporation of the enzyme into members of the xanthine oxidase family of enzymes. Given the highly conserved overall structures of xanthine oxidase family members, an attempt to identify a conserved conformational change allowing for insertion of the molybdenum cofactor has been attempted. Utilizing published structural data of xanthine oxidase family members, specific conserved portions of the enzyme have been compared in attempts to identify portions of enzyme capable of conformational change. Possible targets for the binding of cofactor insertion machinery have also been taken into consideration. We identify a conserved ~125 amino acid motif of the crystallographically characterized xanthine oxidase family members whose connectivity to the remainder of the polypeptide makes possible a "hinge" movement. Published crystal structures for bovine XO and bacterial XDH have been manipulated to create conformations which would allow for access to the

binding site of MPT in the holoenzyme utilizing computational software for simulation and energy minimization of proposed "open" conformations.

Initial expression, purification, and characterization of the 125 amino acid "hinge" motif in *E. coli* has been performed to investigate the possibility of dimerization of the hinge region. Purification suggests several other proteins are associated with the protein fragment, many having molecular weights as proteins involved with the maturation of xanthine dehydrogenase. Based upon the idea of the hinge being part of a complex containing what was believed to be XdhC, a PLP-containing enzyme (assumed to be a NifS homolog), and XDH, investigation into the possibility of a complex based upon current structural data has been conducted. The crystal structures for homologous enzymes to the cofactor insertion machinery of *Rhodobacter capsulatus* XdhC and the NifS-4 homolog IscS have been used to model a number of possible complexes. AutoDock software was used to probe for possible binding sites of both the molybdopterin and molybdopterin cytosine dinucleotide cofactors to the XdhC homolog, identifying a binding pocket in correct proximity to a conserved cysteine proposed to be required for cofactor sulfuration. XdhC has been docked to the crystal structure for the *Rhodobacter capsulatus* XDHAB, providing a model for interaction and region of the protein where the cofactor may be incorporated.

Independently, the docking of the NifS4 homolog IscS to the XdhC homolog from *Bacillus halodurans* has also been conducted to see if the two could possibly interact allowing for sulfuration and subsequent insertion. After initial docking attempts, investigation into the possibility of a complex containing bacterial XDH and both the

XdhC and NifS4 homologs has been begun, producing a plausible model for cofactor sulfuration and insertion in bacterial xanthine oxidase family members.

CHAPTER 2

MATERIALS AND METHODS

2.1 Materials

2.1.1 Reagents and chemicals

Polyethylene glycol 200 (PEG200) and polyethylene glycol 8000 (PEG 8000) used for protein crystallization were obtained from Hampton Research (Aliso Viejo, CA). [8-^{3}H] xanthine was obtained from Moravek Biochemicals and Radiochemicals (Brea, CA). All other chemicals and reagents were obtained from Sigma-Aldrich or Fischer at the highest purity and quality available and used without additional purification.

2.1.2 Enzyme purification

Xanthine oxidase isolation - Xanthine oxidase was purified from freshly collected unpasteurized cow's milk (obtained from Scott Brothers Dairy, Moreno Valley, CA; or from J&M Oostdam Dairy, San Jacinto, CA). Enzyme used for kinetic assays was obtained from a mixture of milk from multiple cows, while enzyme used in crystallography was derived from milk from a single cow in order to avoid possible issues due to genetic variability within the dairy herd.

The protein purification protocol was modified from the previous method developed by Massey et. al. (49). One or two 20 L carboys of fresh raw milk in (totaling 20-40 L of milk for multiple source milk or 10 -16 L of milk from a single cow) was obtained from the local dairy and kept at 4^{o}C. While stirring with a heavy-duty overhead stirrer, the following reagents were added in order to each 20 L of milk: 50 mL 0.3 M

EDTA, pH 7.0; 20 mL 0.1 M PMSF in Ethanol; 20 mL 1.0 M Sodium salicylate, pH 7.0; 316 g $NaHCO_3$ (added slowly to avoid frothing); 6.0 g cysteine-HCl; and 31.6 g pancreatin. The mixture was stirred for 20 minutes and then allowed to stand overnight. On the second day, 3780 g of ammonium sulfate was slowly added to the carboy while stirring and allowed to stir for an additional 1 hr after addition. After the hour of sitting, 3340 mL of butanol which was stored overnight in a -20°C freezer was added while vigorously stirring the mixture. After addition of the butanol, stirring speed was reduced and stirred for another 30 min. The mixture was then allowed to stand overnight at 4°C. On day three, the lower aqueous phase from the carboy was transferred into a large open-topped carboy. Cheese cloth was used to remove any residual floating lipid. 160 g of ammonium sulfate was added per liter of the collected lower aqueous phase while stirring the mixture. The mixture was stirred an additional 30 minutes and allowed to stand for an additional hour. The crude protein aggregated and floated to the top of the liquid and was removed into a large glass beaker on ice. After excess butanol was decanted, the brownish aggregate was centrifuged for 30 minutes at 5000 rpm. After centrifugation, bottom and top aqueous layers were then discarded. The protein was then resuspended in 100-200 ml of 0.1 M potassium phosphate, 0.3 mM EDTA, 1 mM salicylate, 0.01 mM PMSF, pH 6.0. The resuspended protein solution was placed in Spectra/Por dialysis membrane from Spectrum Laboratories, Inc. with a 12-14 KDa molecular weight cutoff and dialyzed against 20 L of the same buffer at 4°C. The 20 L of buffer were changed at least five times over the course of 2-3 days. The dialysis solution was stirred only after the first day of dialysis.

Once dialyzed, the solution was centrifuged for 1 hour at 10,000 rpm and then supernatant was poured through cheese cloth to remove any leftover lipid. The solution was then concentrated to 70-100 ml via a 250 ml Amicon stirred ultrafiltration cell with a 100 kDa molecular weight cutoff membrane. The concentrated solution was then centrifuged at 6000 rpm for 15 minutes to remove any precipitate. A hydroxyapatite (HAP) column from BIO-RAD was equilibrated with and the protein sample was loaded onto the column at 0.3 ml/min. The column was washed with 0.5 column volumes and eluted over 6 column volumes at 0.5 mL/min with 0.1 M potassium phosphate, 0.3 mM EDTA, 1 mM salicylate, 0.01 mM PMSF, pH 6.0 supplemented with 20% ammonium sulfate. Fractions with a absorbance ratio of A_{280nm}/A_{450nm} less than 10 and spectra lacking the presence of a 420nm shoulder were combined and concentrated to less than 5 ml via a 50 ml Amicon stirred ultrafiltration cell with a 100 kDa molecular weight cutoff membrane. The concentrated protein (~200-250 mg total protein) was then run over a S-300 column (BIO-RAD) equilibrated with 0.1 M sodium pyrophosphate, 0.3 mM EDTA, pH 8.5. and eluted with the same buffer. Larger preps were run over a large S-200 which could handle loading up to 20 mL of sample containing up to 1 g of protein. Fractions with an absorbance ratio of A_{280nm}/A_{450nm} less than 7 were pooled and 1mM salicylate was added to protect the activity of the enzyme. The final protein solution was frozen in liquid nitrogen and stored in liquid nitrogen.

Before use, the enzyme was run through a G-25 column (BIO-RAD) to remove the salicylate and functional activity was determined based upon the methods previously

described by Massey and Edmondson (50). Purified enzyme was typically between 40-80% active due to variability in the amount of desulfo and demolybdo enzyme present.

Recombinant Rhodobacter capsulatus xanthine dehydrogenase expression and isolation – Recombinant xanthine dehydrogenase from *R. capsulatus* was provided by the laboratory of Dr. Silke Leimkühler (University of Potsdam, Germany). The enzyme was purified using previously published methods (51). By using PCR mutagenesis, amino acid substitutions were introduced to make each of the XDH variants (E232A, E232Q, Q197A, Q197E, E730A, and R310M). The protein was expressed in TP1000 cells grown on Luria broth media. The enzyme variants were expressed under the same conditions as the wild-type enzyme and purified by nickel-NTA chromatography. Isolated protein was then dialyzed overnight in 50mM Tris, 1mM EDTA, pH7.5 buffer to remove the imidazole. The dialyzed sample was loaded onto a Q-Sepharose column (GE Healthcare) equilibrated with 50mM Tris, 1mM EDTA, pH7.5 buffer. The sample was eluted from the Q-sepharose column with a linear gradient of 50mM Tris, 1mM EDTA, 1 M NaCl pH7.5 buffer. The enzyme-containing samples were then run on a Superpose 6 column (GE Healthcare) equilibrated with 50mM Tris, 1mM EDTA, pH7.5 buffer. The enzyme containing samples were then run on a superpose 6 column (GE Healthcare) equilibrated with 50mM Tris, 1mM EDTA, pH7.5 buffer. For some samples, the final step was instead an affinity chromatography step on a Sepharose 4B/folate gel. The purified enzymes were concentrated by ultrafiltration and in the case of the affinity chromatography step, those enzymes were exchanged into 50 mM Tris, 1mM EDTA, 2.5

mM DTT, pH 7.5 using a PD-10 gel filtration column (GE Healthcare), which was also equilibrated with the same buffer. The final product was then stored at -80°C until needed.

XDH hinge cloning – Initial cloning of the hinge was conducted by Dr. Wilcoxen while visiting the laboratory of Dr. Silke Leimkühler. The PCR product of the genetic sequence encoding for residues 465-606 of *R. capsulatus* xdhB subunit was cloned from the pSL207 plasmid into the pJet plasmid. The sequence was then digested out of pJet and ligated into the pACYC-Duet plasmid (Figure 2.1). Calculated properties for the hinge were a molecular weight of 15770.7 Da, a theoretical pI of 7.26, an extinction coefficient of 10095 at 280nm, and an estimated half-life of more than 10 hours in *E. coli*. The initial expression conditions for the XDH hinge were also described by Jarett Wilcoxen. BL21 (DE3) cells were grown 4-5 hours at 37°C on LB broth containing chloramphenicol. 100mM IPTG was added and the cells were grown an additional 4-5 hours at 30°C. The cells were lysed and centrifuged to remove cell debris. The supernatant was run over a Ni-NTA gravity column followed by concentration of the elution. The concentrated elution sample was then run through a superdex 75 column (GE Healthcare). Peak fractions containing an enzyme the apparent size of the hinge were isolated and the circular dichroism spectrum was taken, showing similarities to the calculated spectrum (Figure 2.3).

Figure 2.1 *The DNA sequence of XDH hinge region incorporated into the pACYC-Duet plasmid.* The DNA sequence for the "hinge" region of *R. capsulatus* xanthine dehydrogenase (XDH) compared to the sequence of the pACYC-Duet plasmid containing the digested fragment from pJet.

*HHHHHHSQDP***NQAGALVQIYTDGSVALNHGGTEMGQGLHAK**
MVQVAAAVLGIDPVQVRITATDTSKVPNTSATAASSGADMNG
MAVKDACETLRGRLAGFVAAREGCAARDVIFDAGQVQASGKS
WRFAEIVAAAYMARISLSATGFYATPK

Figure 2.2 *Amino acid sequence of the expressed XDH "hinge."* The sequence of the XDH hinge is shown in black with the 6-His tag and linker region shown in blue.

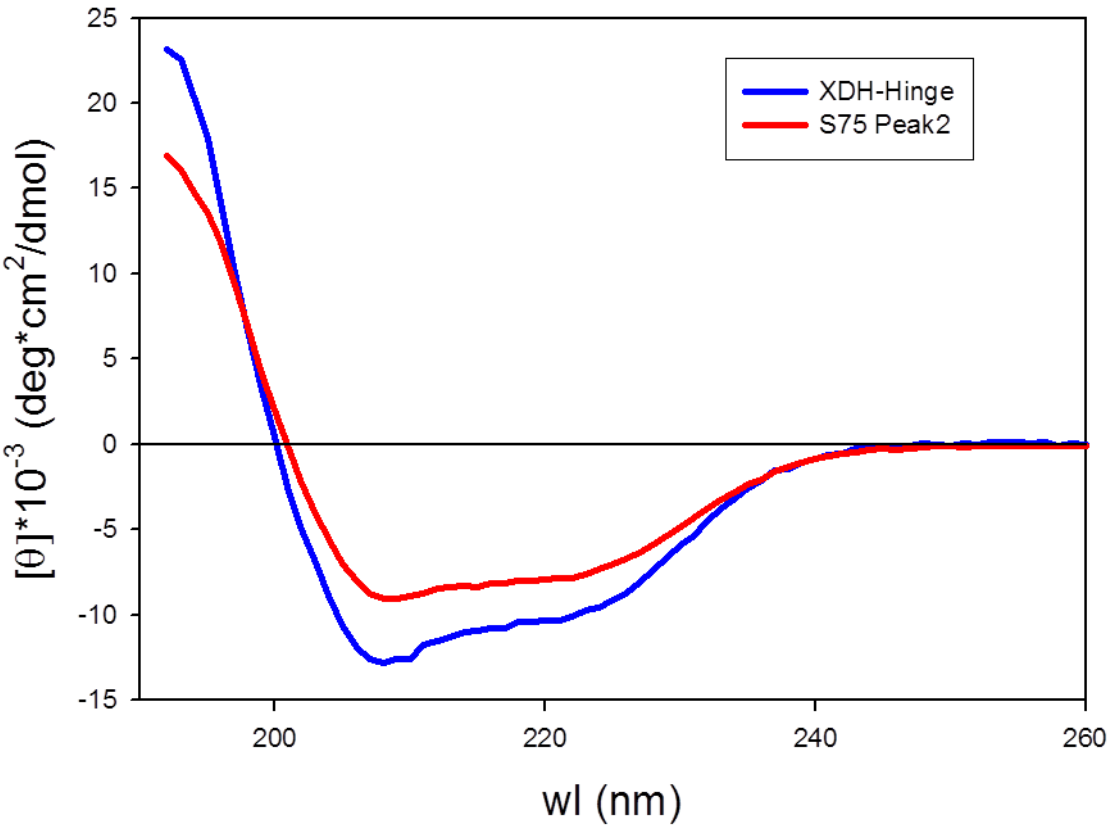

Figure 2.3 *Circular dichroism spectra for the recombinant XDH hinge.* The calculated CD spectrum (blue) and the CD spectrum of the presumed hinge-containing Superose 75 protein peak (red) are shown.

Hinge expression and buffer optimization – Hinge was expressed and purified using a protocol modified from the initial Wilcoxen protocol. BL21 (DE3) was grown on LB broth at 30°C to OD 0.5. 100µM IPTG was added and the cells were continued to be grown for 5 more hours at the same temperature. Cells were resuspended and lysed in 50mM sodium phosphate, 300 mM NaCl, pH 8.0 buffer. The supernatant was run over a Ni-TED gravity column. Washes were performed with 10 mM and 20 mM imidazole and elution as performed with phosphate buffer containing 250 mM imidazole. The eluted sample was concentrated and run through a Superdex 75 column (GE Healthcare) equilibrated with 50 mM Tris, 1 mM EDTA, 150mM NaCl pH 8.0 buffer.
Purified hinge protein was exchanged into various buffer conditions and screened utilizing florescence-based thermal shift assay (Thermoflor) to find stable buffer conditions. Phosphate buffers pH range 7-8 each had the highest stability ratings and similar stability profiles. (Figure 2.4)

The protocol was modified in the Hille laboratory. BL21 (DE3) cells were grown at 37°C on LB media, to an OD of 2.5-3.0. The cells were then induced with 250 µM IPTG and incubated for 5-8 hours. Cells were centrifuged for 30 minutes at 8000 rpm and the pellet was resuspended in 50 mM potassium phosphate buffer with 300 mM NaCl, pH 8.0. Cells were lysed and cell debris was removed via centrifugation for one hour at 35,000 rpm. The supernatant was incubated with Ni-TED resin (Macherey-Nagel) for 1 hour with light shaking. The column is washed with 50 mM potassium phosphate buffer with 150 mM NaCl, pH 8.0. Protein is eluted with the same buffer supplemented with 250 mM imidazole. The eluate was is concentrated via an Amicon ultra centrifugal filter

with a 10,000 molecular weight cutoff. The concentrated sample was then loaded onto a superpose 12 column equilibrated with 50 mM potassium phosphate buffer with 150 mM NaCl, pH 8.0.

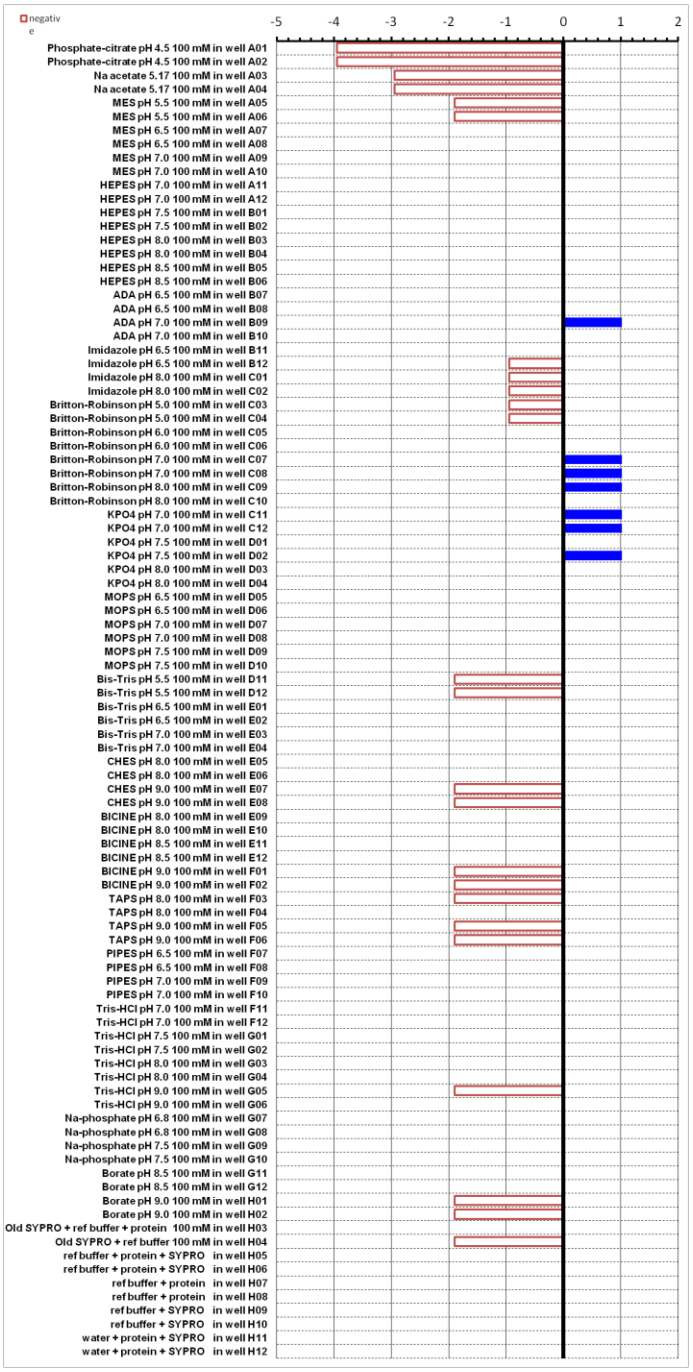

Figure 2.4 *List of buffers probed via florescence-based thermal shift assay.* The buffer conditions are shown on the left and the perturbation of protein stability from the reference buffer shown in degrees Celsius on the right. The reference buffer was 50mM sodium phosphate, 300 mM NaCl, pH 8.0.

2.2 X-ray crystallography

Materials **–** Magnetic bases for the automated system at LRL-CAT were obtained from MAR-USA (Evanston, IL). Mounted cryoloops, magnetic cryovials, microbridges, 24 well plates, cover slides, and other crystal growth materials were obtained from Hampton Research (Aliso Viejo, CA).

Isolation of fully active xanthine oxidase via folate column – Single source bovine oxidase of lower than 70% activity was subject to affinity chromatography on a Sepharose 4B/folate gel to provide a protein sample that contained 80-90% active enzyme (52).

Crystallization, data acquisition and structure determination – All xanthine oxidase crystals were grown based upon a slight modification of the method described by Pauff et. al. (53). The protein was prepared by exchanging single source xanthine oxidase into 40mM Tris-HCl, 20mM sodium pyrophosphate pH 8.4 buffer. The enzyme concentration was then adjusted to 35 µM total monomer concentration based upon the extinction coefficient of xanthine oxidase at 450 nm of 37.8 $mM^{-1}cm^{-1}$ (this concentration corresponds to ~5mg/ml protein) (49). The enzyme was then incubated with 0.2 mM EDTA, and 5mM DTT for 1-2 hours.

The crystals were grown in microbridges that held batch solutions in the sealed wells of a 24-well tray (53-56). Each well contained 10 µl of the enzyme solution and 5-6 µl of a 12% PEG 8000, 0.1 M potassium phosphate (initial pH 6.5), 0.2mM EDTA

solution. The final pH of the batch was about 7.2. The crystals grew in the dark for 2-3 days at 25°C. Wells containing suitable crystals had the mother liquor exchanged via micropipette with a 42% PEG 2000 solution containing all proportions of the enzyme and precipitant solution. Substrate was introduced to the xanthine oxidase crystals via soaking to reach a final concentration of substrate of about 1mM in the well. Wells were allowed to soak with the substrate for between 1-10 minutes, and then crystals were harvested and frozen in liquid nitrogen. Diffraction data was collected at Argonne National Laboratory on the LRL-CAT beamline using a wavelength of 0.9793 Å and a MARCCD 165 detector.

Crystallographic data received from the beamline was processed using the MOSFLM package of the Collaborative Computational Project No. 4 (CCP4) program suite (57). Molecular replacement was used for phase solution and determination of the structure of each complex utilizing the MOLREP package of CCP4 with the basis for fitting being the previously reported crystal structure of xanthine oxidase of Enroth et al. as the search model (Protein Data Bank code 1FIQ;(27)). The output structure was refined first by rigid body refinement and subsequently by restrained refinement using the REFMAC program of the CCP4 suite (57-61). The weighting term for geometric restraints was adjusted in REFMAC to minimize R_{cryst} while at the same time minimizing the difference between R_{cryst} and R_{free}. No non-crystallographic symmetry restraints were used during refinement of the structures. Water molecules were added to both the crystal structures (using REFMAC) prior to building in the substrates.

Structure files for substrate molecules were constructed using the PRODRG2 server (62), and the respective Protein Data Bank codes were added into the corresponding $2F_0 - F_c$ and $F_0 - F_c$ omit electron density maps observed in the active sites using Crystallographic Object-Oriented Toolkit (COOT) (63). After merging the substrate structure files with those for the refined protein structures, the results were refined again using the restrained refinement mode in REFMAC.

Published final structure files were deposited into the Protein Data Bank (PDB) at www.rcsb.org with the PDB accession numbers 3NVZ (xanthine oxidase in complex with indole-3-aldehyde) and 3NVW (xanthine oxidase in complex with guanine). All structures in the figures have been rendered using PyMol (64).

2.3 Enzyme kinetics

2.3.1 Rapid reaction kinetics

The reductive half-reaction was studied using an Applied Photophysics, Inc. SX-18MV stopped-flow spectrophotometer. Enzyme was made anaerobic in glass tonometers by evacuating and flushing with oxygen scrubbed argon gas (obtained from Airgas) for between 30-60 minutes. Substrate solutions were made anaerobic by bubbling solutions in glass syringes for 15-30 minutes. Standard buffer conditions for xanthine oxidase were 100 mM sodium pyrophosphate, 0.3 mM EDTA, pH 8.5 at 25°C. Reactions were observed at 450nm, monitoring the disappearance of absorbance due to reduction. For bacterial xanthine dehydrogenase, standard buffer conditions were 50 mM potassium phosphate, 0.1 mM EDTA, pH 7.8. Reactions involving the bacterial xanthine

dehydrogenase were monitored at 465nm. The reaction mixtures after mixing typically had 5-10 μM enzyme, and varying concentrations of substrate. The reaction with each substrate concentration used was repeated in triplicate. The kinetic transients were fit to single exponentials to obtain rate constants, which were averaged for each substrate concentration. Each k_{obs} was then plotted against substrate concentration, [S], and the hyperbolic curve was fit using SigmaPlot to obtain values for k_{red} (the maximum rate constant observed at high substrate concentration) and the dissociation constant, K_d.

pH dependence studies on the reductive half-reaction were conducted between pH units of 6-11 using conditions previously reported by Kim et. al. (65). Buffers at the various pH units included 0.1 M MES (pH 6.0), 0.1 M MOPS (pH 7.0), 0.1 M Tris-HCl (pH 8.0), 0.1 M CHES (pH 9.0, 9.5), 0.1 M CAPS (pH 10, 10.5, 11.0), each also supplemented with 0.3 mM EDTA and 0.1 M KCl.

2.3.2 Enzyme assay methods

UV-visible absorption spectra were obtained and steady-state experiments were performed using a Hewlett-Packard 8452 diode-array spectrophotometer. To follow the fractional conversion of xanthine to uric acid by xanthine oxidase, substrate and enzyme were added to 1 ml of air equilibrated buffer (0.1 M sodium pyrophosphate, 0.3 mM EDTA, pH 8.5). The formation of uric acid was monitored at 295nm ($\Delta\varepsilon_{295nm}$ = 9600 $M^{-1}cm^{-1}$). For bacterial XDH, xanthine, NAD+ and enzyme were subsequently added to 1mL of air-equilibrated buffer (50mM potassium phosphate, 0.1 mM EDTA, pH 7.9).

The formation of NADH ($\Delta\varepsilon$340nm = 6200 $M^{-1}cm^{-1}$) was monitored in addition to the formation of uric acid.

2.3.3 Kinetic isotope effects

Following a slight modification of the methods outlined by D'Ardenne and Edmondson (66), steady-state kinetic analysis was used to determine the primary deuterium isotope effects and the deuterium isotope effects on the chemical step of the reaction for bovine xanthine oxidase, bacterial wild-type XDH, and the bacterial XDH Q197A variant. Xanthine and bacterial enzyme were subsequently added using Hamilton syringes to 2.5 ml buffer solution at pH 7.8 containing 50 mM potassium phosphate, 0.1 mM EDTA and 500 μM NAD^+ as the terminal electron acceptor. The solutions were made anaerobic by bubbling argon gas through it for 20 min in a sealed quartz cuvette. The buffer solution, including NAD^+, was preincubated at 25°C and mixed via inversion after addition of xanthine and enzyme. Changes in absorbance change at 295 nm were monitored. The initial reaction mix contained a fixed concentration of functional *R. capsulatus* xanthine dehydrogenase (~ 2 nM functional active sites) and varying concentrations of substrates (5-200 μM). The initial rates were calculated from linear fits of the first 20-120s of each transient. Xanthine oxidase assays used 5nM functionally active sites and were measured in air equilibrated 0.1 M sodium pyrophosphate, pH 8.5 that did not contain NAD^+.

Competition experiments were used to determine the tritium isotope effect on (V/K) for bovine xanthine oxidase, bacterial wild-type XDH, and the bacterial XDH

Q197A variant following slight modification of the methods as described by D'Ardenne and Edmondson (66). Catalytic amounts of enzyme (5nM functional active sites for XO and 2nM functional active sites for bacterial XDH) were incubated at room temperature with xanthine concentrations of 40µM for bovine XO and 200 µM xanthine for bacterial XDH. Air saturated buffers were used for xanthine oxidase, while 500 µM NAD^+ was used as the final electron acceptor for the bacterial XDH samples. Levels of radiolabeled [8-^{3}H] xanthine in each sample were about 0.1 µCi/ml. Fractional conversion of xanthine to uric acid was determined via UV/Vis spectroscopy, monitoring the reaction to completion and determining the point at which 10-20% of the total absorbance change at 295nm was reached. Once 10-20% fractional conversion was reached, the reaction mixture was quenched by the addition of 10% (w/v) trichloroacetic acid. Substrate ([8-^{3}H] xanthine) and product (^{3}H-labeled water) were separated by HPLC (Supelco C18 column, isocratic conditions, 1ml/min, 50mM sodium phosphate, pH 6.0) with tritiated water eluting around 3 minutes and [8-^{3}H] xanthine eluting around 10 minutes.

The competitive (V/K) isotope effects were calculated from quantitation of the radioactivity in the tritiated water and the [8-^{3}H] xanthine using the following equation (66,67):

$$\frac{(V/K)_H}{(V/K)_T} = \frac{ln\ (1-f)}{ln((1-f)\frac{R_p^{\ t}}{R_s^{\ 0}})}$$

Where f is the fractional conversion of substrate to products, $R_p^{\ t}$ is the ^{3}H ratio of products at time t and $R_s^{\ 0}$ is the ^{3}H ratio of the substrate at t = 0. The ratio at 0%

conversion was monitored to correct for the naturally occurring ^{3}H exchange with water in the absence of enzyme.

The intrinsic isotope effect was calculated using the equation:

$$\frac{^{H/D}(V/K)}{^{H/T}(V/K)} = \frac{^{D}k-1}{^{D}k^{1.44}-1}$$

By solving for the ratio of the isotope effects on (V/K) for both deuterium and tritium, the value of ^{D}k was solved by plotting the function and finding the intercept point of the ratio and the function.

With both the primary deuterium isotope effect ($^{H/D}V$) and the intrinsic isotope effect (^{D}k), the f_v or fractional velocity of the chemical step in relation to the overall rate of the reaction can be calculated using the equation:

$$f_v = \frac{^{H/D}V-1}{^{D}k-1}$$

100 f_v gives the percentage of k_{cat} the chemical step ($k_{C\text{-}H}$) comprises while the inverse of f_v gives how much faster the chemical step of the reaction is in relation to k_{cat}, thus multiplying the inverse of f_v by the value for k_{cat} gives the approximate rate of the chemical step.

2.4 Calculation and representation of molecular orbitals

Calculation of the molecular orbitals of indole-3-aldehyde was carried out in the ChemDraw 3D Pro 12.0 program of the ChemDraw Ultra 12.0 suite of programs.

Structures of various purine substrates were built in ChemDraw and were the MM2 force field method was utilized to energy minimize the structure. The minimized structures then had extended Hückel charges calculated for all atoms and the molecular orbitals rendered in wireframe.

2.5 Computational modeling and molecular dynamics

Structures of bovine xanthine dehydrogenase (PDB ID: 1FO4) and *R. capsulatus* xanthine dehydrogenase (PDB ID: 2W3S) were obtained from the RCSB Protein Data Bank and modified by removing all waters, the molybdenum centers, the 2Fe-2S clusters and the FAD molecules. Then using the Crystallographic Object-Orientated Toolkit (COOT) (63), the residues corresponding to the hinge region were selected (residues 1011-1139 in the bovine enzyme and residues 466-604 in the alpha subunit of *R. capsulatus* XDH). Using the Rotate/Translate zone tool, the hinge regions were rotated towards one another into 15-20Å wide groove that spans the non-crystallographic two fold axis of symmetry in the dimer. A second region, corresponding to residues 561-576 in bovine xanthine dehydrogenase, was rotated toward the loop comprised of residues 192-201. The bond angles of these rotated residues were checked using the regularize zone function in the COOT software. With the newly modified structure in the proposed open configuration, a PDB file was generated. Energy minimization was carried out in NAMD (68) and was run at a temperature of 300K using the Charmm force field

parameters (69). The minimization coordinates were converted to PDB files using VMD (70). All figures were generated using PyMol (64).

2.6 Protein-substrate and protein-protein docking

An unannotated XdhC homolog from *Bacillus halodurans* was identified in the RCSB Protein Data Bank (PDB ID: 3ON5) and the structure file was modified by removing all waters. The MPT and MCD versions of the molybdopterin cofactor were docked to the protein using AutoDock 4.2.5.1 (71,72). Both versions of the cofactor were modeled without molybdenum due to the inability of the software to recognize the atom type. After docking, the molybdenum was added back into the model to simulate where the molybdenum lies in relation to the pterin cofactor and the protein. All models were then represented using PyMol (64).

The calculation of intramolecular cavities in the *Bacillus halodurans* XdhC-like enzyme was carried out by MOLE 2.13.9.6 (73). Cavity paths were traced and rendered in PyMol(64).

Positioning of the *Bacillus halodurans* XdhC-like enzyme to the *R. capsulatus* xanthine dehydrogenase (PDB ID: 2W3S) was done in PyMol while taking into account complimentarity between secondary structures and the residues along the face of the enzymes that would come into contact. Independently, positioning of IscS (PDB ID: 1KMJ) onto the *Bacillus halodurans* XdhC-like enzyme was done in PyMol while taking into account complimentarity between secondary structures and the residues along the face of the enzymes that would come into contact. Finally, positioning of the *Bacillus*

halodurans XdhC-like enzyme, *R. capsulatus* xanthine dehydrogenase, and the NifS4 homolog IscS together was constructed in PyMol.

CHAPTER 3

THE CATALYTIC ROLE OF GLUTAMATE 802/232 OF XANTHINE OXIDOREDUCTASE AND THE pH PROFILE OF THE E232Q VARIANT

3.1 Introduction

The active site of xanthine oxidoreductase is highly conserved across many species. The active site of the bovine enzyme consists of: Phe 914, Phe 1009, Glu 802, Glu 1261, Gln 767, and Arg 880, all of which are universally conserved. The crystal structure of the xanthine dehydrogenase from *Rhodobacter capsulatus* illustrates the highly conserved architecture of the active site, providing a convenient system to conduct mutational studies. Due to the fact that the FAD and Fe/S-binding domains are found in a separate subunit from the mo-binding part of the enzyme, the numbering in the bacterial enzyme is as follows: Phe 344, Phe 459, Glu 232, Glu 730, Gln 197, and Arg 310 (Figure 1.8).

Based upon crystallographic data, substrates bind between the phenylalanines, which serve to orient the substrate for catalysis. Glutamate 1261 (730 in the bacterial enzyme), is oriented beneath the molybdenum center. Being within hydrogen bonding distance, this "bottom" glutamate is universally conserved and is required for activity (35,36). Arginine 880 and glutamate 802 (residues 310 and 232 in the bacterial enzyme, respectively), sit below and above the substrate, respectively. Structural and kinetic studies suggest that residues Arg 880 and Glu 802 play a role in substrate binding and orientation, as well as transition state stabilization (36,37,56).

Previous amino acid substitution studies of glutamate 232 in the recombinant *R. capsulatus* enzyme involved substitution of glutamate 232 to alanine (36). In steady state experiments the E232A variant exhibited a 25 -fold decrease in k_{cat} and there was a 12-fold decrease in k_{red} in rapid reaction studies observing the reductive half-reaction of the variant with xanthine. It is to note that similar kinetic characteristics were also seen in the steady state kinetics of E803V variant of the human enzyme (74). Based upon the variations in K_d and k_{cat}, initial conclusions were that glutamate 232 was involved with both substrate binding and transition state stabilization. In addition to the kinetic work, computational and structural analysis points towards glutamate 232/802 playing a role in the facilitation of proton tautomerization between N3 and N9 positions on hypoxanthine and xanthine over the course of catalysis (36,54,75,76).

In the structure of xanthine oxidase with the slow substrate FYX-051(77), the crystal structure exhibited what was likely a protonated glutamate 802/232. The likely protonation is also observed in crystal structures displaying “upside down” orientations of substrates in the active sites in which the C6 oxygen of the xanthine/uric acid is within hydrogen bonding distance of glutamate 802/232. These structures have led to the argument that glutamate 802/232 acts as a hydrogen bonding donor with the substrate. However, in order for glutamate 802/232 to facilitate in tautomerization, the residue must be deprotonated.

In order to further investigate the role of Glu 232 and the effect of its protonation, kinetic studies on the reductive half-reaction of E232Q variant of the recombinant *R. capsulatus* enzyme have been conducted. We find that the E232Q mutant exhibits a 12-

fold decrease in k_{red}, comparable to the effect that was observed in previously published kinetic studies of the E232A variant. This result is inconsistent with the argument that glutamate 802/232 acts as a hydrogen bonding donor to the substrate during catalysis, as glutamine also acts as a hydrogen bonding donor. The reductive half-reaction has also been conducted at several pH points to investigate the effects of pH on activity in comparison to previously published parameters.

3.2 Results and discussion

3.2.1 The reductive half-reaction of E232Q with xanthine

Structural evidence indicates that Glu 802/232 is within hydrogen-bonding distance of substrate and that it can act as either a hydrogen bonding acceptor (and play a role in tautomerization of hypoxanthine or xanthine), or hydrogen bonding donor (and form stabilizing interactions with the substrate) (FIGURE 3.1). Past mutational studies of the E232A XDH variant by Leimkühler et. al. have demonstrated a 25-fold decrease in k_{cat} and a 12-fold decrease in k_{red}, as compared to the wild-type enzyme (36). While the alanine variant allows for the investigation of the absence of the glutamate, it does not allow for insight into the role of protonation of the glutamate on catalysis. The current work has investigated the reductive half-reaction of the *R. capsulatus* E232Q xanthine dehydrogenase variant under identical conditions to the wild-type *R. capsulatus* xanthine dehydrogenase. If glutamate 232 were to act as a hydrogen bonding donor during catalysis, then the E232Q variant should still be able to hydrogen-bond with the substrate and it would be expected that there would be little change in activity; however, if Glu 232

is not protonated, a decrease in activity would be expected. At pH 7.8, 25°C conditions, the limiting rate of reduction, k_{red}, for the wild-type enzyme with xanthine was found to be 217 ± 13 s^{-1} and the apparent dissociation constant, K_d, was found to be 42.1 ± 10.0 μM. Both of these agree with the previously published results after taking into account the difference in the temperature of the kinetic assays. The E232Q variant exhibits a 12-fold decrease in k_{red} and a ~3 fold increase in K_d compared to wild-type. When compared to the published results of the E232A variant (which exhibited a 12-fold decrease in k_{red} and 12-fold increase in K_d compared to wild-type), both variants are seen to exhibit similar decreases in k_{red}, however K_d is affected less in the E232Q mutant. This suggests that protonation of glutamate 802/232 alters substrate binding and significantly alters catalysis and that the glutamate must be deprotonated to stabilize the transition state. This is consistent with the interpretation that glutamate 802/232 is in fact deprotonated and functions catalytically to facilitate tautomerization of the substrate in the course of catalysis (36,54,75,76).

A

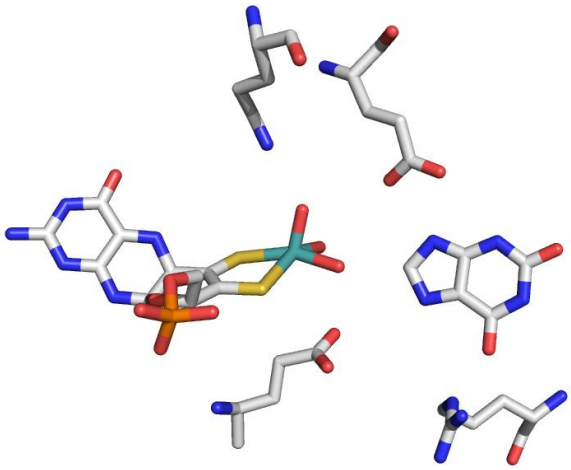

B

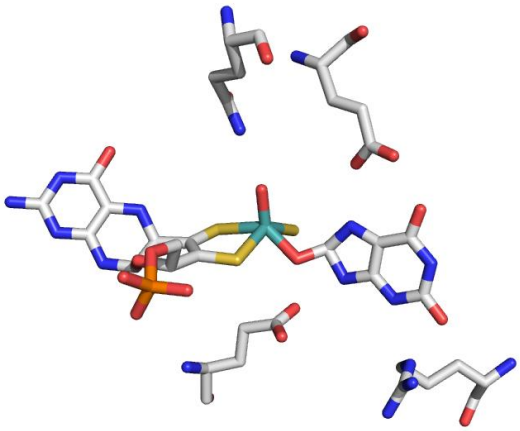

Figure 3.1 *Crystal structures of xanthine oxidase with substrate*. The x-ray crystal structures of (A) desulfo bovine xanthine oxidase with xanthine bound (PDB ID: 3EUB), where glutamate 802 is acting as a hydrogen bonding acceptor and (B) reduced bovine xanthine oxidase with urate bound (PDB ID: 3AMZ), with glutamate 802 acting as a hydrogen bonding donor.

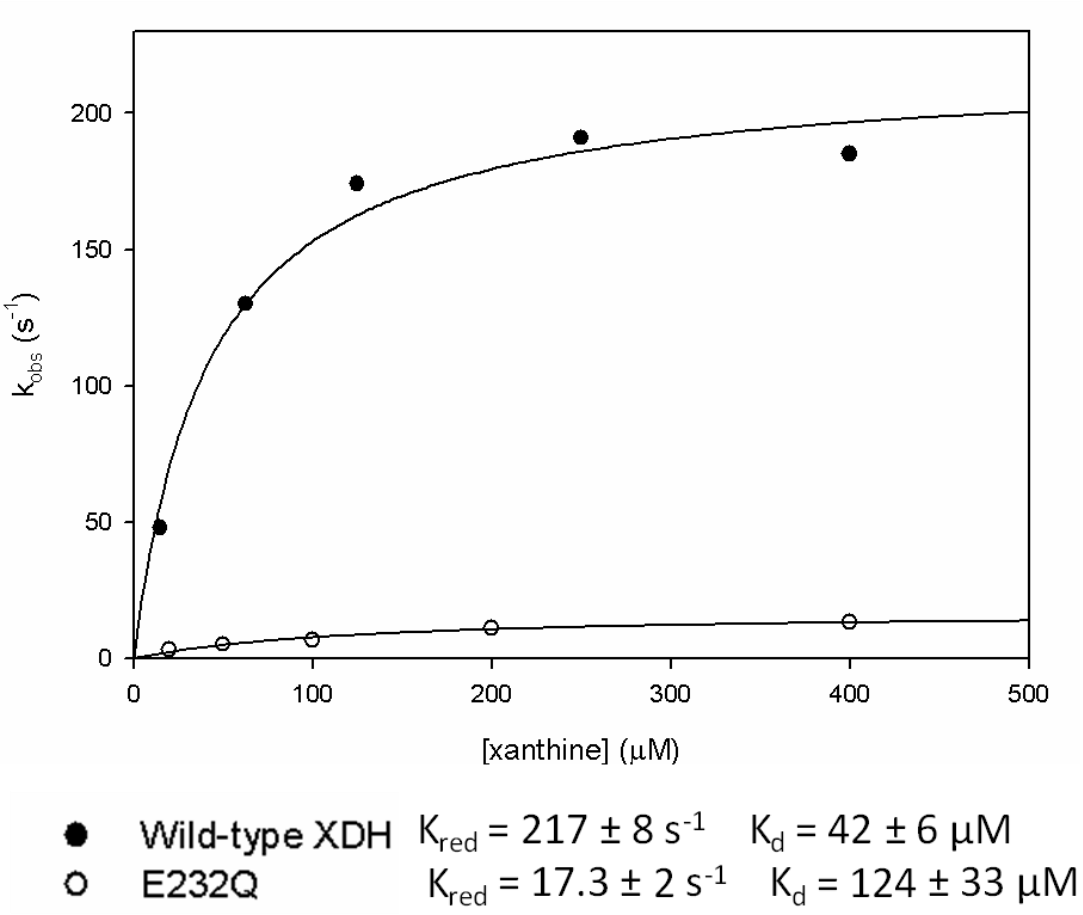

Figure 3.2 *Plots of observed rate constant k_{obs} versus [substrate] for the anaerobic reductive half-reaction of wild-type Rhodobacter capsulatus xanthine dehydrogenase and the E232Q variant with xanthine at pH 7.8, 25°C.*

.

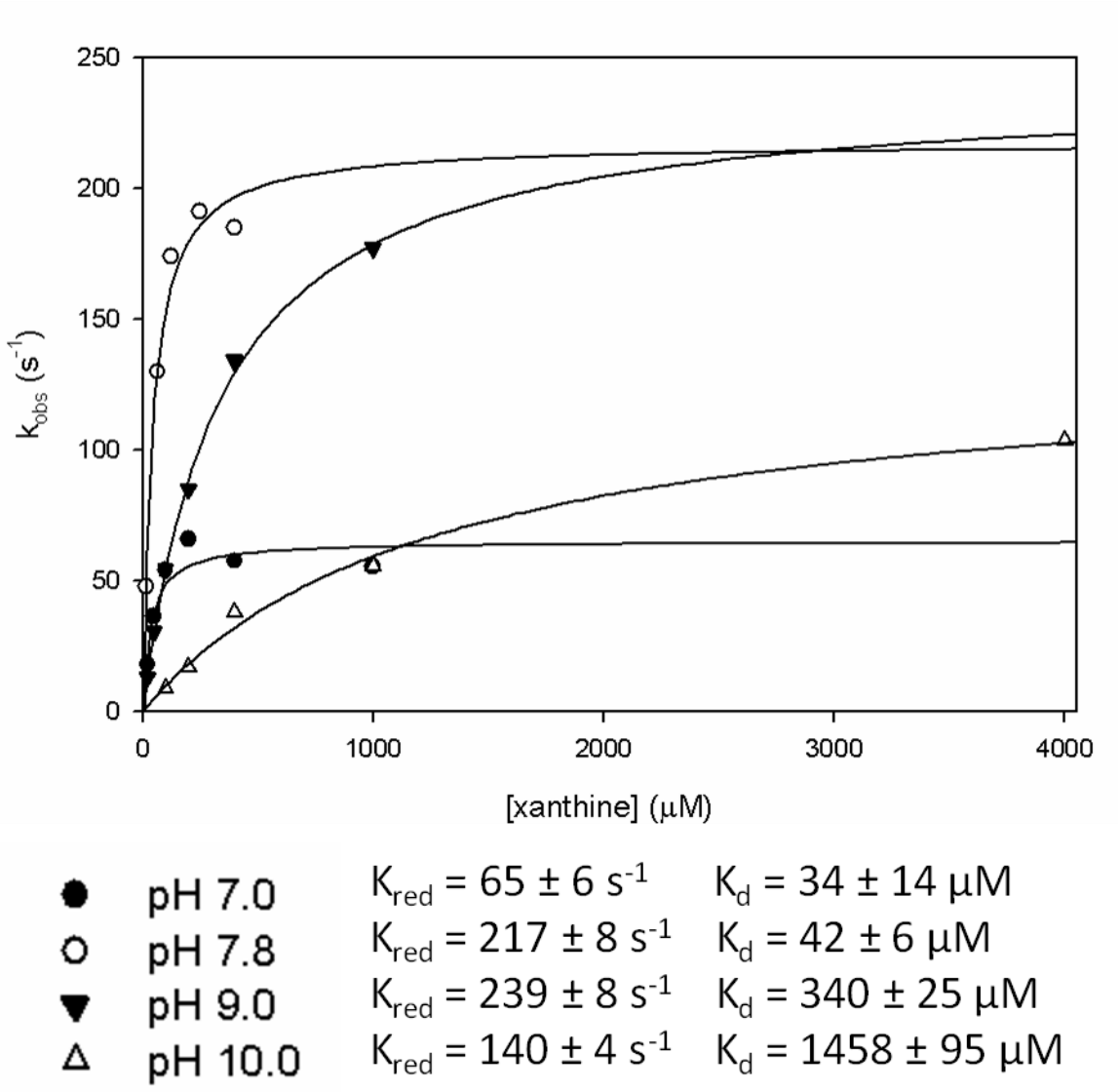

Figure 3.3 *Plots of observed rate constant k_{obs} versus [substrate] for the anaerobic reductive half-reaction of wild-type Rhodobacter capsulatus xanthine dehydrogenase at various pH values.*

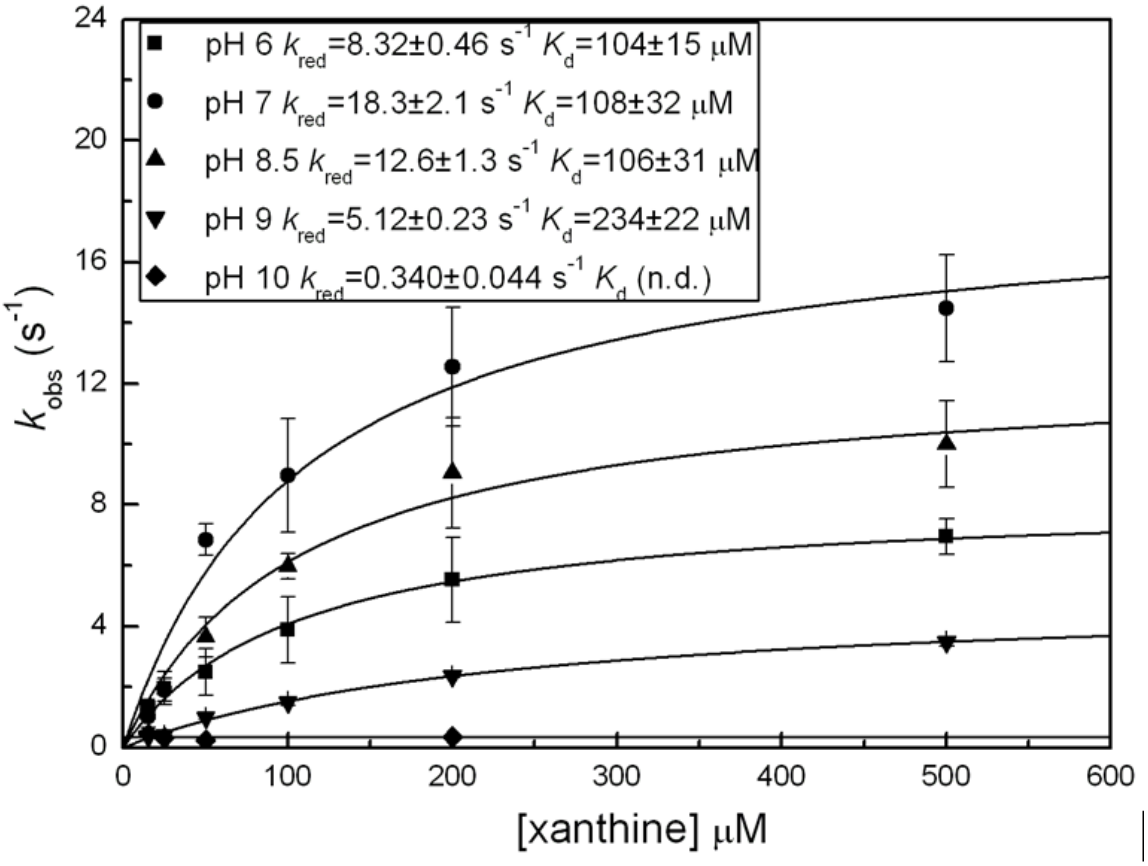

Figure 3.4 *Plots of observed rate constant k_{obs} versus [substrate] for the anaerobic reductive half-reaction of wild-type Rhodobacter capsulatus xanthine dehydrogenase and the E232Q variant with xanthine.*

Table 3.1 *Kinetic parameters for the reductive half-reactions of wild-type R. capsulatus xanthine dehydrogenase and the E232Q variant*

	Wild-type *R. capsulatus* XDH				E232Q *R. capsulatus* XDH		
pH	k_{red} (s^{-1})	*Kd* (μM)	k_{red}/K_d ($x10^6 M^{-1}s^{-1}$)		k_{red} (s^{-1})	*Kd* (μM)	k_{red}/K_d ($x10^6 M^{-1}s^{-1}$)
6.0					**8.3 ± 0.46**	**104 ± 15**	**0.080**
7.0	**65 ± 6**	**34 ± 14**	**1.9**		**18.3 ± 2.1**	**108 ± 32**	**0.17**
7.8	**217 ± 8**	**42 ± 6**	**5.16**		**17.3 ± 1.9**	**124 ± 33**	**0.14**
8.5					**12.6 ± 1.3**	**106 ± 31**	**0.12**
9.0	**239 ± 8**	**340 ± 25**	**0.70**		**5.12 ± 0.23**	**234 ± 22**	**0.022**
10.0	**140 ± 4**	**1458 ± 95**	**0.096**		**0.340 ± 0.044**	**N.D.**	

3.2.2 The pH profile of R. capsulatus xanthine dehydrogenase and the E232Q variant with xanthine

Previous pH dependence studies of bovine XO with the substrate xanthine have yielded bell-shaped curves of k_{red}/K_d versus pH corresponding to a double ionization model, with *pKa* values of 6.6, assigned to an active site base (protonation of the terminal sulfido ligand in the Mo^{VI} form or more recently attributed to protonation of Glu1261/730 (78)), and of 7.4, attributed to substrate. This suggests the active enzyme/substrate system must be in its intermediate (singly protonated) state for catalysis to occur (65). Similar *pKa* values of 6.3 and 7.7 were also reported for the pH dependence on k_{cat}/K_m of the bacterial enzyme (79). In both instances, maxima for the curves were at pH 7. While the bacterial XDH and bovine xanthine oxidase exhibit similar profiles for k_{cat}/k_m, the pH profiles for k_{red} and k_{red}/K_d do not precisely match. A plot of k_{red} versus pH for the wild-type bacterial XDH is bell-shaped curve, with rate constants roughly 10-fold greater than the bovine enzyme; while previously published curves for the pH dependence for k_{red} of bovine xanthine oxidase follow a sigmoidal curve (Figure 3.5). The plot for k_{red}/K_d versus pH for the wild type enzyme exhibits a bell-shaped curve, but it does not mimic that of the bovine enzyme. Assuming a double-ionization mechanism, curves can be fit using the equation $y = \frac{a}{1+\frac{[H^+]}{K1}+\frac{K2}{[H^+]}}$ where *a* is the theoretical maximum for k_{red} or k_{red}/K_d. The fit for the pH dependence of k_{red} for wild-type bacterial XDH gives pKa values of ~7.3 and ~10 for the ascending and descending limbs of the pH profile and a theoretical maximum value of ~270 s^{-1} (Figure 3.6).

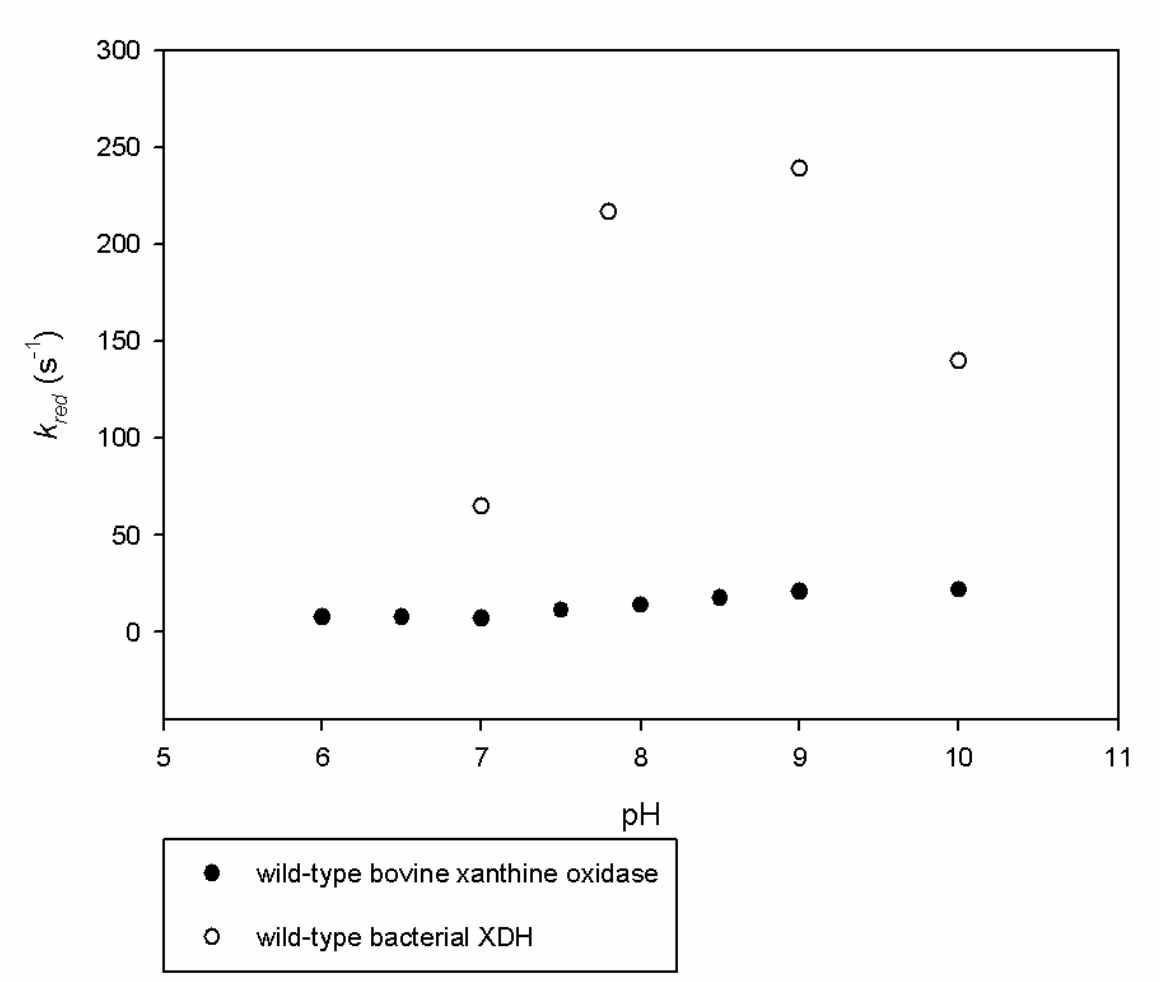

Figure 3.5 *Comparison of the pH-dependence of k_{red} for wild-type xanthine oxidase (white circles) and bovine xanthine oxidase (black circles) with xanthine.* The values for bovine enzyme were obtained from Kim *et al* (65).

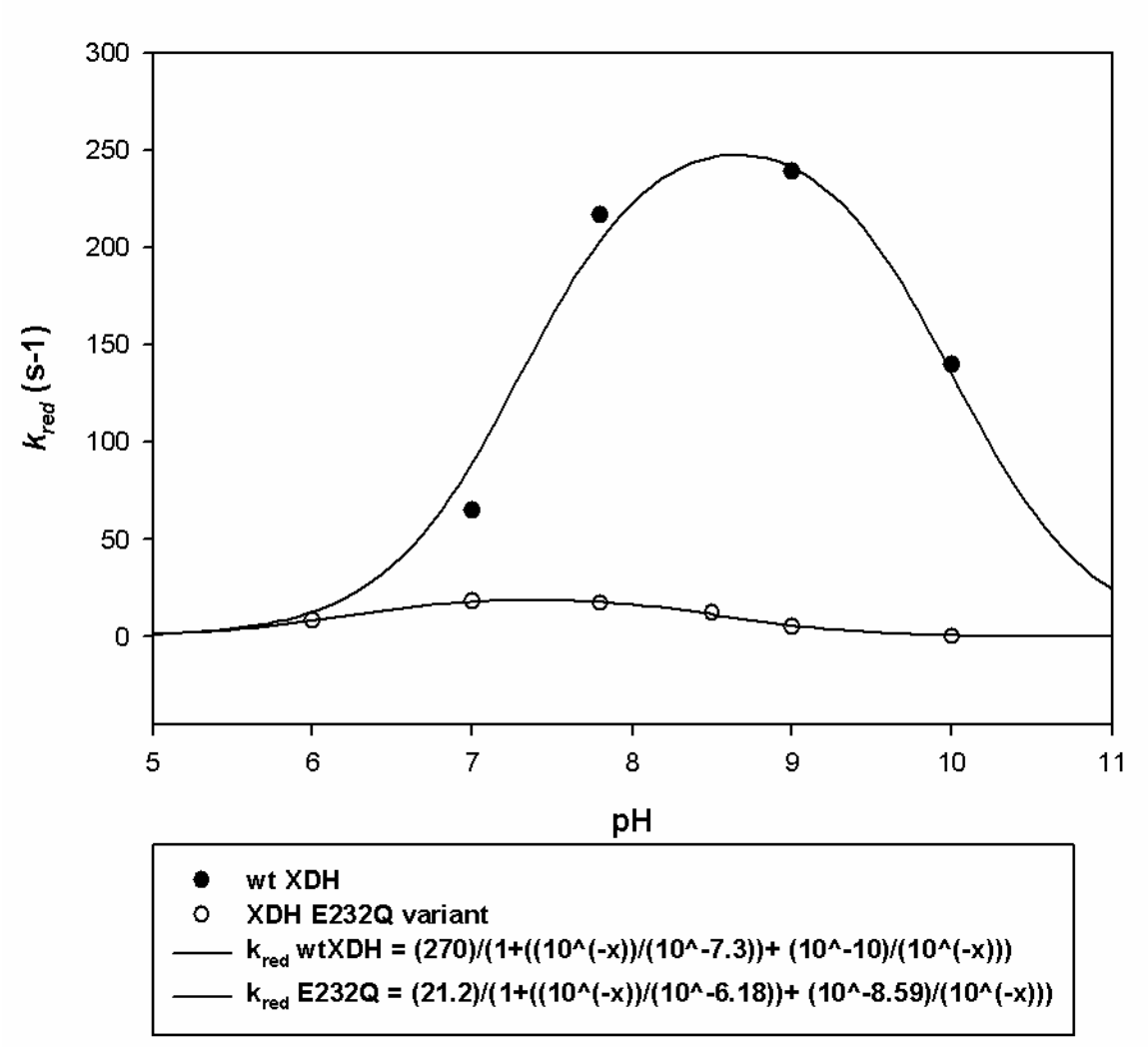

Figure 3.6 *The pH-dependence of k_{red} for wild-type xanthine dehydrogenase (black circles) and the E232Q variant (white circles) with xanthine.* The fit for the pH dependence of k_{red} for wild-type bacterial XDH gave pKa values of ~7.3 and ~10 and a theoretical maximum value of ~270 s^{-1}. The fit for the pH dependence of k_{red} for XDH E232Q variant gave pKa values of 6.18 and 8.59 and a theoretical maximum value of 21.2 s^{-1}.

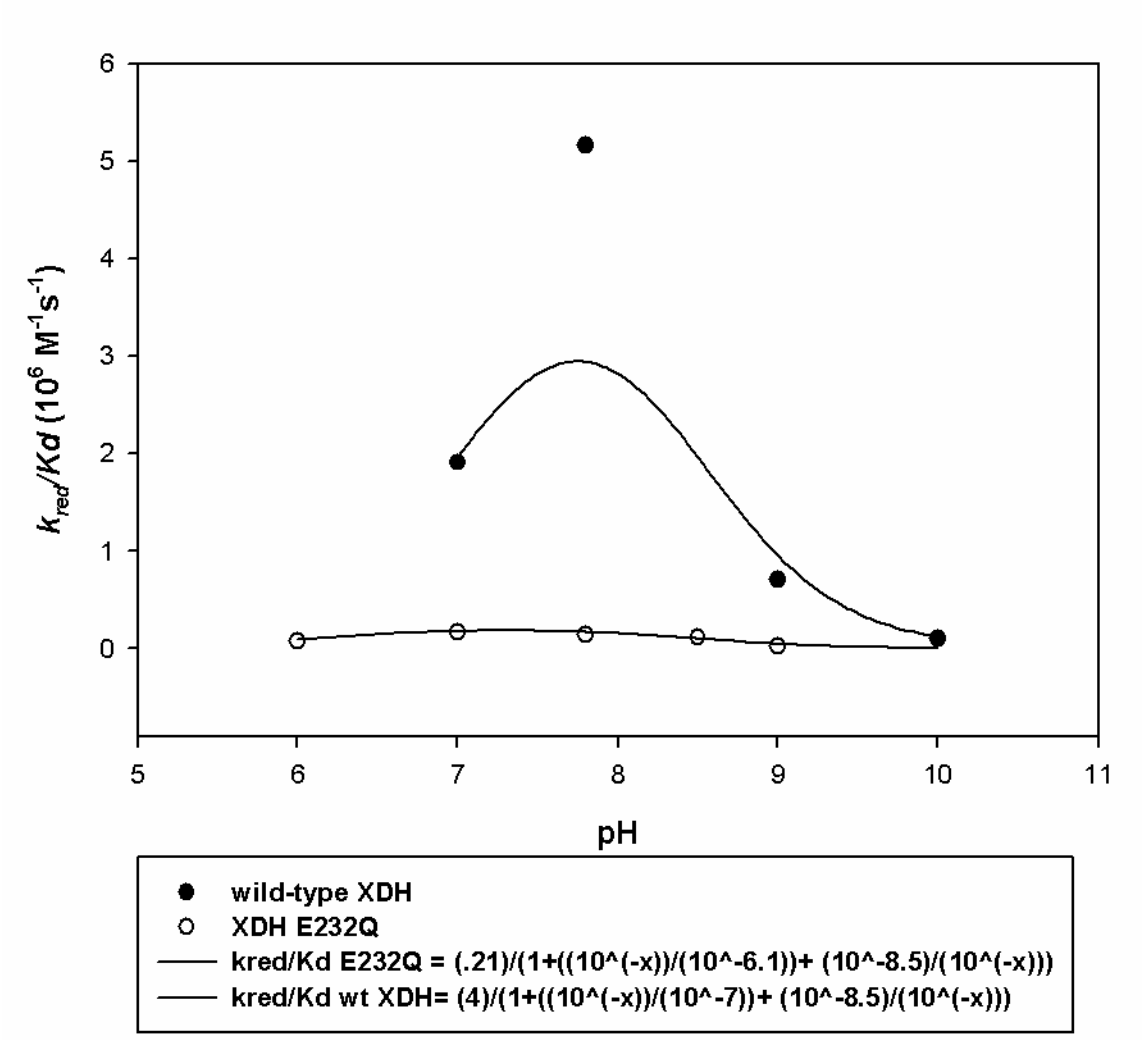

Figure 3.7 *The pH-dependence of k_{red}/K_d for wild-type xanthine dehydroganase (black circles) and the E232Q variant (white circles) with xanthine.* The fit for the pH dependence of k_{red}/K_d for wild-type bacterial XDH gave *pKa* values of ~7 and ~8.5 and a theoretical maximum value of ~4 x 10^6 $M^{-1}s^{-1}$. The fit for the pH dependence of k_{red}/K_d for XDH E232Q variant gave *pKa* values of 6.1 and 8.5 and a theoretical maximum value of 0.21 x 10^6 $M^{-1}s^{-1}$. It is to be noted that due to the two *pK*'s values for k_{red}/K_d for wild-type bacterial XDH being close to each other, the theoretical maximum is significantly underestimated.

Taking advantage of the ability of glutamine to act as a hydrogen bonding donor without becoming deprotonated, the pH profile of the E232Q mutant has been investigated. In the case of the bacterial E232Q variant, the pH profile observed for k_{red} is bell-shaped and does not exhibit significant activity above pH 9.0, unlike the wild-type bacterial XDH (which had significant activity observed up to pH 10.0) (Figure 3.6). The pH dependence on k_{red}/K_d also exhibited bell-shaped curve with *pKa* values of 6.1 and 8.6 (Figure 3.7).

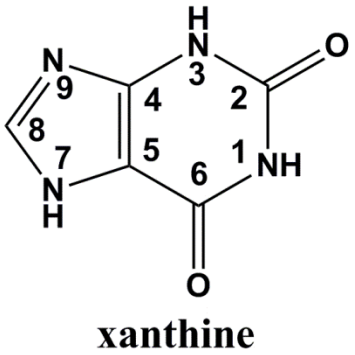

Figure 3.8 *The numbering scheme of xanthine*.

A possible explanation for the decrease in range for which k_{red} is finite in the E232Q variant is that it has lost specificity towards only the neutral form of xanthine. Previously published studies on wild-type bovine xanthine oxidase have demonstrated the requirement for neutral substrate for catalysis, consistent with a reaction mechanism involving proton abstraction from C-8, as the negative charge of the ionized substrate would be expected to significantly destabilize the accumulating negative charge on C-8 in the course of deprotonation (65). Xanthine has a pKa of 7.7 and at neutral pH it is found

in an equilibrium between neutral and monoanionic species (Figure 3.9), but is predominately the former (80). Deprotonation of xanthine typically occurs at N3(75,80), so based upon the orientation of xanthine in the crystal structure of wild-type xanthine oxidase from Pauff et al. (81), the negative charge of glutamate 802/232 would repel xanthine exhibiting a negative charge resonating between N3 and the C2 oxygen (Figure 3.10 B). Substitution of glutamate 232 to glutamine effectively permanently protonates the residue. In addition to the loss of ability of the residue to participate in tautomerization of substrate, the neutral polar group would also allow enzyme to bind both the neutral and negative forms of the substrate. Glutamine would be able to stabilize the binding of the monoanionic form of xanthine via its polar amide group, an interaction that could result in partial stabilization of the negative charge of the ionized substrate allowing the monoanionic xanthine to act as a competitive inhibitor against the population of neutral xanthine that can react with the enzyme (Figure 3.10 C/D).

The current data, do not rule out that the E232Q variant could accommodate more than one substrate orientation for the different substrate forms, a process which would be influenced by the pH. Ionization of xanthine to the monoanion could also be stabilized by the positively charged Arg 310, resulting in substrate binding in an inverted orientation so that the positively charged Arg 310 interacts electrostatically with the negative charge resonating on N3/O2 of xanthine while glutamine 232 would then form a hydrogen-bond with the C6 oxygen (Figure 3.10 E/F). In the wild-type enzyme, the negative charge on glutamate 232 could destabilize an interaction with the C6 oxygen making this binding mode unlikely under physiological conditions; however this

orientation has been observed crystallographically in the case of demolybdo rat xanthine oxidoreductase complexed with urate and the crystal structure of reduced bovine xanthine oxidoreductase with urate bound (82). In both cases, at neutral pH urate (which has a *pKa* values of 5.8 and 10.9 (83)) would be in monoanionic, accounting for the observed inverted orientation seen in Figure 3.1 B. The pH dependence of k_{red} for the E232Q variant (Figure 3.6) exhibits a bell-shaped curve that peaks at a maximum around a pH of 7.5. As the pH increases from pH 6.1 to 7.5 the rate of reduction also increases. Xanthine is predominantly in its neutral form and able to react with the enzyme if it is in its correct tautomeric state. As pH rises there is an increase in the population of deprotonated Glu 730 which acts as a general base to abstract the Mo-OH proton catalyzing the chemical step of the reaction to occur and thus promoting faster rates of reduction. As the *pKa* of xanthine is reached, increasing amounts of the monoanion accumulates. Based on the studies with bovine xanthine oxidase, the monoanionic form of the substrate is not acted upon by the wild-type bacterial enzyme because the negative charge on xanthine would repel the incoming nucleophilic attack by the Mo-OH (65). If the neutral form of the substrate is also the only form that can be acted upon by the E232Q enzyme, then as pH increases, the population of monoanionic xanthine increases and outcompetes the neutral form xanthine for binding to the enzyme, resulting in an expected loss of observed activity. This loss in activity is observed in the k_{red} of the E232Q mutant, however the wild-type XDH does not observe a loss in k_{red} until much higher pH as expected since the wild-type enzyme has the ability to discriminate between forms of the substrate and primarily binds the neutral substrate.

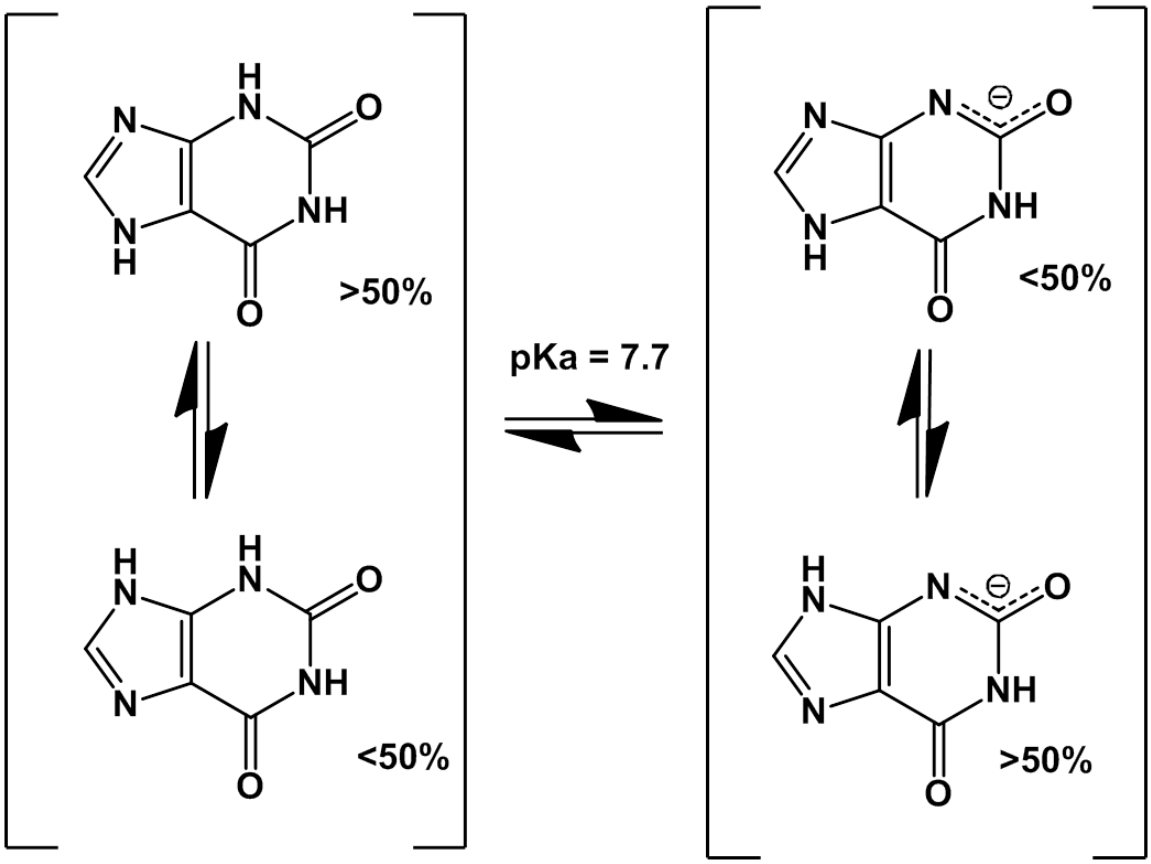

Figure 3.9 *Structures of the neutral and monoanionic forms of xanthine*

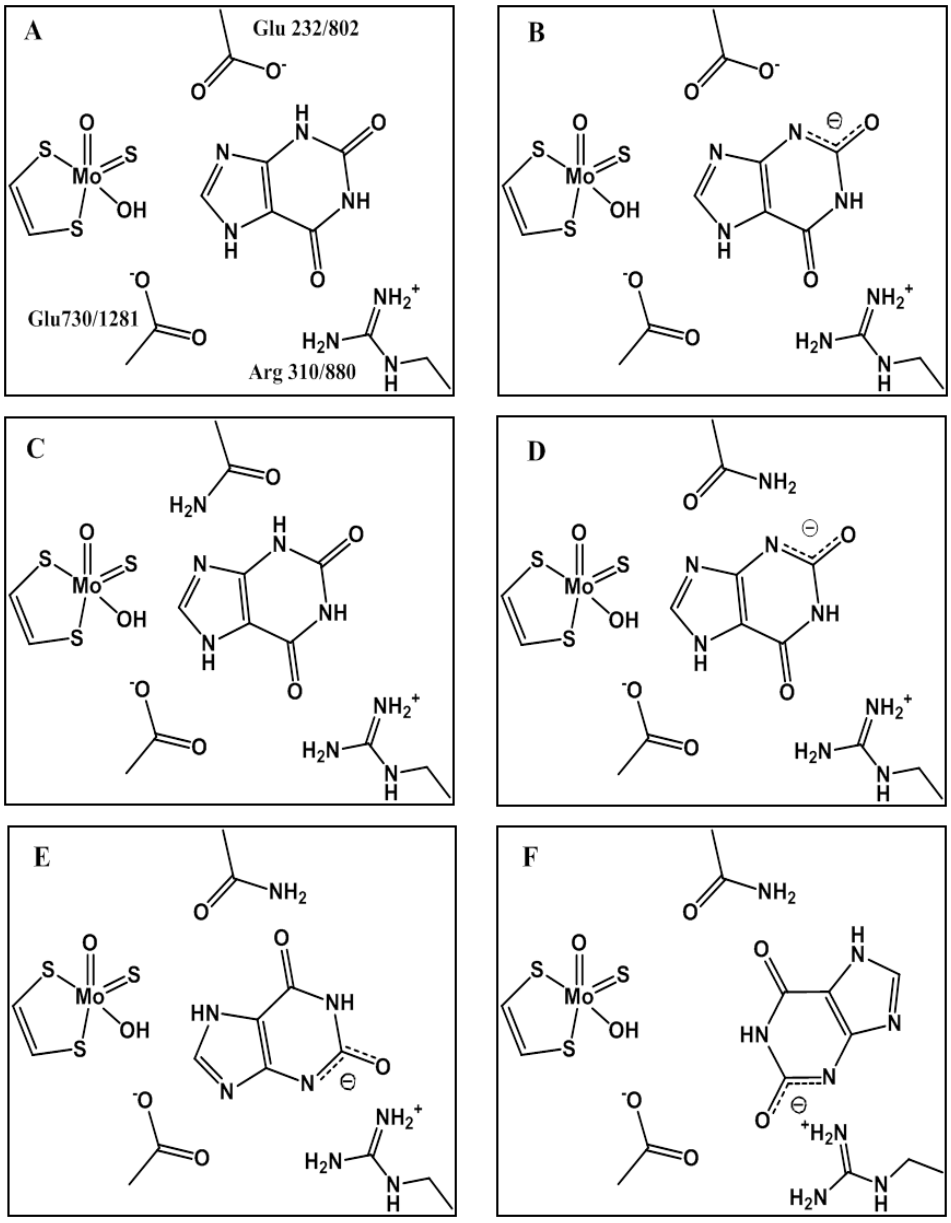

Figure 3.10 *Proposed orientations of xanthine binding in the active site of xanthine oxidoreductase.* (A) The "right-side" up conformation of xanthine oxidase with neutral xanthine, as seen in the crystal structure by Pauff et al. (PDB ID: 3EUB (81)). (B) A model of the "right-side" up conformation of xanthine oxidoreductase with monoanionic xanthine, an unlikely conformation based on the proximity of negative charge on enzyme and substrate. (C) The proposed "right-side" up conformation of the E232Q variant with neutral xanthine. (D) The proposed "right-side" up conformation of the E232Q variant with monoanionic xanthine. (E and F) Proposed "upside down" conformations of the E232Q variant with monoanionic xanthine

In summary, removal of the ionizable group of Glu 232 resulted in a shift in the observed pH profile of k_{red} and a decrease in k_{red} for the E232Q variant of *R.* capsulatus xanthine dehydrogenase. Given the drastic decrease in k_{red}, it is clear that Glu 232 is in fact deprotonated and functions catalytically to facilitate tautomerization of the substrate in the course of catalysis. In a solution containing multiple forms of xanthine, Glu 232 is suggested to play an essential role in substrate specificity and catalytic efficiency towards the neutral form of xanthine. The decrease in k_{red} as pH increased above pH 7.4 for the E232Q variant (which does not occur in the wild-type enzyme until above pH 8.5) suggests that the negative charge of Glu 232 allows discrimination against the binding of the monoanionic form of xanthine. The monoanionic form of xanthine is not acted upon by the wild-type enzyme because the negative charge of the ionized substrate would be expected to significantly destabilize the accumulating negative charge on C-8 in the course of deprotonation (65). In the E232Q variant, the monoanionic form of xanthine is not discriminated against and can then outcompete the neutral form of xanthine for binding in the active site. In the observed crystal of reduced bovine xanthine oxidoreductase with urate bound, the conditions allow the reverse reaction to occur in small quantities. Under these conditions to force a reaction with urate, the positive charge on Arg 310 likely interacts with the negative charge on the monoanionic form of urate, explaining the inverted binding orientation. The C6 oxygen of xanthine would be repelled by the negative charge on Glu 232, destabilizing the overall binding of monoanionic xanthine preventing catalysis from occurring.

CHAPTER 4

SUBTRATE ORIENTATION AND SPECIFICITY IN XANTHINE OXIDASE: Crystal Structures of the Enzyme in Complex with Indole-3-Acetaldehyde and Guanine – Implications for the roles of Glutamate 802/232 and Arginine 880/310

4.1 Introduction

While xanthine is the physiological substrate for xanthine oxidase, the enzyme can act upon a broad variety of heterocycles and aldehydes (39). The reductive half-reaction follows a mechanism where substrate is hydroxylated at specific sp^2 hybridized carbon centers. The reaction begins with Glutamate 1261 (Glu 730 in the *R. capsulatus* xanthine dehydrogenase) abstracting a proton from the equatorial molybdenum hydroxyl group, which allows the $Mo\text{-}O^-$ to make a nucleophilic attack on the substrate. Simultaneously, a hydride transfer occurs from the carbon to the Mo=S group. At this point, an intermediate is formed where the heterocycle is now coordinated to the molybdenum center by the newly incorporated hydroxyl group. This intermediate has been shown in the crystal structures in complex with two slow substrates, FYX-051 (77) and 2-hydroxyl-6-methylpurine (53). The reaction is completed with the displacement of product from the molybdenum center by solvent hydroxide, thus regenerating the equatorial molybdenum hydroxyl group.

As mentioned before, the active site is highly conserved among the xanthine-hydroxylating enzymes from various species, and Glu 1261(Glu 730 in the bacterial XDH) has been shown to be required for activity. Mutational studies of this residue to

alanine in the *R. capsulatus* XDH demonstrated a 10^7-fold decrease in the limiting rate of reduction by xanthine (36). Based upon the crystal structure, substrates wedge in between the phenylalanines 914 and 1009 (Phe 344 and Phe 459 in the *R. capsulatus* XDH), which together serve to orient the substrate perpendicular to the equatorial plane of the molybdenum center, allowing for simultaneous nucleophilic attack and hydride transfer. Arginine 880 (Arg 310 in the bacterial XDH) is only conserved in enzymes acting upon aromatic heterocycles, and is often a methionine in the otherwise closely related aldehyde-hydroxylating molybdenum-containing enzymes. Arginine 880, being located within hydrogen-bonding distance of the C6 oxygen on xanthine is proposed to carry a positive charge which acts to stabilize any charge accumulation on the C6 oxygen of xanthine during catalysis. As discussed in Chapter 3, we propose that Arg 880/310 acts in concert with glutamate 802 (Glu 232 in the bacterial XDH) in order to provide specificity towards the neutral form of the substrate, thereby enhancing the efficiency in catalysis and broadening the pH range for which the enzyme maintains activity.

Previous studies have shown that some substrates such as hypoxanthine (54) and allopurinol (unpublished) can occupy multiple orientations of which only one can be acted upon by the enzyme. In Chapter 3, the substrate ionization state and orientations in the active site were proposed to influence reactivity and catalytic efficiency. In this chapter, the crystal structures of xanthine oxidase in complex with the poor substrate indole-3-aldehyde and the non-substrate guanine provide new insight into how the active site residues of xanthine oxidase can determine catalytic efficiency and discriminate

against substrates such as guanine, which if hydroxylated would produce the highly mutagenic 8-hydroxyguanine causing problems for the cell.

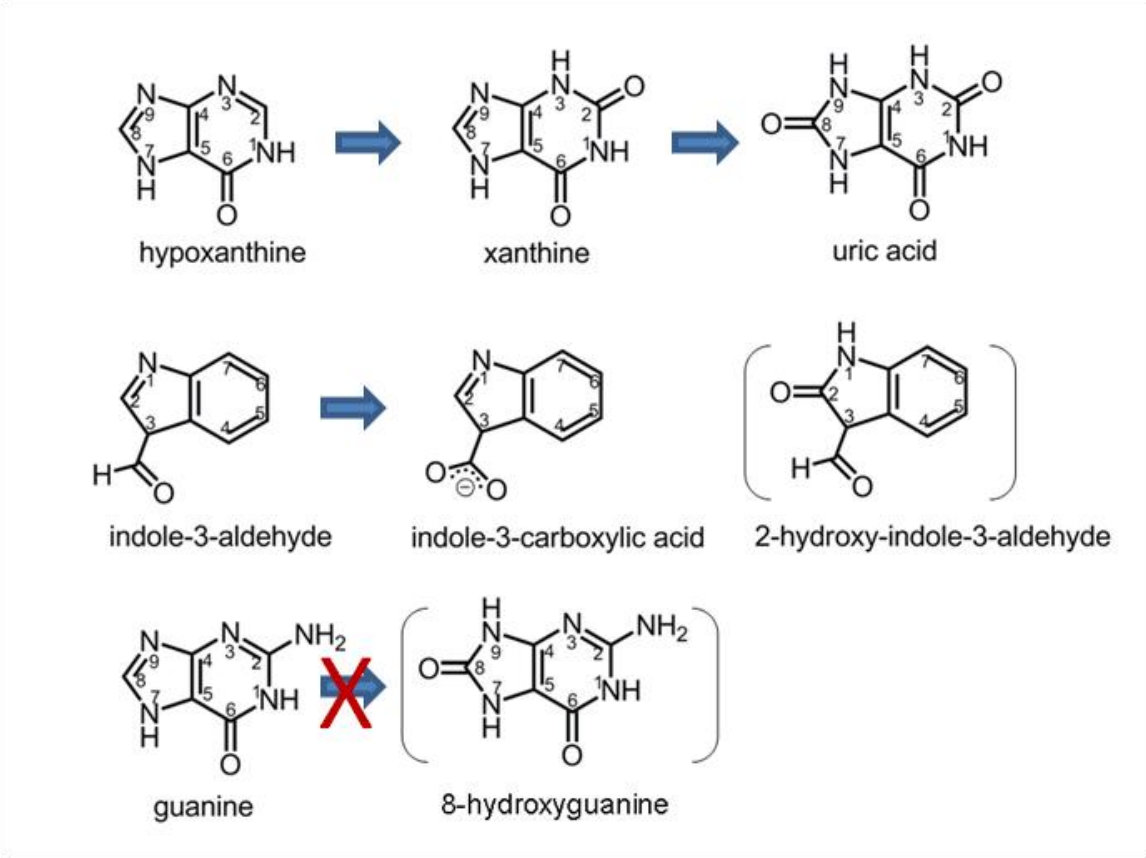

Figure 4.1 *The chemical structures and numbering scheme of compounds used in the present work.* The top row shows the chemical structures and numbering scheme for the physiological reaction with hypoxanthine to xanthine to uric acid. The second row depicts indole-3-aldehyde and the hydroxylation product indole-3-carboxylic acid. The third row depicts the non substrate guanine and its proposed hydroxylation product 8-hydroxyguanine. The hydroxylation products that are not observed to be produced are shown in brackets.

4.2 Results and discussion

4.2.1 The reaction of indole-3-acetaldehyde with xanthine oxidase

Indole-3-acetaldehyde is the physiological substrate for aldehyde oxidase (AOX) III from *Arabidopsis thaliana* that converting it to indole-3-carboxylic acid, a plant hormone. Bovine xanthine oxidase can also act on indole-3-acetaldehyde, converting it to the corresponding carboxylic acid, but only slowly. Hydroxylation of indole-3-acetaldehyde occurs at the exocyclic aldehyde to produce indole-3-carboxylic acid. When looking at the highest occupied and lowest unoccupied molecular orbitals of substrate (Figure 4.2), the carbon position of the exocyclic aldehyde can accept a nucleophilic attack and donate a hydride (both are required for catalysis to occur) as compared to the C2 position (corresponding to the C8 on xanthine) which does not exhibit an overlap of the C2 hydrogen and a highest occupied molecular orbital that would allow a hydride transfer to occur.

The reaction was examined spectrophotometrically to determine if the reaction of bovine xanthine oxidase with indole-3-aldehyde actually produced indole-3-carboxylic acid. Figure 4.3 shows the UV/visible spectra of indole-3-acetaldehyde, authentic indole-3-carboxylic acid and the hydroxylation product of indole-3-acetaldehyde by the enzyme. The spectra are distinct with local maxima at 244 nm, 260 nm, and 300 nm for indole-3-acetaldehyde and 278 nm for indole-3-carboxylic acid. Comparison of the reaction product of xanthine oxidase with indole-3-aldehyde and the normalized spectrum of indole-3-carboxylic acid agree well, and we conclude that indole-3-aldehyde is being acted on by xanthine oxidase and the product is indole-3-carboxylic acid.

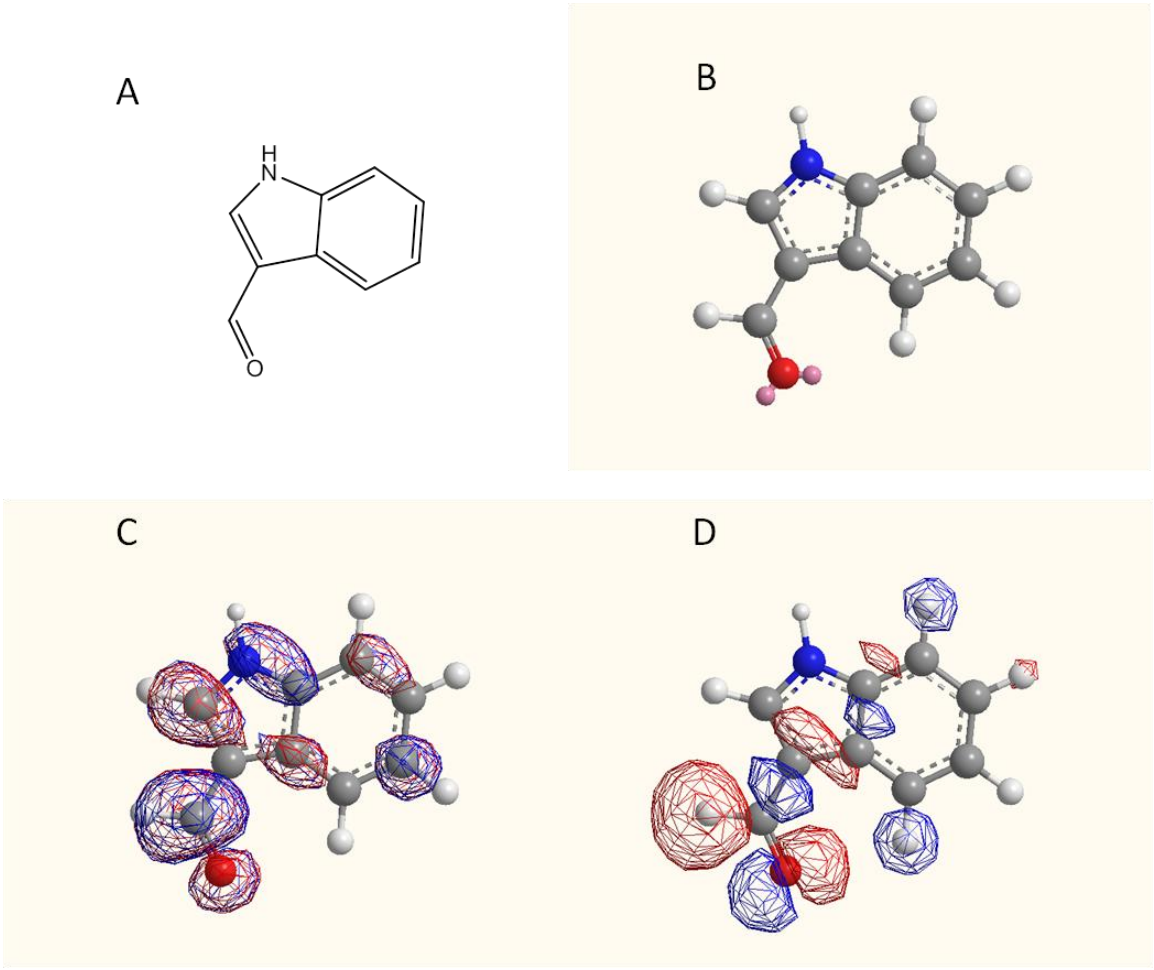

Figure 4.2 *Structure of indole-3-aldehyde and the highest occupied and lowest unoccupied molecular orbitals.* The structure of indole-3-aldehyde represented in lines (A) and ball and stick (B). (C) The lowest unoccupied molecular orbitals (LUMO) and (D) the highest occupied molecular orbitals (HOMO). Hydrogen atoms are represented in white, nitrogen atoms in blue, oxygen atoms in red, and carbon atoms in grey.

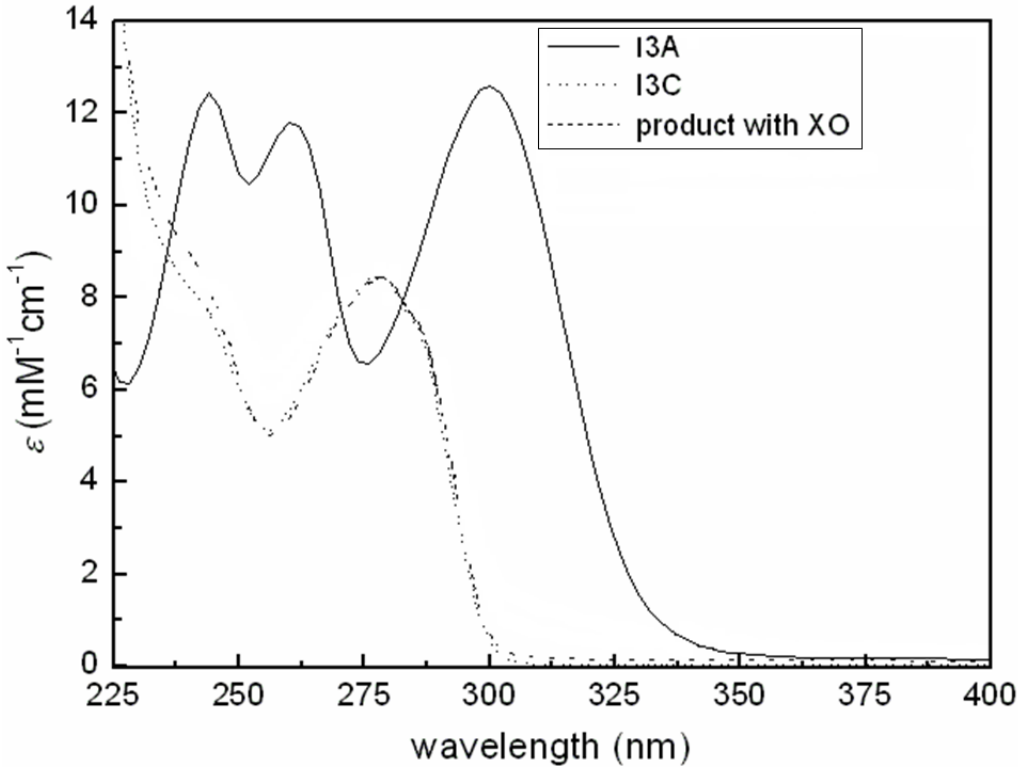

Figure 4.3 *The UV-visible absorption spectra of indole-3-acetaldehyde, indole-3-carboxylic acid and the hydroxylation products of indole-3-acetaldehyde by bovine xanthine oxidase*. Spectra shown are for indole-3-acetaldehyde, indole-3-carboxylic acid and the reaction product of indole-3-acetaldehyde with xanthine oxidase. The extinction coefficient of the reaction products are normalized at 278 nm where local maximum is observed for the characteristic UV-vis absorption spectrum of indole-3-carboxylic acid. For the reaction with bovine xanthine oxidase, 118 nM of enzyme was added prior to a one-day incubation and its absorption was subtracted as the baseline from that of the final reaction mix. Abbreviations used: XO, xanthine oxidase; XDH, xanthine dehydrogenase; WT, wild-type; I3A, indole-3-acetaldehyde; I3C, indole-3-carboxylic acid.

4.2.2 The reductive half-reaction of xanthine oxidase with indole-3-aldehyde.

Due to the low rate of reactivity of indole-3-aldehyde and the uncertainty of in the results of steady-state assays, analysis of the reductive half-reaction via stopped-flow spectroscopy was performed. The rate of reduction was followed by monitoring the loss in absorbance at 450nm corresponding to the reduction of the FAD and iron-sulfur clusters of XDH. The limiting rate of reduction, k_{red}, was found to be 0.13 s^{-1} with a K_d of 95 µM (Figure 4.4). Compared to the wild-type enzyme with xanthine (k_{red} = 18 s^{-1} K_d = 15 µM), the reaction with indole-3-aldehyde is less than 1% of the rate observed with xanthine as the substrate, however, the binding affinity only drops by a factor of six.

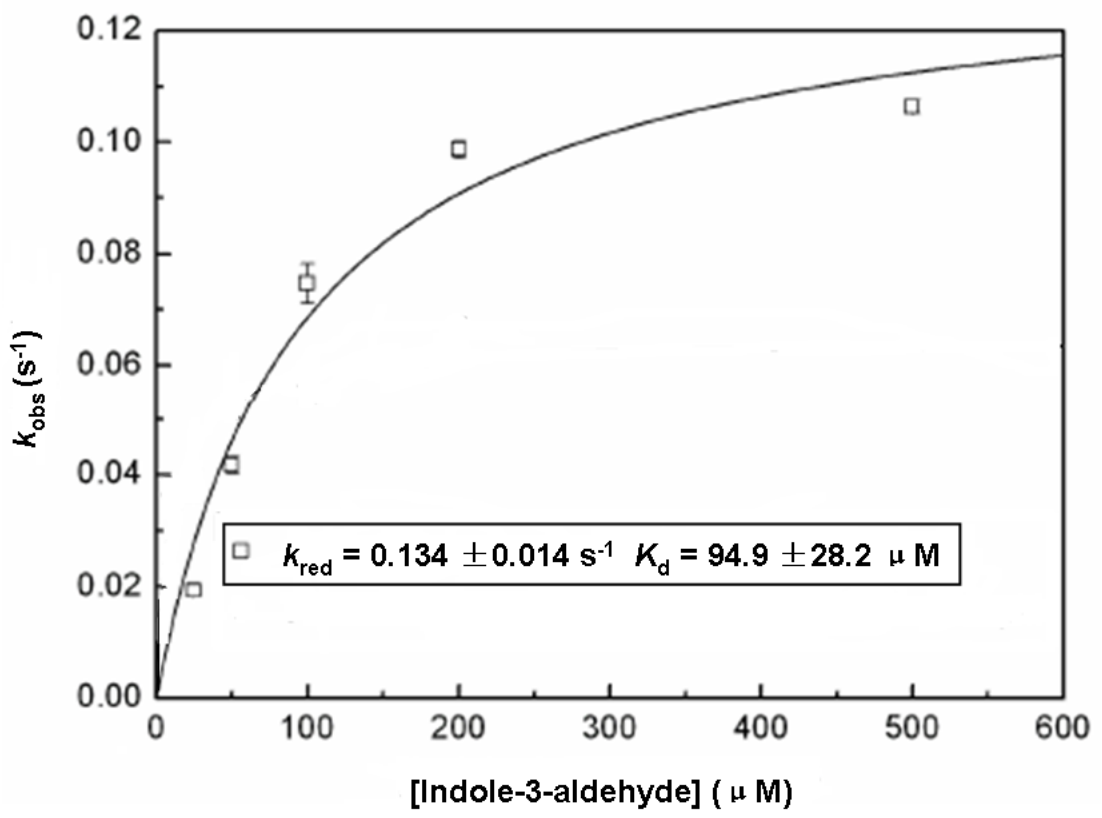

Figure 4.4 *Plot of k_{obs} vs. [indole-3-acetaldehyde] for the reaction with xanthine oxidase.* The reaction conditions were 0.1 M pyrophosphate buffer, 0.3 mM EDTA, pH 8.5, 25°C. The hyperbolic fit to the data indicated yields a k_{red} of 0.13 s^{-1} and K_d of 95 μM.

4.2.3 The crystal structure of bovine xanthine oxidase in complex with indole-3-aldehyde

The X-ray crystal structure of bovine xanthine oxidase in complex with indole-3-aldehyde was solved at a resolution of 1.6 Å using molecular replacement, using the previously published crystal structure of xanthine oxidase by Enroth et al (PDB ID: 1FIQ (27)) as the search model. The final R-factors obtained were an R_{cryst} of 21.5% and R_{free} of 24.6% (Table 4.1). The asymmetric unit contained a single homodimer of the enzyme and exhibited an overall structure that highly resembled that of the previously published structures (27,53,54,81). Figure 4.5 shows F_0-F_c and $2F_0$-F_c omit electron density maps for indole-3-acetaldehyde bound in each of the two active sites in the asymmetric unit, contoured at 3.0σ and 1.0σ, respectively. Each active site contains a single dominant orientation of indole-3-aldehyde found bound between the phenylalanine residues 914 and 1009 (Figure 4.6 B and D). The indole nitrogen makes hydrogen bonding interactions with glutamate 802 (2.78 and 2.86 Å in the two active sites, respectively) while the exocyclic aldehyde oxygen makes hydrogen bonding interactions with arginine 880 (2.89 and 3.15 Å to two of the guanidinium nitrogens in one active site, 2.99 and 3.36 Å in the other). The binding of the indole-3-aldehyde in each active site along with hydrogen bonding distances can be seen in Figure 4.6. The lack of bridging electron density between the equatorial molybdenum hydroxyl and the substrate indicates that catalysis has not progressed in either active site of the asymmetric unit, likely due to the observed low reactivity of the substrate with the enzyme.

Table 4.1 *Statistics for data collection and refinement of the crystal structures of xanthine oxidase in complex with indole-3-acetaldehyde and guanine*

Statistic	XO with indole-3-acetaldehyde	XO with guanine
Protein Data Bank code	3NVZ	3NVW
Space Group	$P2_1$	$P2_1$
Cell dimensions		
a, b, c (Å)	133.4, 73.7, 138.9	132.7, 73.4, 138.1
α, β, γ (°)	90.0, 97.1, 90.0	90.0, 97.0, 90.0
Resolution (Å)	45.2 – 1.6	131.7 – 1.6
Wavelength (Å)	0.9793	0.9793
Unique Reflections (test set)	339,741 (17094)	334,928 (16908)
Completeness % (highest resolution shell, Å)	96.5 (93.3)	96.6 (94.3)
I/s (highest resolution shell)	6.1 (2.2)	18.2 (2.4)
R_{cryst} (highest resolution shell)	21.5 (37.9)	18.4 (23.8)
R_{free} (highest resolution shell)	24.6 (44.3)	21.2 (26.8)
Ramachandran Statistics (%)	90.4, 9.0, 0.3, 0.3	90.0, 9.7, 0.1, 0.2
Mean coordinate error based on free *R* value (Å)	0.103	0.091
Mean coordinate error based on maximum likelihood (Å)	0.076	0.059
Rmsd bond length (Å)	0.011	0.008
Rmsd bond angles (°)	1.3	1.2
Average B value ($Å^2$)	21.6	18.0
Number of non-hydrogen atoms in refinement	20,672	21,495
Number of waters	1600	2173

Ramachandran statistics indicate the percentage of residues in the most favored, additionally allowed, generously allowed, and disallowed regions of the Ramachandran diagram as defined by the program PROCHECK (34). I/σ is defined as the ratio of the averaged value of the intensity to its standard deviation.

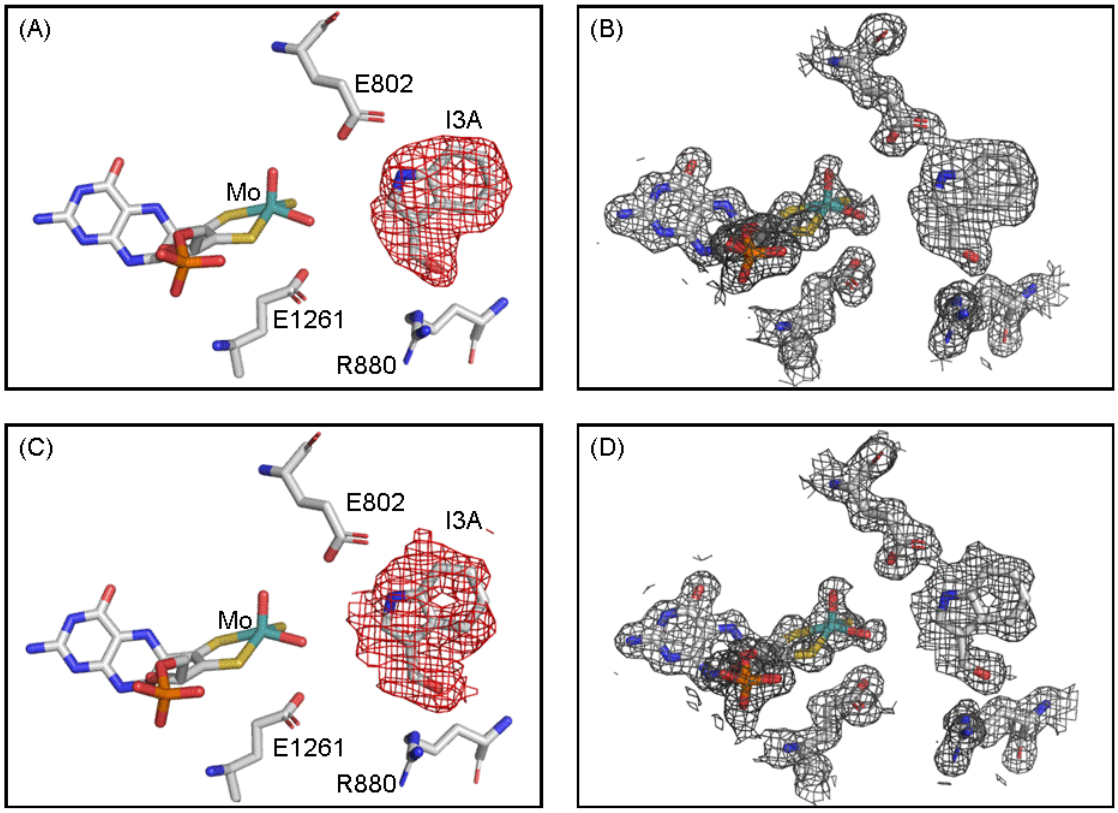

Figure 4.5 *Electron density maps of xanthine oxidase complexed with indole-3-acetaldehyde.* Both active sites of the asymmetric unit (A and B, and C and D, respectively) have the same single dominant orientation with C-2 proximal to molybdenum center. (A) and (C) show F_o - F_c omit maps contoured at 3.0σ, while (B) and (D) show $2F_o$ - F_c omit maps contoured at 1.0σ, all within 2.0 Å of all atoms shown. All omit maps were constructed prior to addition of indole-3-acetaldehyde in the refinement model, and subsequently overlaid with the final model. The atoms were color coded as follows, molybdenum is in cyan, carbon in white, nitrogen in blue, oxygen in red, sulfur in yellow, and phosphorus in orange. All structures were rendered with PyMol (64). Abbreviation used: I3A, indole-3-acetaldehyde.

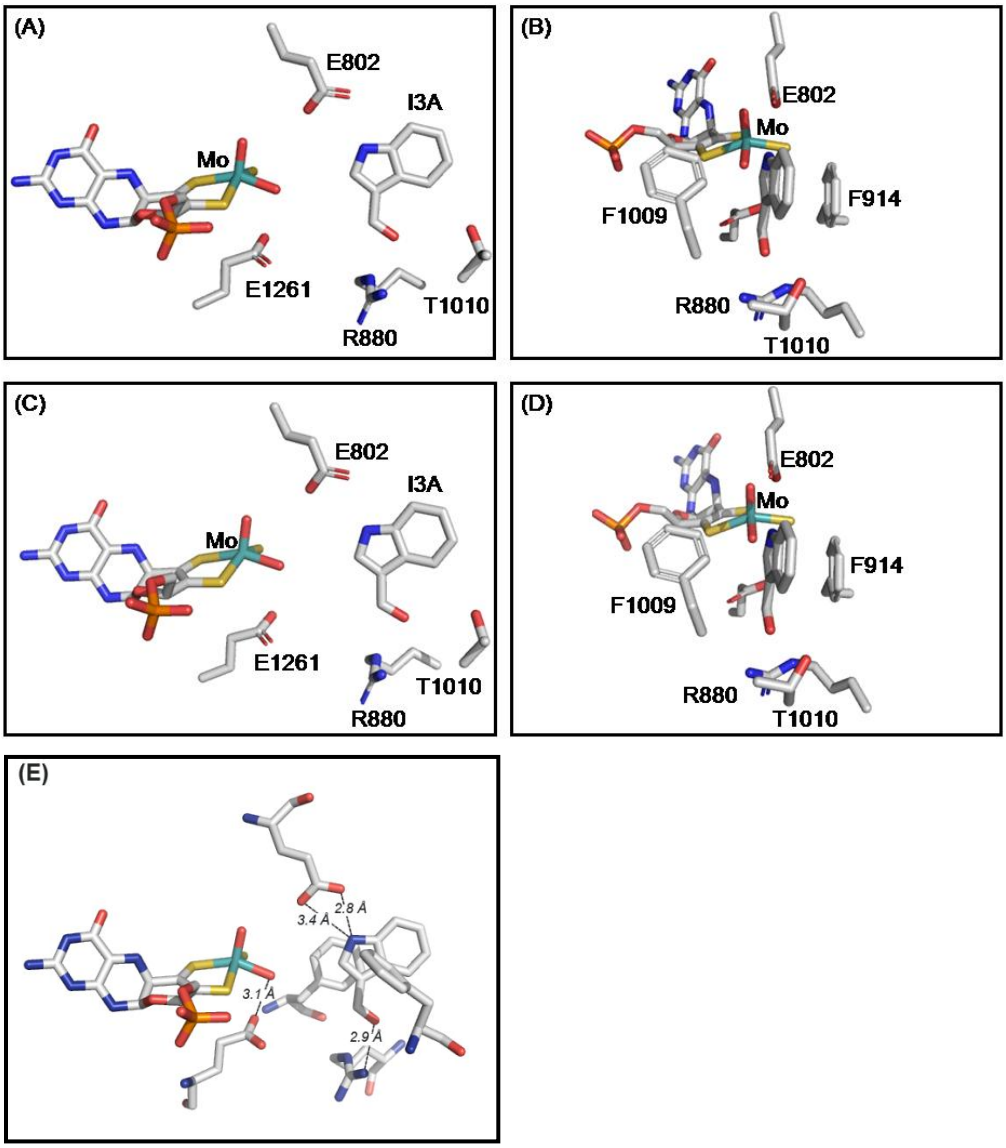

Figure 4.6 *Structures of xanthine oxidase complexed with indole-3-acetaldehyde.* (A) and (B) show one active site, while (C) and (D) show the other active site in the asymmetric unit. (B) and (D) are rotated approximately 90°C about the vertical from (A) and (C). Atoms are colored the same as described in Figure 3. (E), Indole-3-acetaldehyde bound in the active site with Phe 914 and 1009 shown, with the hydrogen bonding distances indicated. All structures were rendered with PyMol (64).

As observed in the crystal structure, the orientation of indole-3-aldehyde is not correctly positioned for hydroxylation of the exocyclic aldehyde, which is located 5.4 Å from the equatorial molybdenum hydroxyl group. This unfavorable orientation is primarily the result of arginine 880, which hydrogen bonds to the exocyclic aldehyde and pulls it away from the molybdenum center. In the aldehyde oxidases, the arginine is typically a methionine (16), which would not cause the substrate to bind in such a unfavorable, non-productive conformation. Previous reductive half-reaction studies have demonstrated that xanthine oxidase is indeed able to act upon indole-3-aldehyde, so in order for hydroxylation to occur the interaction with arginine 880 must be broken and the substrate must rotate approximately 30° in order to bring the exocyclic aldehyde within range of the molybdenum center for catalysis. This slight rotation in the active site does not appear to have any major steric restrictions in the active site and because the reaction with indole-3-aldehyde is observed experimentally, the energetics of the motion must be small compared to kT at room temperature.

` Multiple substrate orientations in xanthine oxidase have been characterized previously with hypoxanthine and 6-mercaptopurine (54). In each case, two orientations are observed, one being catalytically relevant and the other non-productive. In the case of hypoxanthine, the nonproductive orientation occurs when C2 is oriented away from the molybdenum center (C8 is oriented towards the center). This situation applies generally to any given substrate, where a distribution of substrate orientations can be expected, with each having a given intrinsic reactivity. This would result in the overall observed catalytic rate being a weighted average of the catalytic rates of the various substrate

orientations. The individual contributions of each rate would be based upon the fractional population of a given orientation and its intrinsic catalytic rate. Mathematically, this can be described by the equation $k_{red} = \Sigma_n (q_i * k_i)$ where k_{red} is the experimentally observed limiting rate of reduction, q is the fractional population of a given orientation i, and k_i is the intrinsic rate of catalysis for orientation i. The situation illustrates the principle of near attack conformations, in which thermally populated configurations of the Michaelis complex play an important role in facilitating the transition state and accelerating the rate of reaction (84-86). One extreme is that substrate can occupy a strictly nonproductive orientation having no contribution to the overall rate of enzyme reduction, resulting in a lower overall observed rate. Such an interpretation is consistent with the small but finite value seen for k_{red} with indole-3-acetaldehyde. Such an extreme has been observed in the case of hypoxanthine (54), where hypoxanthine can bind with the C8 position oriented towards the molybdenum center. This orientation has been shown to be nonproductive as the expected 6,8-dihydroxypurine product is not produced over the course of the reaction of hypoxanthine with xanthine oxidase (54).

4.2.4 The reductive half-reaction of wild-type R. capsulatus xanthine dehydrogenase and the R310M variant with xanthine, indole-3-aldehyde and benzaldehyde.

To further investigate the involvement of Arg 310 (Arg 880 in the bovine enzyme) in increasing the population of substrate in a nonproductive orientation, the reductive half-reactions of wild-type *R. capsulatus* xanthine dehydrogenase and an R310M variant were examined. In comparison of the wild-type enzyme and the R310M variant with xanthine, the limiting rate of reduction was less than 1% of the overall rate of the wild-type bacterial XDH, with the k_{red} for the R310M mutant being 0.11 s^{-1} and the k_{red} for the bacterial XDH being 217 s^{-1} (Figure 4.7). In the case of the indole-3-aldehyde as the substrate, the wild-type enzyme showed very little activity with a k_{red} <0.001s^{-1}, as compared to the R310M mutant which showed a higher activity, with a k_{red} of 0.0648 s^{-1} (Table 4.2). A similar trend was observed with benzaldehyde, a much faster reacting aldehyde substrate than the indole-3-aldehyde. k_{red} for the R310M variant was 47 s^{-1}, nearly double that of the wild type enzyme which had a k_{red} of 25 (Figure 4.8). Interestingly, in the case of the reaction with benzaldehyde as a substrate, the K_d for both the wild-type and the R310M were about the same (~14 mM). It is thus clear that Arg 310 plays a key role in specificity towards the binding of xanthine while also preventing efficient catalysis of aldehyde substrates. By removing the positively charged arginine and replacing it with a nonpolar residue, the enzyme loses specificity towards xanthine and abolishes the predominant nonproductive orientation observed in the crystal structure with indole-3-aldehyde. With fewer nonproductive substrate orientations in the R310M

variant, the overall observed k_{red} increases, as observed with the reductive half-reactions of both indole-3-aldehyde and benzaldehyde.

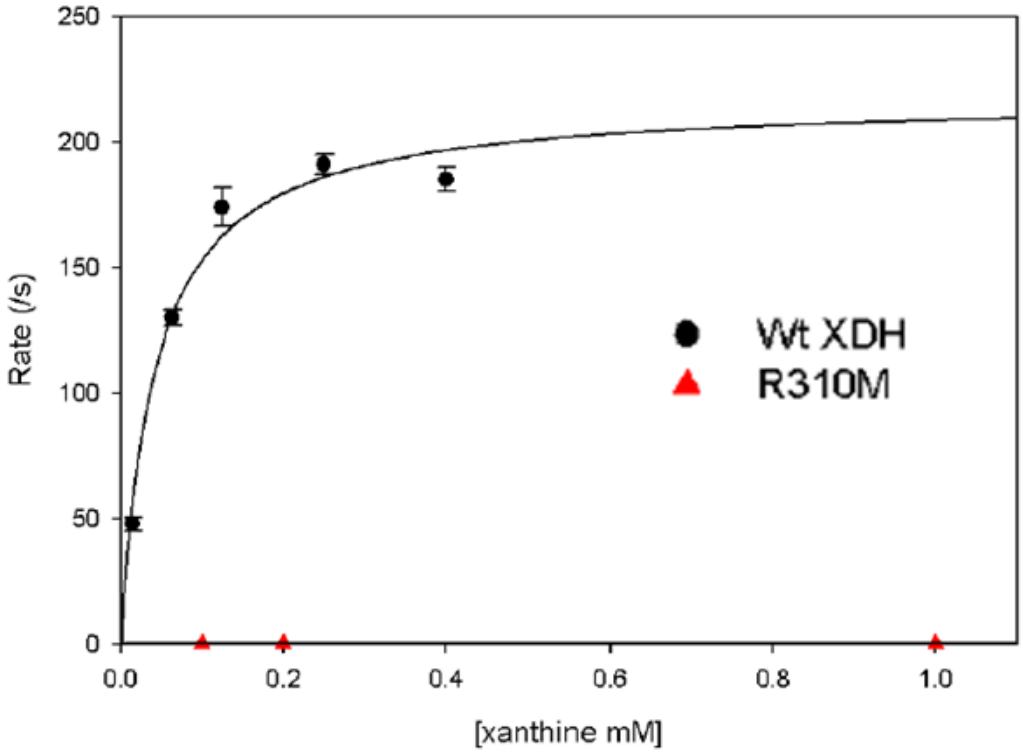

Figure 4.7 *Plot of k_{obs} vs. [xanthine] for the reductive half-reaction of R. capsulatus xanthine dehydrogenase and xanthine.* The reaction conditions were 50 mM potassium phosphate, 0.1 mM EDTA, pH 7.8, 25°C. The hyperbolic fit to the data for the wild-type enzyme (black circles) yields a k_{red} of 217 s^{-1} and K_d of 42 µM. The hyperbolic fit to the data for the R310M variant (red triangle) yields a k_{red} of 0.11 s^{-1} and K_d of 0.08 µM.

Table 4.2 *Kinetic parameters for the reductive half-reactions of wild-type R. capsulatus xanthine dehydrogenase and the R310M variant*

	Substrates					
	xanthine		indole-3-aldehyde		benzaldehyde	
Enzyme	k_{red} (s^{-1})	K_d (μM)	k_{red} (s^{-1})	K_d (μM)	k_{red} (s^{-1})	K_d (mM)
WT XDH	217 ± 13	42 ± 10	<0.001	N.D.	25 ± 1.1	14 ± 1.3
R310M	0.11 ± 0.03	0.08 ± 0.1	0.0648 ± 0.0054	11.3 ±4.4	47 ± 9.1	13 ± 5.6

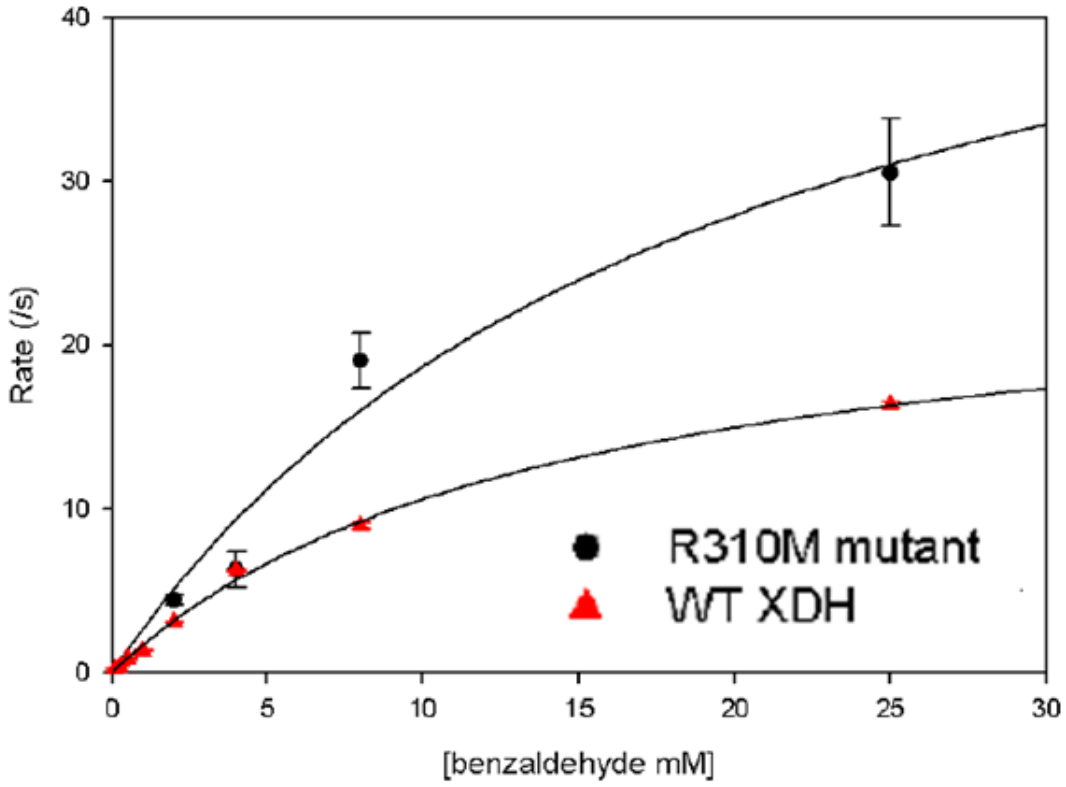

Figure 4.8 *Plot of k_{obs} vs. [benzaldehyde] for the reductive half-reaction of R. capsulatus xanthine dehydrogenase and xanthine.* The reaction conditions were 50 mM potassium phosphate, 0.1 mM EDTA, pH 7.8, 25°C. The hyperbolic fit to the data for the wild-type enzyme (red triangles) yields a k_{red} of 25 s^{-1} and K_d of 14 mM. The hyperbolic fit to the data for the R310M variant (black circles) yields a k_{red} of 47 s^{-1} and K_d of 13 mM.

4.2.5 The crystal structure of bovine xanthine oxidase in complex with guanine

The x-ray crystal structure of bovine xanthine oxidase in complex with guanine has also been solved at a resolution of 1.6 Å. The overall structure is very similar to those previously reported with all the differences limited to the active site. Table 4.1 gives a summary of the structural refinement parameters and Figure 4.9 shows both active sites of the asymmetric unit with the F_0-F_c and $2F_0$-F_c omit electron density maps for guanine bound in each of the two active sites in the asymmetric unit, contoured at 3.0σ and 1.0σ, respectively. The electron density shows a single dominant orientation for guanine bound which has the C2 amino group oriented towards the molybdenum center while the C8 position, that would be expected to be hydroxylated, is oriented away from the molybdenum center. In addition to the single orientation observed, no electron density appears to bridge between the molybdenum center and substrate that might suggest partial catalysis.

Just as in the case of the indole-3-aldehyde structure, guanine makes van der Waals contacts with the phenylalanines and is held in place by a network of hydrogen bonds. Glu 802 makes interactions with the C2 amino group and N3, and Arg 880 interacts with the C6 oxygen via hydrogen-bonding interactions. The equatorial molybdenum hydroxyl group is also close enough to make a hydrogen-bonding interaction with the C2 amino group. These interactions with their distances are shown in Figure 4.9 E. While the overall orientation resembles that seen with hypoxanthine (54) or allopurinol (unpublished) in which C2 is hydroxylated, guanine cannot be hydroxylated due to the amino group at the C2 position. This leaves C8 as the only site for which

hydroxylation can occur. While in the case of indole-3-aldehyde, a 30° rotation and disruption of just the interaction with Arg 880 is sufficient for the hydroxylation of substrate to occur (Figure 4.10), in the case of guanine a 180° rotation be necessary. A rotation of that magnitude would require the vast network of hydrogen bonds to be broken, and there is also significant steric hindrance with Glu 802 and Arg 880. Guanine would have to dissociate and re-associate with the protein in the correct orientation for C8 to be hydroxylated. The unfavorable binding of guanine is highly advantageous for the cell due to the fact that 8-hydroxyguanine is highly mutagenic. It is likely that the enzyme's active site has evolved in such a way to be able to preferentially bind guanine in a dominantly nonproductive manner in order to minimize the potential for production of 8-hydroxy purine.

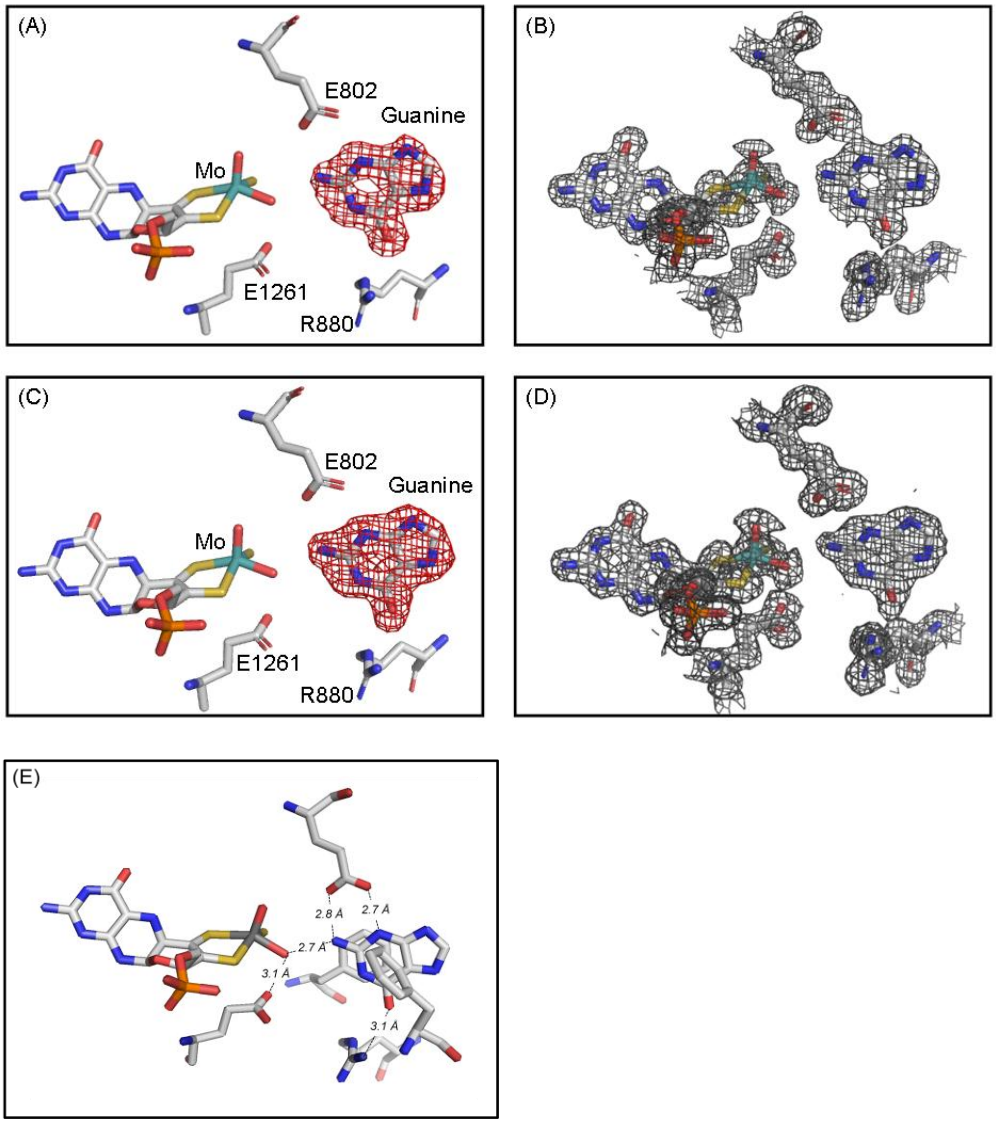

Figure 4.9 *The structures of xanthine oxidase complexed with guanine.* (A) and (B) show one active site, while (C) and (D) show the other active site in the asymmetric unit. (A) and (C) have F_o - F_c omit maps contoured at 3.0σ and (B) and (D) show $2F_o$ - F_c omit maps contoured at 1.0σ, all within 1.8 Å of all atoms shown. All the omit maps were constructed before the introduction of guanine for the refinement of the model and overlaid with the final model. Molybdenum is in teal, carbon in white, nitrogen in blue, oxygen in red, sulfur in yellow, and phosphorus in orange. (E), guanine bound in the active site with Phe 914 and 1009 shown, with the hydrogen bonding distances indicated. All structures were rendered with PyMol (64).

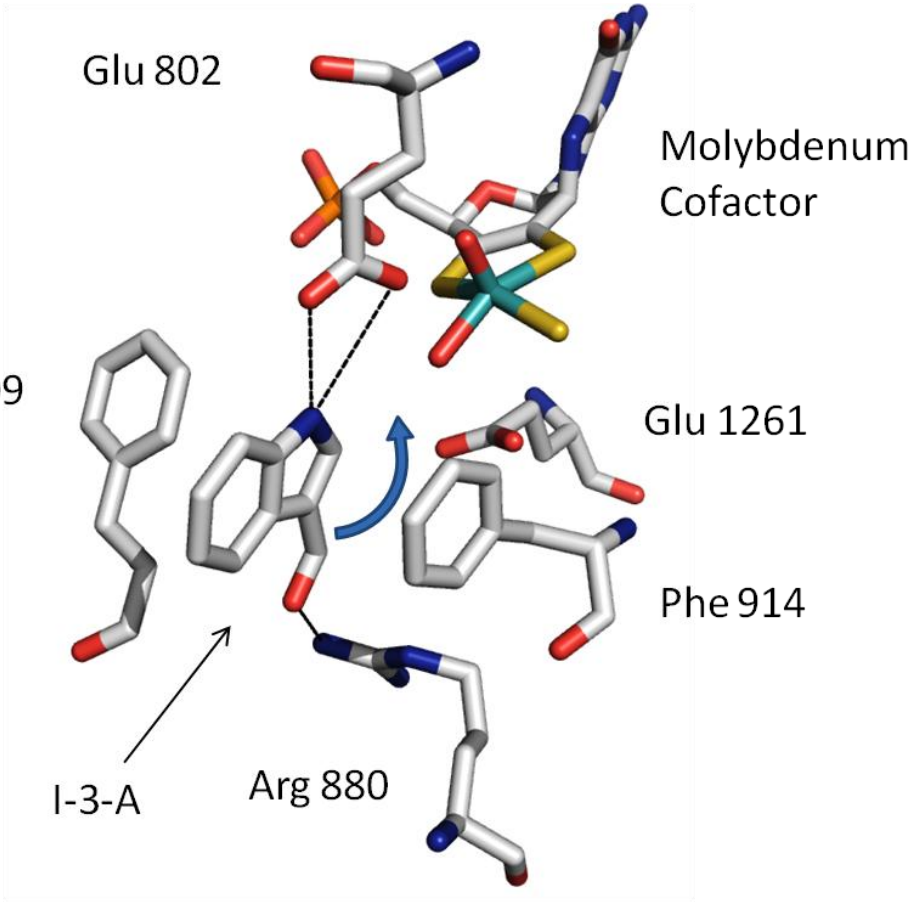

Figure 4.10 *The proposed motion of indole-3-acetaldehyde in order for catalysis to occur.* The proposed 30° motion of indole-3-aldehyde (abbreviated I-3-A) is indicated by the blue arrow. Hydrogen bonding interactions are indicated by black dashed lines. The amino acid residues are numbered for the bovine xanthine oxidase. The atoms are shown in CPK color scheme, with the molybdenum atom in cyan. Image was rendered in PyMol (64).

CHAPTER 5

KINETIC ISOTOPE EFFECT STUDIES ON BOVINE XANTHINE OXIDASE AND BACTERIAL XANTHINE DEHYDROGENASE

5.1 Introduction

As mentioned earlier, xanthine oxidase catalyzes the conversion of hypoxanthine to xanthine, and further catalyzes the conversion of xanthine to uric acid. The overall mechanism, shown in Figure 1.10, depicts the reaction with xanthine that has been well agreed upon in the literature (16). The reaction begins with glutamate 1261 (Glu 730 in the bacterial enzyme), abstracting a proton from the equatorial Mo-OH, which can then make a nucleophilic attack on the sp^2 hybridized center of the substrate to be hydroxylated. In the case of hypoxanthine, this is C2 and in the case of xanthine, it is C8. A simultaneous hydride transfer to the Mo=S group results in reduction of the molybdenum center from Mo^{VI} to Mo^{IV}. The intermediate thus formed has product coordinated to the molybdenum center via the catalytically introduced hydroxyl oxygen. The intermediate then breaks down by displacement of product by hydroxide from the solvent, and electron transfer out of the active site, readying the enzyme for another round of catalysis.

As shown in previous chapters of this thesis, the active site residues of xanthine oxidoreductase have evolved to provide specificity towards substrate, as seen in the reactions of indole-3-aldehyde and guanine (56). While the roles of specific active site residues have been explored using mutational studies in the *Rhodobacter capsulatus*

system (36,37), determination of why the limiting rates of reduction for the *R. capsulatus* xanthine dehydrogenase variants vary have not completely been described.

The rate of reduction in xanthine oxidoreductase is observed through following the spectroscopic loss in absorbance that accompanies the reduction of the flavin and iron-sulfur clusters of xanthine oxidoreductase. Given the constitution of redox-active centers, each independent enzymatic subunit requires three equivalents of substrate (six electrons) to be completely reduced (39). The reaction of xanthine can be broken down into two major steps consisting of the chemical step of the reaction (nucleophilic attack and hydride transfer) and product release. In the wild-type bovine enzyme, the rate-limiting step is the product release step (18) and is some 75-fold slower than the chemical step of the reaction (66). Amino acid substitutions of the active site residues can affect the two steps differently. Glu 197, while not being a residue involved in substrate binding, substitution of Glu 197 in the bacterial enzyme to alanine was shown to produce a 1.5-fold increase in k_{red} compared to wild-type and the Q197E variant showed a 4.6-fold decrease in rate compared to wild-type (Table 5.1) . It has also been previously documented that there is a significant difference between the rates observed in the bovine xanthine oxidase and the wild-type *R. capsulatus* xanthine dehydrogenase (51). The higher rate of catalysis found in the bacterial enzyme is assumed to be attributed to more rapid product release, but that has not been examined. In order to more specifically examine the reason for the differences in reduction rate of the wild-type bovine xanthine oxidase, wild-type *R. capsulatus* xanthine dehydrogenase, and the effect of mutagenesis on the chemical step of the reaction and product release of the *R. capsulatus* XDH

Q197A variant, kinetic isotope effect studies were performed to gain insight into the extent that the chemical step is rate-limiting.

Due to product release being the principal rate-limiting step of the reaction, the apparent primary kinetic isotopic effect on k_{cat} using xanthine deuterated at position 8 is small, with values for bovine xanthine oxidase of 1.1 and chicken liver xanthine dehydrogenase of 1.2 have been reported previously by D'Ardenne and Edmondson (66). Similar values were reported by Dr. Cao when studying the primary deuterium isotope effect on both bovine xanthine oxidase and bacterial dehydrogenase (Table 5.2,(87)). In order to determine the intrinsic isotope effect for the chemical step of the reaction, the tritium isotope effect on (V/K) must also be determined, which allows for the calculation of the intrinsic deuterium isotope effect (^{D}k) and the subsequent calculation of the extent that the chemical step is rate limiting. In this chapter we describe the tritium isotope effects and intrinsic deuterium isotope effects for bovine xanthine oxidase, bacterial xanthine dehydrogenase and the bacterial Q197A variant, in addition to the extent that the chemical step is rate-limiting in each.

Table 5.1 *Kinetic parameters for the reductive half-reaction of R. capsulatus xanthine dehydrogenase and variants with xanthine at pH 7.8, 25°C*

Enzyme	k_{red} (s^{-1})	K_d (μM)	k_{red}/K_d ($\mu M^{-1}\ s^{-1}$)
Wild-type	**217 ± 13**	**42.1 ± 10.0**	**5.15**
Q197E	**46.6 ± 2.6**	**34.2 ± 5.4**	**1.36**
Q197A	**328 ± 20**	**83.7 ± 11.3**	**3.92**
E232Q	**17 ± 1.9**	**124 ± 33**	**0.14**

Table 5.2 *Kinetic parameters for the steady state reactions of bovine xanthine oxidase, wild-type R. capsulatus xanthine dehydrogenase and the Q197A xanthine dehydrogenase variant with xanthine.*

Enzyme	$^{H/D}(V/K)$	$^{H/T}(V/K)$	^{D}k	$^{H/D}V$	fv
wt XDH	**2.12**[a]	**3.64**	**5.44**	**1.39**[a]	**0.087**
wtXO	**1.98**[a]	**3.62**	**7.01**	**1.1**[a]	**0.016**
XDH Q197A	**3.03**[a]	**6.00**	**6.15**	**3.03**[a]	**0.39**

[a] The values for $^{H/D}(V/K)$ and $^{H/D}V$ were previously reported by Dr. Cao (87).

5.2 Results and Discussion

Using the methods outlined in Section 2.3.3, steady-state kinetics for the various enzymes with xanthine were observed for both normal xanthine and deuterated xanthine. The primary deuterium isotope effects previously reported by Dr. Hongnan Cao were determined for bovine xanthine oxidase, the bacterial XDH and several bacterial XDH variants (Table 5.2) (87). The deuterium kinetic isotopic effect on k_{cat} was observed to be very small for the wild-type enzyme (1.39), and even smaller for the Q197E mutant (1.14), but larger for the Q197A mutant (2.23). The deuterium isotope effect on (*V/K*) for bovine xanthine oxidase, the bacterial XDH and the Q197A variant were 1.98, 2.12, and 3.03, respectively.

Using a modification of the method of D'Ardenne and Edmondson (66) detailed in Section 2.3.3, tritium isotope effect values were successfully determined for bovine xanthine oxidase, wild-type bacterial XDH and the Q197A variant (Table 5.2). The tritium isotope effect on (*V/K*) for bovine and the bacterial XDH were comparable (3.62 and 3.64, respectively). For the Q197A XDH variant, the tritium KIE on (*V/K*) was larger with a value of 6.00. The intrinsic isotope effects calculated for bovine XO, the bacterial wild-type XDH and the Q197A mutant were 7.01, 5.44, and 6.15 respectively. The intrinsic deuterium isotope effect value for bovine XO agrees fairly well with the previously published value of 7.4 (66). After calculating the fractional velocity (f_v) of the chemical step for each of the enzymes (refer to Section 2.3.3 for equations), the percentage of the overall k_{cat} that the chemical step of the reaction ($k_{C\text{-}H}$) comprised was calculated ($100f_v$). The inverse of f_v gave how much faster $k_{C\text{-}H}$ was compared to k_{cat}. It

was observed that for bovine XO that $k_{C\text{-}H}$ was ~62-fold faster than k_{cat}, for wild-type XDH that $k_{C\text{-}H}$ is ~11.5-fold faster than k_{cat}, and for the Q197A variant $k_{C\text{-}H}$ is ~2.6-fold faster than k_{cat}.

With the k_{cat} values for each enzyme (Table 5.3), the rate constant for the chemical step of the reaction for each of the enzymes could be estimated, yielding values of 930 s^{-1} and 802 s^{-1} for bovine xanthine oxidase and the bacterial xanthine dehydrogenase, respectively had similar rates. . When calculated using the equation $\frac{1}{k_{cat}} = \frac{1}{k_{C-H}} + \frac{1}{k_D}$, the estimated values for the rate of product dissociation (k_D) for the bovine and bacterial enzyme were found to be 15.2 s^{-1} and 76.9 s^{-1}, respectively. These results indicate that the increased rate of the bacterial enzyme is not due to a faster chemical step of the reaction, but to an increase in the rate of product release. With regard to the Q197A XDH variant, the increase in k_{cat}, as compared to the wild-type actually accompanied by a decrease in the rate constant for the chemical step, the higher k_{cat} value being due to an increase in the rate of product release, which is also supported by a k_D value of 263.2 s^{-1}. We note that replacing the glutamine with alanine creates a small pocket in the active site above the molybdenum center that could accommodate one or more water molecules, thus increasing the local concentration of water around the molybdenum center and in turn increasing the rate of product displacement from the molybdenum coordination sphere by hydroxide. The change in the rate constant for the chemical step of the reaction for the Q197A variant along with the observed decrease in k_{cat} of the Q197E variant suggest that the hydrogen-bonding interaction of Gln 197 with

the axial Mo=O directly modulates the reactivity of the molybdenum center, possibly by electrostatically facilitating its two-electron reduction in the course of electron transfer.

Table 5.3 *k_{cat} and the rate of the chemical step, k_{C-H}, of bovine xanthine oxidase, wild-type R. capsulatus xanthine dehydrogenase and the Q197A xanthine dehydrogenase variant with xanthine.*

	Comparative rates (Substrate: xanthine)		
Enzymes	k_{cat}	k_{C-H}	k_D
wt XO	**15 s^{-1}**	**930 s^{-1}**	**15.2 s^{-1}**
wt XDH	**69.7 s^{-1}**	**766 s^{-1}**	**76.9 s^{-1}**
XDH Q197A	**164 s^{-1}**	**426.4 s^{-1}**	**263.2 s^{-1}**

The tritium kinetic isotope effects for some of the bacterial XDH variants could not be reliably determined. The E730A variant of the bacterial XDH did not exhibit any detectable activity towards xanthine, for example, and so no kinetic isotope effects could be determined. Similarly, while the E232A and R310M variants exhibited finite reactivities towards the rates were still too slow to allow for reliable determination of fractional conversion via spectroscopic methods. For these variants, accumulation of uric acid and NADH was observed over the course of the reaction, as in the wild-type reaction. At a certain point in the reactions, consumption of NADH began to occur (loss in absorbance at 340nm) along with a decrease in uric acid (a decrease in absorbance at 295nm), which does not occur in the wild-type enzyme. This could be attributed to the reverse reaction of bacterial XDH with uric acid and NADH. Given the decrease in the limiting rate of reduction of the variants as compared the wild-type enzyme, the E232A and R310M XDH variants would exhibit a smaller difference between the rates of the forward and backward reactions, resulting in accumulation of uric acid and NADH until the concentration of xanthine falls, thus slowing the rate of the forward reaction allowing for the reverse reaction to occur much more quickly than the forward reaction. Eventually the two reactions would go back and forth until equilibrium between the forward and reverse reactions is reached, as seen in Figure 5.1.

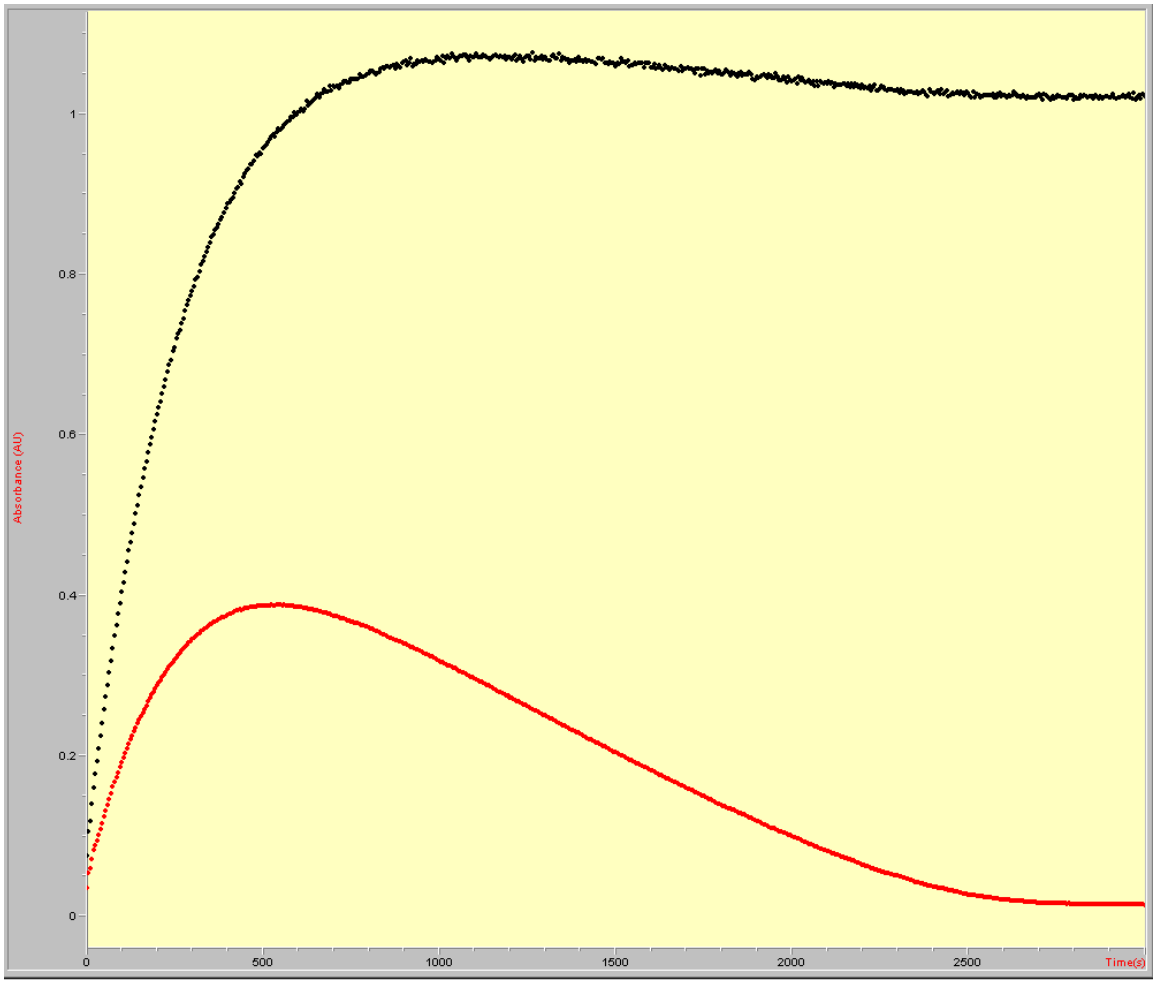

Figure 5.1 *The reaction of the R. capsulatus E232Avariant with xanthine and NAD*$^+$. The absorbance at 295 nm, associated with uric acid production (black dots), and the absorbance at 340 nm, associated with NADH production (red dots), are shown over a time course of 3000 seconds.

CHAPTER 6

MATURATION AND INSERTION OF THE MOLYBDENUM COFACTOR INTO THE XANTHINE OXIDASE FAMILY OF MOLYBDENUM-CONTAINING ENZYMES

6.1 Introduction

The manner in which prosthetic groups are incorporated into apoproteins has been of interest since the reports of the first two protein X-ray crystal structures of hemoglobin (88) and myoglobin (89), and the process by which metal centers are assembled and inserted in vivo remains an active area of research at the interface of biochemistry and chemical biology (40,90-93). The molybdenum-containing hydroxylases and related enzymes of the xanthine oxidase family constitute a large and broadly distributed group of enzymes that typically catalyze the oxidative hydroxylation of biologically important heterocycles and aldehydes(39). The X-ray crystal structures of several members of this family are known, including aldehyde oxidoreductase from *Desulfovibrio gigas* (17), mouse aldehyde oxidase 3 (26), bovine xanthine dehydrogenase (27), CO dehydrogenase from *Oligotropha carboxidovorans* (28,29), xanthine dehydrogenase from *Rhodobacter capsulatus* (30), quinoline-2-oxidoreductase from *Pseudomonas putida* (31), 4-hydroxybenzoyl-CoA reductase from *Thauera aromatica* (32,33), and nicotinate dehydrogenase from *Eubacterium barkeri* (34)(Figure 6.1). Although each has some distinctive variation in structural elements, all possess

significant sequence identities and profound structural homologies, particularly in the two domains that constitute the molybdenum-binding portion of the polypeptide.

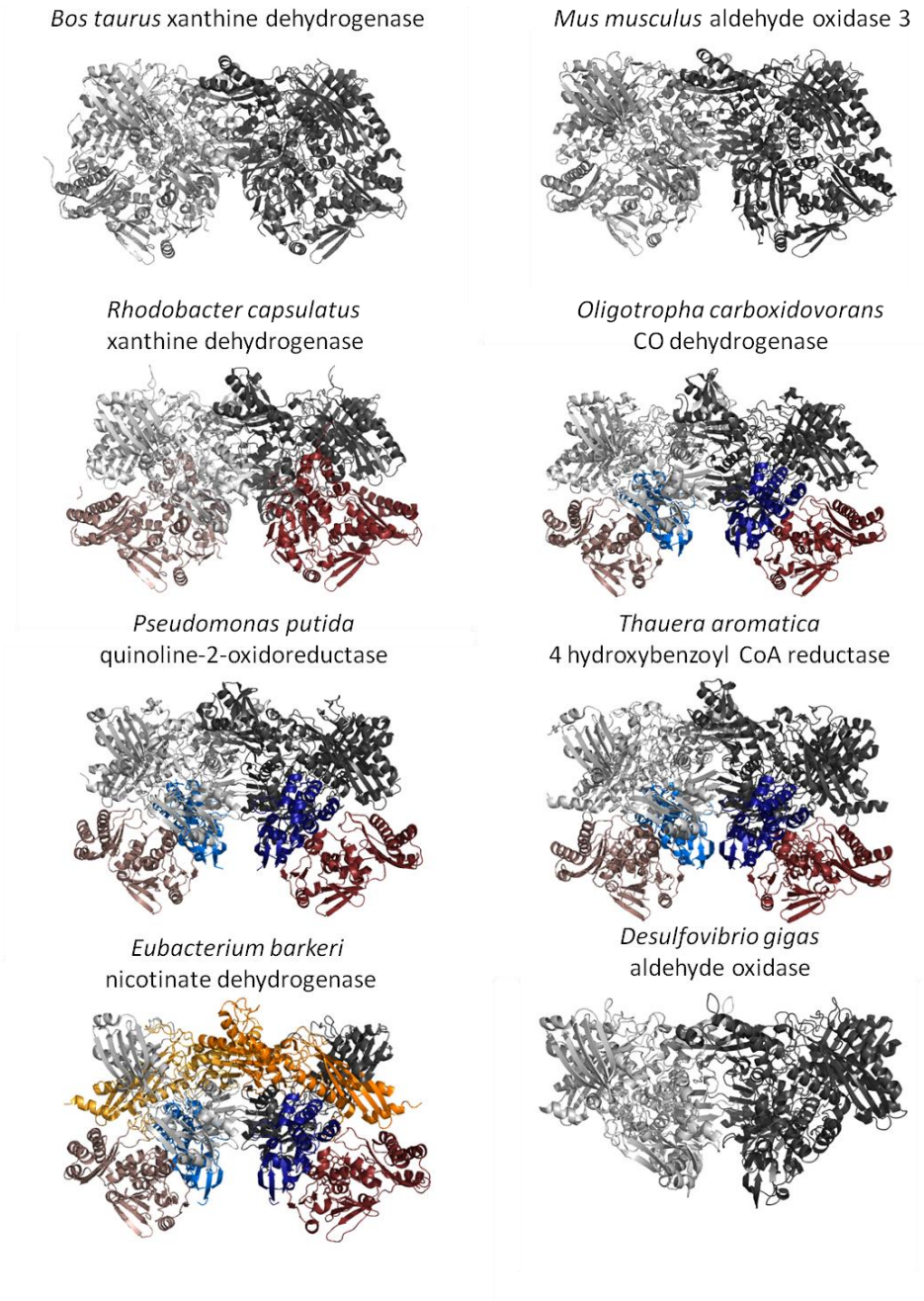

Figure 6.1 *X-ray crystal structures of several xanthine oxidase family members*. The structures in order above are: *Bos taurus* xanthine dehydrogenase (PDB ID: 1FO4), *Mus musculus* aldehyde oxidase 3 (PDB ID: 3ZYV), xanthine dehydrogenase from *Rhodobacter capsulatus* (PDB ID: 2W3S), carbon monoxide dehydrogenase from *Oligotropha carboxidovorans* (PDB ID: 1N5W), quinoline-2-oxidoreductase from *Pseudomonas putida* (PDB ID: 1T3Q), 4-hydroxybenzoyl-CoA reductase from *Thauera aromatica* (PDB ID:1SB3), nicotinate dehydrogenase from *Eubacterium barkeri* (PDB ID: 3HRD), and aldehyde oxidoreductase from *Desulfovibrio gigas* (PDB ID: 1VLD). The enzymes are shown in cartoon representation with each subunit in different colors and with different shades of the same color given to identical subunits within the holoenzymes.

In all molybdenum-containing enzymes other than nitrogenase, the molybdenum atom is coordinated to a pyranopterin cofactor. Biosynthesis of this cofactor has been extensively worked out for the three families of mononuclear molybdenum containing enzymes (39,40,93). For enzymes of the xanthine oxidase family, the final two steps of involve coordination of the metal to the pyranopterin and insertion of a catalytically essential sulfur into the molybdenum coordination sphere. Given the molybdenum center's sensitivity to oxidation and the fact that it is deeply buried (~15 Å from the protein surface) in the polypeptide, cofactor insertion is expected to be a complex process. While a number of proteins involved in the final steps of cofactor maturation and insertion into the xanthine oxidase family have been identified, it has been only recently that structural and mechanistic information has been obtained for some of these enzymes.

In *R. capsulatus*, the XdhC gene product has been shown to be specifically involved in binding the immature desulfo form of cofactor, facilitating its sulfuration by a specific sulfurase (NifS-4) and subsequently inserting the mature cofactor into the apo form of xanthine dehydrogenase (43-47,94). Genes homologous to *xdhC* have also found in gene clusters encoding a wide variety of confirmed and proposed enzymes of xanthine oxidase family, suggesting that XdhC-like proteins allow for targeting of the molybdenum cofactor to specific xanthine oxidase family enzymes (43).The sulfuration of the molybdenum cofactor involves replacement of a Mo=O group of the molybdenum center with a catalytically essential Mo=S (Figure 6.2) whose sulfur atom is derived from cysteine (47). *R. capsulatus* NifS-4 shows high structural homology to a wide variety of cysteine desulfurases such as CsdB or IscS in *E. coli*. The current accepted mechanism of

action by these pyridoxalphosphate-dependent cysteine desulfurases remove the sulfur atom from cysteine, releasing alanine, with the sulfide transferred to a cysteine residue on of the enzyme as a persulfide (Figure 6.3A) (95). The cysteine-containing loop with bound persulfide has been shown to be highly flexible and able to deliver the sulfide to destinations many angstroms away (96). An example of the flexibility of the loop involved with sulfide delivery can be seen in Figure 6.3 B, depicting IscU (an iron-sulfur cluster assembly protein) bound to IscS (a cysteine desulfurase homologous to NifS-4) where the loop is unresolved and located between the active site of IscS and the bound IscU.

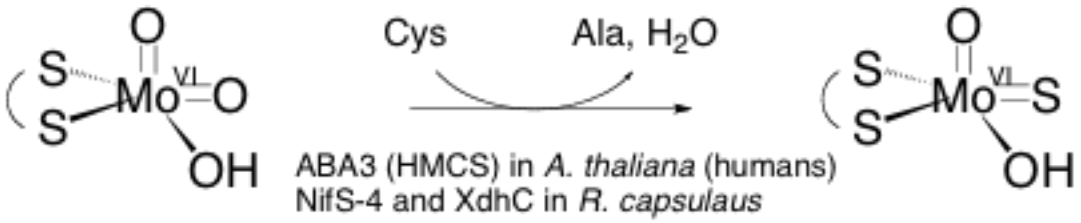

Figure 6.2 *Sulfuration of the molybdenum center of xanthine dehydrogenase.* The site is sulfurated by ABA3 in *Arabidopsis thaliana* (analogous to HMCS in Humans), or NifS-4 and XdhC in *Rhodobacter capsulatus*, is indicated.

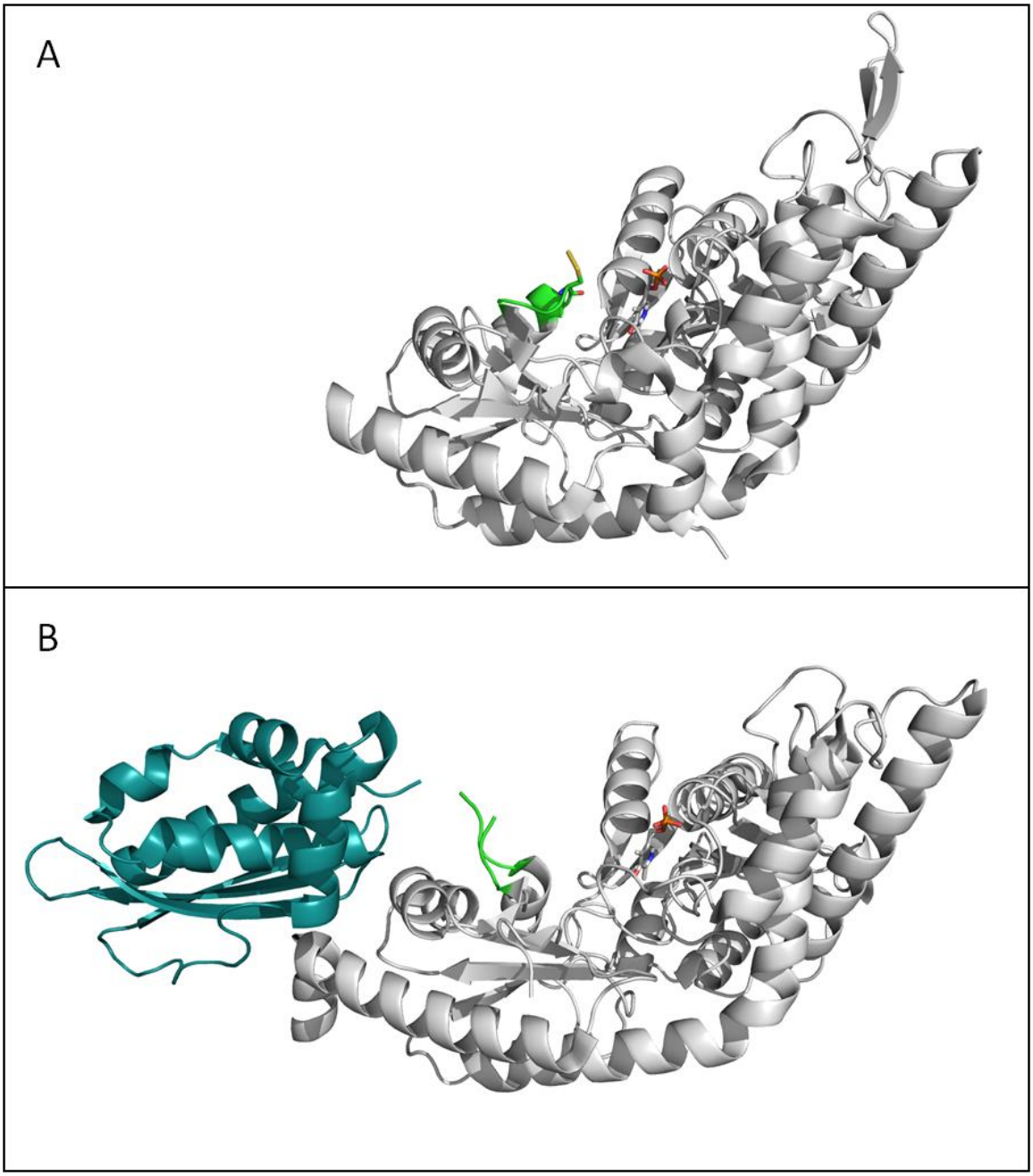

Figure 6.3 *Structural basis for how sulfur is transferred by NifS-like enzymes.* (A) The structure of a monomer of the CsdB/NifS from *E. coli* (PDB ID: 1KMJ) shows persulfide formed on Cys 364 after catalytic turnover of the enzyme. (B) The structure of IscU (*teal*) bound to a monomer of IscS (*grey*) from *E. coli* (PDB ID: 3LVL) is shown in an orientation identical to that of the CsdB monomer shown in A. The loop which would contain the persulfide is not resolved in the IscU structure. Both loops are colored *green* to highlight the range of motion of the loop.

In the *R. capsulatus* system, XdhC binds only to the apo form of bacterial xanthine dehydrogenase (94), and only after the two [2Fe-2S] clusters and FAD of the enzyme have been incorporated into apoprotein and the subunits assembled into an $(\alpha\beta)_2$ heterotetramer (45). These results strongly suggest that the apoprotein has complete (or nearly complete) structural integrity at the point at which the molybdenum center is incorporated, but exists in a distinct configuration from the holoenzyme. This places serious structural constraints on the manner in which insertion might occur and any conformational change that might be associated with the process.

Among eukaryotes, the ABA3 gene product of *Arabidopsis thaliana* has also been identified to be involved in cofactor sulfuration and insertion (48,97,98). ABA3 is a bifunctional protein that has an N-terminal portion with cysteine desulfurase activity analogous to NifS-like enzymes in bacterial systems (including the one that sulfurates the immature molybdenum cofactor bound to XdhC)(98). The C-terminal portion of ABA3 also binds the molybdenum cofactor, and is thought to provide a scaffold on which the sulfuration occurs. While this C-terminal portion is functionally equivalent to the bacterial XdhC in having insertase activity, however, there is negligible sequence identity between it and XdhC (98) and the two cannot complement one another *in vivo* (43). In *in vitro* assays, ABA3 is able to sulfurate the desulfo form of aldehyde oxidase (98), a plant enzyme which, like the xanthine oxidoreductases, requires the sulfur for activity. The cognate to ABA3 in humans is human molybdenum cofactor sulfurase (HMCS), and the family appears to be well-conserved in eukaryotes (93). The fact that ABA3 can restore activity to desulfo aldehyde oxidase suggests that eukaryotes have evolved a way to

restore activity to enzyme that has spontaneously desulfurated without having to synthesize new apo protein (43). A D428A mutant of rat xanthine oxidoreductase has also been crystallized in the apo form exhibiting a structure identical to the holoenzyme (82), suggesting that apo eukaryotic xanthine dehydrogenases may not exhibit an alternate conformation than the holoenzyme as appears to be the case with their bacterial counterparts.

In the present work, analysis of reported X-ray crystal structures of several members of the xanthine oxidase family and homologs of XdhC and NifS-4 has been used to construct multiple models to explain how the cofactor is sulfurated and inserted. Based upon the similarities between members of the xanthine oxidase family, we propose that this mode of insertion is common to all family members. In attempts to identify a conserved motif which could act as a target for cofactor insertion machinery, a ~125 amino acid region of the "closed" configuration of the crystallographically characterized bovine holoenzyme has been identified whose connectivity to the remainder of the polypeptide makes possible a "hinge" movement that would allow access to the interior to the protein. We have compared this "hinge" region to other members of the xanthine oxidase family to offer insight into likely differences in the insertion process between prokaryotic and eukaryotic systems.

6.2 The hinge rotation model

The very considerable amino acid sequence identities and structural homologies of the xanthine oxidase family of molybdenum-containing enzymes have been previously

noted (31,33,34), and the shared overall architecture of these enzymes strongly suggests a common mechanism by which the deeply buried cofactor is inserted into the (largely folded (45)) apoprotein. The published holoenzyme structures show very limited solvent access to the molybdenum center, primarily via a 15 Å long substrate binding channel; these structures thought of as being in a "closed" conformation which must somehow open in the apoenzyme to allow cofactor insertion. An attempt to identify regions of the bovine xanthine dehydrogenase/oxidase structure that might be involved in conformational changes associated with the cofactor insertion process has led to the proposal that portions of the enzyme may function as hinges or flaps whose motions relative to the rest of the protein would allow access to the molybdenum center binding site when the apoprotein is in a punitive "open" conformation (39). A candidate hinge region is readily identified consisting of amino acid residues 1011 to 1137 in the bovine enzyme, which is a contiguous subdomain towards the amino-terminal end of the molybdenum binding domain. The polypeptide backbone makes a single entry into this punitive hinge region, tracing out in its entirety and exiting near the point of entry. The close spatial proximity of the entry and exit points in the three-dimensional structure (Figure 6.4) allows for a significant range of motion for this portion of the protein. The putative hinge domain itself consists of two α helices, one longer than the other, that lie across a three-stranded β-sheet (Figure 6.5). The domain is capped by a short helix-turn-helix motif that is solvent-exposed. Despite the complete absence of contacts with other portions of the protein the amino acid sequence of this cap portion of the hinge region is very strongly conserved among eukaryotic xanthine- and aldehyde oxidizing enzymes as

KNPxGS/TxWxDW (Figure 6.6). Interestingly, while the putative hinge domain lies at the dimer interface of the holoenzyme, it has only modest interactions with the remainder of the protein; the two hinge regions themselves are separated by a 15-20 Å wide groove on the dimer surface that spans the non-crystallographic two-fold axis of symmetry. Most importantly from the standpoint of a possible role in cofactor insertion, the molybdenum center of each monomer lies at the base of its respective hinge domain, and it is clear that relatively modest motion of the latter would expose the molybdenum center binding site.

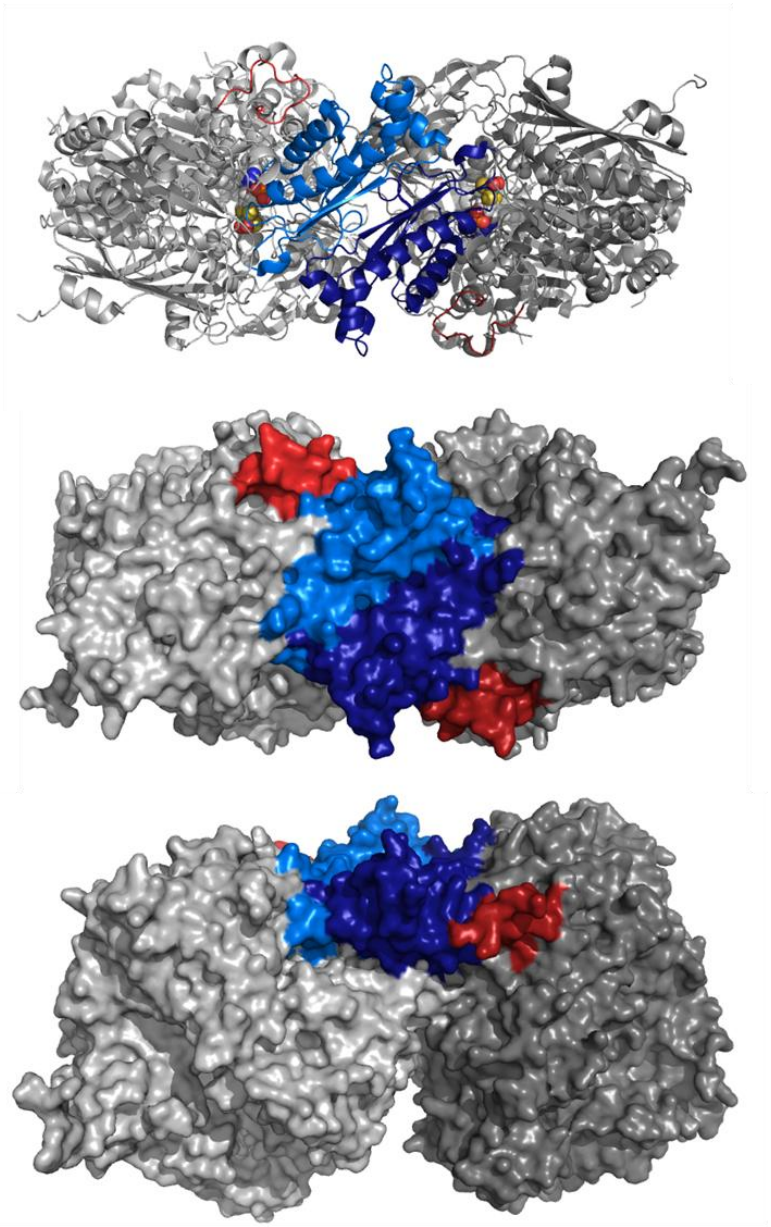

Figure 6.4 *The structure of xanthine dehydrogenase*. The dimeric holoenzyme (PDB ID: 1FO4) is shown, with the two subunits shaded light and dark, to the left and right, respectively. The putative hinge region of each subunit is indicated in blue, and the loop region discussed in the text is indicated in red. (Top) The ribbon representation of the structure, as viewed along the non-crystallographic twofold axis of symmetry, looking down onto the large groove separating the two hinge regions in the dimer. (Middle) A surface representation of the structure from the same perspective. (Bottom) The structure as seen rotated 90° about the horizontal from that shown in the two previous orientations.

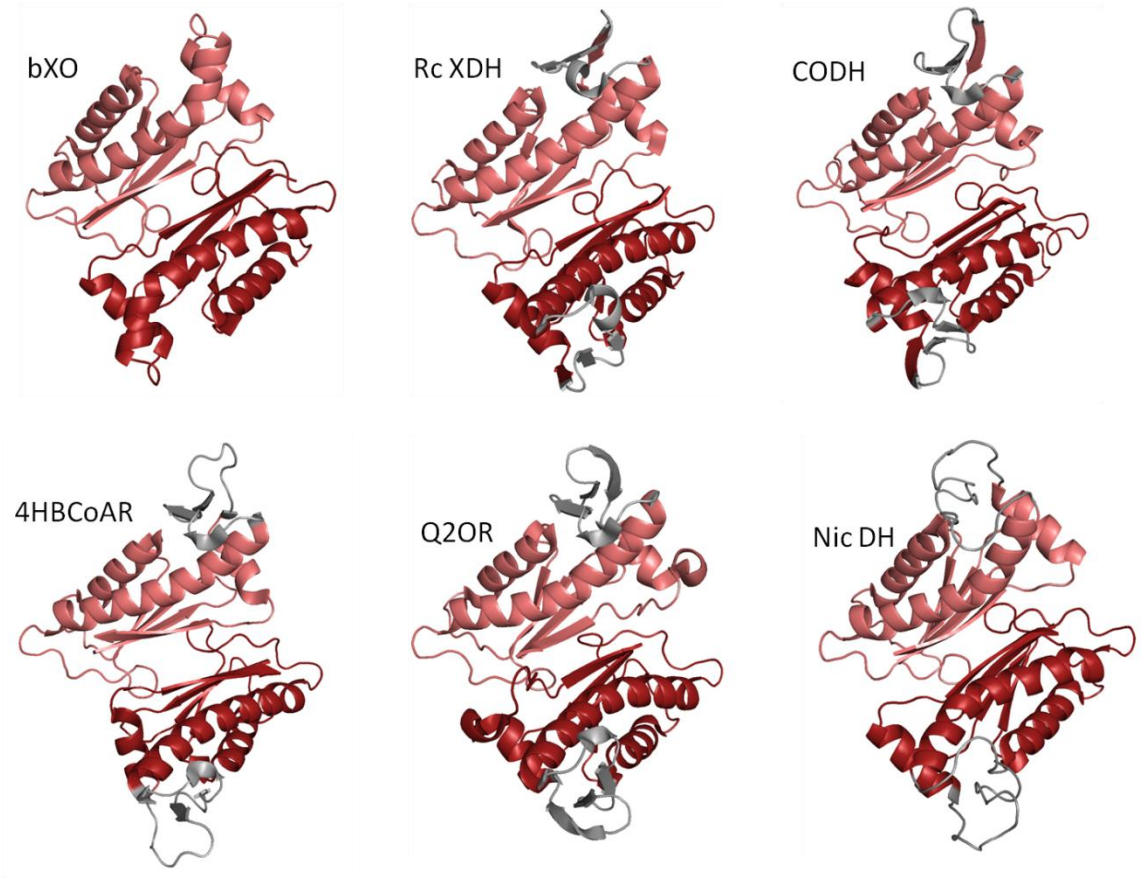

Figure 6.5 *Structural homologies in the hinge region among members of the xanthine oxidase family of molybdenum enzymes*. In all cases the orientation is comparable to that shown in Figure 6.4, and with the dimers designated in light and dark shading. In the five prokaryotic enzymes shown, the insert region referred to in the text is shaded in gray. *Top*, from left to right, bovine xanthine oxidase (Abbreviated bXO; PDB ID: 1FIQ), *R. capsulatus* xanthine dehydrogenase (Abbreviated Rc XDH; PDB ID: 1JRP), *O. carboxydovorans* CO dehydrogenase (Abbreviated CODH; PDB ID:1N5W), *T. aromatica* 4-hydroxybenzoyl-CoA reductase (Abbreviated 4HBCoAR; PDB ID: 1RM6), *P. putida* quinoline 2-oxidoreductase (Abbreviated Q2OR; PDB ID: 1T3Q), and *E. barkeri* nicotinate dehydrogenase (Abbreviated Nic DH; PDB ID: 3HRD).

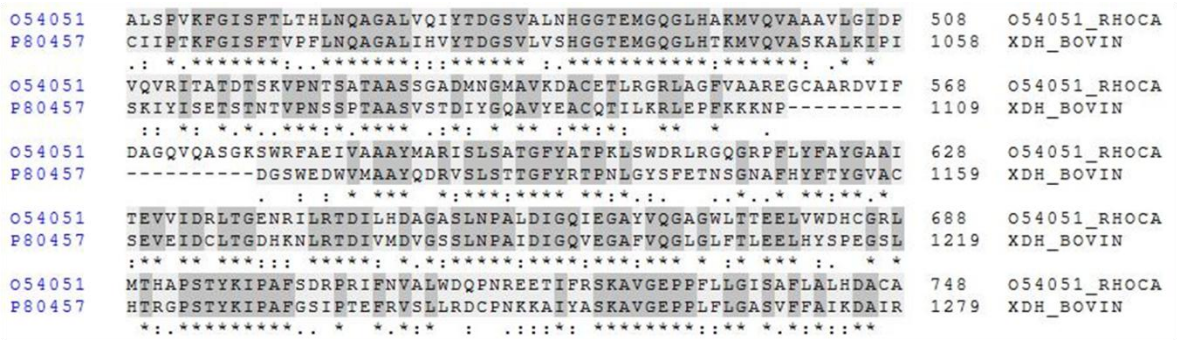

Figure 6.6 *Sequence alignments of bovine xanthine dehydrogenase and R. capsulatus xanthine dehydrogenase*. The 19 amino acid insert seen in the hinge region of the bacterial enzyme is also shown.

Inspection of the structure of the xanthine oxidase dimer suggests that a symmetrical pivoting of the two putative hinge domains toward one another about an axis defined by the outermost strand of the β sheet of the hinge brings complementary portions of the hinge regions into close proximity and closes the large gap that exists between the two hinge regions on the surface of the dimeric holoenzyme. This motion also opens a large channel at the base of each hinge domain that lies on the opposite the substrate access channel from the molybdenum center binding site of each monomer. Significantly, the strand of β sheet about which this motion might occur is the C-terminal portion of the hinge domain, the end of which constitutes the exit of the polypeptide trace out of the hinge domain back to the remainder of the protein. The amino terminus of the hinge domain lies at the N-terminal end of the immediately adjacent (middle) strand of β sheet, and as a result the proposed motion is minimally constrained by the covalency of the polypeptide backbone: a simple twisting motion of each hinge region is sufficient to accommodate the proposed rotation.

Energy minimization of the structure after hinge rotation (with the molybdenum center, iron-sulfur clusters and FAD removed) readily converges to a stable conformation (Figure 6.7). Specific hydrogen bonding interactions between the two hinges were observed: Lys 1099_1 – Glu 1092_2, Lys 1099_1–Thr 1096_2, Thr 1096_1 – Lys 1099_2, and Glu 1092_1 - Lys 1099_2 (here, the subscript designates the first or second subunit monomer within the dimer). The two Thr 1092 residues are also within hydrogen-bonding distance, although their orientations are less than fully optimal. It is to be emphasized that this new energy-minimized configuration does not disrupt the dimer interface: substantially

stronger interactions between the two hinge domains are created, and the majority of the dimer interface region (not involving the hinge domains) remains undisturbed.

In this "open" conformation, the two hinge domains create a large, relatively flat, solvent-exposed surface. We propose that these regions constitute a recognition site for the ABA3/HMCS in the "open" conformation proposed in this model and allow the ABA3/HMCS to distinguish apo- from holoprotein. The cap motifs (solvent facing portions of the α helices) of the hinge region are extremely acidic, suggesting that the complementary portion of the insertion machinery is positively charged. Importantly, while the two new channels to the cofactor binding sites of the dimer lie at opposite ends of the now merged hinge domains, they lie on the same face of the overall dimer, allowing the dimeric insertion machinery to insert the molybdenum centers simultaneously.

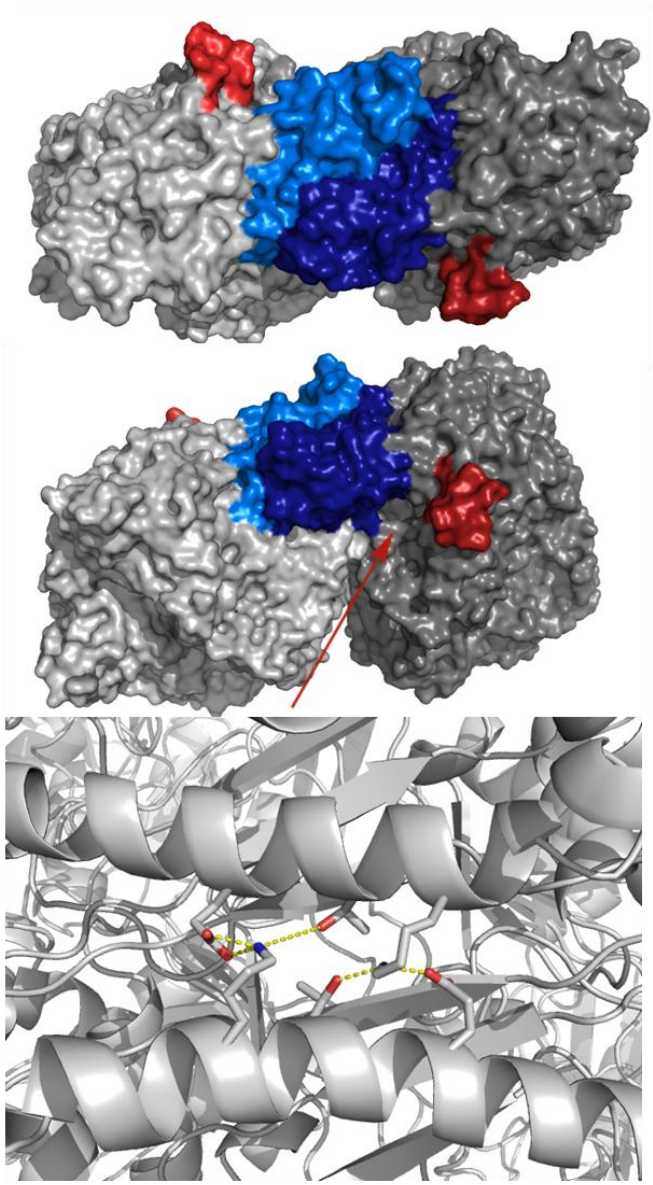

Figure 6.7 *Structure of the energy-minimized open configuration for bovine xanthine oxidase.* The color scheme is the same as in Figure 6.4. (Top) a representation of the open configuration viewed from along the non-crystallographic two-fold axis of symmetry, with the two hinge regions rotated into the groove separating them in the structure of the holoenzyme (compare with Figure 6.4); (Middle) the open configuration as viewed from the side, with the large channel opened by the movement of the hinge regions indicated by the arrow in the subunit on the right; (Bottom) a close-up of the view from above showing the specific hydrogen-bonding and electrostatic interactions involving Glu 1092, Thr 1095 and Lys 1099 in each of the hinge regions that are created in the energy-minimized open structure. The two Thr 1095 oxygens are 2.8 Å apart and probably also hydrogen-bonded.

A comparison of the structure of the *R. capsulatus* xanthine dehydrogenase with that of the bovine enzyme indicates that while the molybdenum-binding portion of the bacterial enzyme is a separate subunit from the iron-sulfur- and FAD-binding portion of the protein (and is thus an $(\alpha\beta)_2$ dimer of dimers), the overall structural homology to the bovine enzyme is strong, and in particular the core structure of the putative hinge region is very well-conserved. Still, a comparison of the amino acid sequences for the molybdenum-binding portions of eukaryotic and prokaryotic members of this enzyme family indicate that a 19 amino acid residue insert is present in the putative hinge region of the bacterial enzyme (Figure 6.6). This insert constitutes an elaboration of the cap motif to the hinge region identified above in the bovine enzyme, although the hinge region is otherwise highly conserved in both overall fold (Figure 6.5) and amino acid sequence (60% sequence identity, another 22% sequence similarity). The net effect of this insert is that the cap motif of the bacterial protein is approximately twice the size of that in the eukaryotic protein. It is to note that all bacterial xanthine oxidase family members crystallized so far contain a variation of this hinge insert (Figure 6.5) which we suggest is involved in recruitment of each family member's respective XdhC-like protein. Rotation of the hinge regions in the bacterial enzymes analogously to the motion proposed for the eukaryotic enzyme again closes the large groove on the protein surface, and the energy-minimized structure that results again brings complementary portions of the longer α helix in each hinge into proximity, with a channel providing access to the molybdenum center binding site similar to that seen with the bovine enzyme above again

created. The specific interactions between the two hinge regions of the *R. capsulatus* xanthine dehydrogenase are: Asp 542_1 – Asp 550_2 and Arg 550_1 - Asp 542_2 (Figure 6.8).

A second 20-residue insert (residues 381-398 of the XdhB subunit) in the prokaryotic enzymes is found elsewhere in the molybdenum-binding portion of the proteins that turns out to be adjacent to the rotated hinge regions in the putative "open" conformation (Figure 6.8). The fairly close spatial proximity of the second pair of inserts suggests that they represent structural cassettes which themselves have significant range of motion. Although only a small portion of this second pair inserts is resolved in the crystal structure of, for example, the *R. capsulatus* xanthine dehydrogenase, the N- and C-terminal insertion points are readily identified and indicate that this second insert is not likely to interact directly with any portion of the hinge domains in the "open" configuration. On the other hand, the second inserts do lie on the same face of the dimer as the merged hinge regions and may constitute an approximately linear 80 Å-span on the surface of the protein that may help recruit XdhC (Figure 6.8). Absent these prominent insert regions in the eukaryotic enzymes, it seems likely that the structural landmarks for recruitment of ABA3 and its cognates (possibly in conjunction with other, as yet unidentified, components of the eukaryotic insertion machinery) may be substantially different than is seen in the bacterial systems.

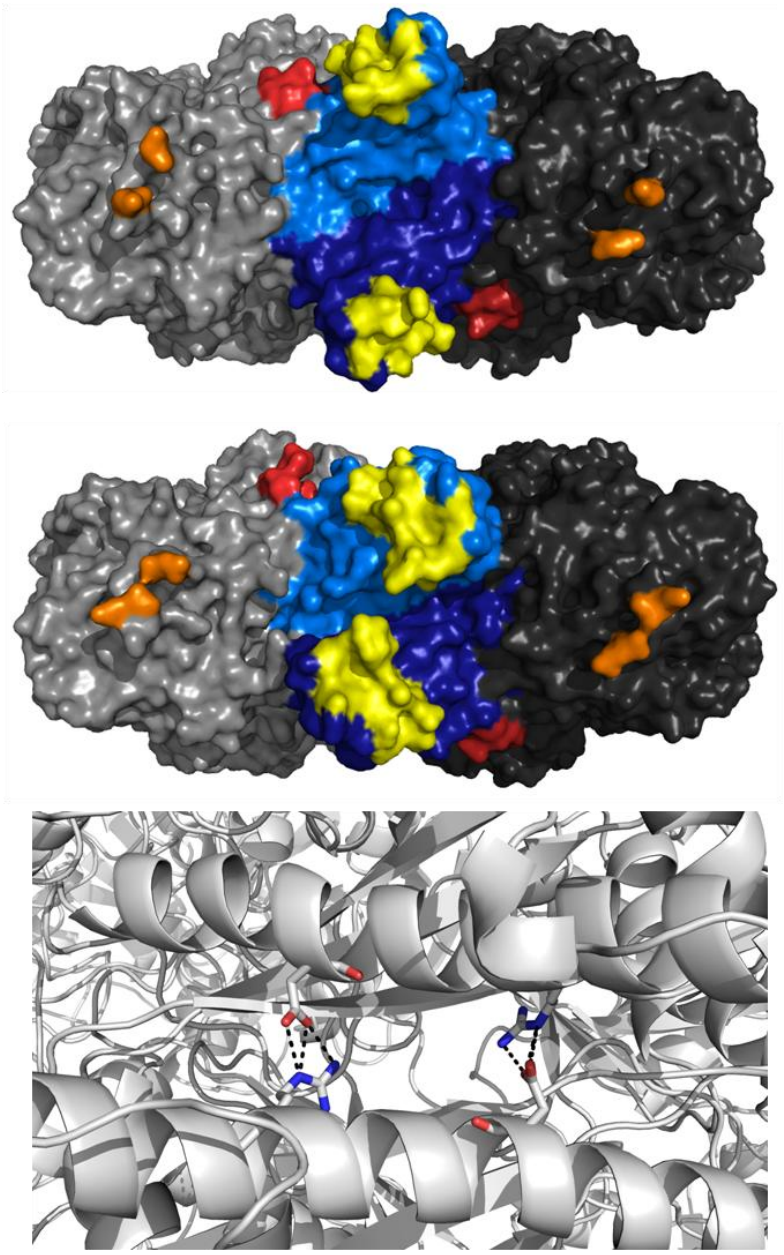

Figure 6.8 *Structure of the energy-minimized open configuration for the R. capsulatus xanthine dehydrogenase*. The color scheme is similar to that used in Figure 6.4, with the insertion in the cap motif of the hinge region indicated in yellow and the insertion points for the second insert referred to is in orange for each subunit. With the hinge region is rotated into the open configuration, the surface shown creates a structural motif that may be involved in recruitment of the dimeric XdhC involved in cofactor sulfuration and insertion. The channel created in the open configuration of each subunit lies at the base of each of its respective hinge region. The channel is partially obstructed by the N-terminus of the molybdenum binding subunit (in red). The two channels are located sufficiently close together as to allow the 2 x 34 kDa XdhC to insert the sulfurated molybdenum centers into the two subunits of the dehydrogenase simultaneously.

The above notwithstanding, there are substantive and fundamental similarities in the bacterial and eukaryotic enzymes with regard to the hinge region itself (Figure 6.5) and the putative channel that is created by rotation of the hinge domains into the "open" configuration. In both eukaryotes and prokaryotes, one side of this channel is provided by the hinge itself, the other by the N-terminal portion of the first molybdenum domain as well as the second [2Fe-2S]-containing domain of the protein (that lying nearer the molybdenum center in the holoenzyme). A loop near the N-terminus of the molybdenum-binding subunit in the bacterial enzymes in fact partially occludes the channel. In the bovine xanthine dehydrogenase, the corresponding loop is part of the long linker peptide between the FAD and the molybdopterin domains composed of residues 561-576. As shown in Figure 6.4, this highly conserved unstructured loop (colored in red) interacts with the shorter α helix of the putative hinge region, with specific interactions including a salt bridge between Asp 571 (in the N-terminal loop) and Lys 1052 (in the hinge region) and hydrogen bonds between Thr 572 (loop) and Gln 1048, and His 579 (loop) and Thr 1044 (hinge). These are some of the few interactions between the hinge region and the remainder of the polypeptide that are ruptured upon rotation of the hinge region as proposed. Immediately C-terminal to this unstructured loop is a short α helix that lies against the second Fe/S domain. A modest rearrangement of the N-terminal loop juxtaposes Asp 571 and Arg 575 with Glu 103 and Arg 104 on the surface of the Fe/S domain, and considerably enlarges the channel. Such a movement subsequent to rotation of the hinge region may well be important, particularly in the bacterial enzymes, given the proximity of the iron-sulfur cluster of this domain to the

inserted molybdenum cofactor. The structural integrity of the Fe/S domain has in fact been shown to be critical in the insertion process in the case of the *R. capsulatus* xanthine dehydrogenase (45). The interaction between Lys 1052 on the hinge region and Asp 571of the loop is broken when rotated away from the hinge domain and new interactions form bringing residues 561-576 to wrap around the loop created by residues 192-201. This reorganization reveals the channel which is about 13 Å wide and 22 Å deep (Figure 6.7, middle).

It is significant that the new channel created in the putative "open" configuration lies opposite the position of the molybdenum atom from the substrate access channel to the active site in both the prokaryotic and eukaryotic enzymes. The implication is that in this model, the molybdenum center is inserted "molybdenum first", entering from what has conventionally been understood to be the back side of the protein structure. The pyranopterin ring portion of the mature molybdenum center enters next (its distal amino group lies close to, and possibly hydrogen bonds, one of the cysteine ligands to the nearer [2Fe-2S] cluster in the adjacent domain of the protein), followed last by the sidechain phosphate of the cofactor (17). In the *O. carboxydovorans* CO dehydrogenase, another member of the molybdenum hydroxylase family that possesses an elaborated cytosine dinucleotide form of the pyranopterin cofactor, the cytidine portion of the cofactor extends toward the protein surface, with the walls of the putative cofactor access channel identified here apparently now collapsed upon the cytidine portion of the cofactor in the "closed" configuration (99). This observation further suggests that the cofactor access channel indeed lies opposite the substrate access channel in the protein structure.

The phosphate group of the molybdenum center, once inserted, could play an important role in triggering the closure of the cofactor access channel. In all known crystal structures, this phosphate group lies at the amino terminus of the longer α helix of the hinge domain. We suggest that the interaction between the negatively charged phosphate and the positively charged amino terminus of the helix dipole would trigger closure of the protein structure once cofactor has been inserted.

In conclusion, we suggest that a symmetric domain-domain motion at the subunit interface of members of the xanthine oxidase family of molybdenum-containing enzymes has been identified that opens a channel in the resulting energy-minimized structure and provides access for insertion of the newly sulfurated molybdenum cofactor. The hinge regions involved in this motion are connected to the remainder of the polypeptide in such a way that the proposed motion is largely unconstrained. The "open" configuration thus obtained is stabilized by several specific sidechain interactions between the two hinge domains, and the cap motif of the putative hinge domains (and possibly the N-terminal of the first molybdenum domain) may constitute recognition sites for recruiting the insertion machinery – XdhC in prokaryotes and ABA3/HMCS in eukaryotes – to the apoprotein. Cofactor insertion appears to occur from the "back" side, opposite the substrate access channel to the active site, implying that cofactor insertion occurs "molybdenum first", and the side chain phosphate appears to play a key role in triggering closure of the cofactor access channel once cofactor has bound.

6.3 Docking of XdhAB to a homolog of XdhC

6.3.1 Analysis of the structures of homologous XdhC-like enzymes and docking studies with the molybdenum cofactor

Utilizing Sequence Annotated by Structure (SAS) software on the EMBL-EBI website, the sequence of *R. capsulatus* XdhC was used as the basis of a search to identify homologous protein structures. Two unpublished structures were found deposited in the protein database that were classified as having homologous sequence to XdhC, one from *Mycobacterium smegmatis* (PDB ID: 2WE7) and the other from *Bacillus halodurans* (PDB ID: 3ON5) (Figure 6.9). Like the previously characterized XdhC-like proteins (43), both were dimers and exhibited some sequence homology to one another; most importantly, they both contained the conserved cysteine (residue Cys 92 in the *Bacillus halodurans* structure) residue proposed to be involved with sulfuration of the molybdenum cofactor (Figure 6.10). The regions containing the conserved cysteine lie on a portion of the dimer interface and are poorly defined in both crystal structures, suggesting that they are highly flexible. This region is resolved in one of the asymmetric units of the *Bacillus halodurans* structure, allowing for the docking of both the molybdopterin cofactor and the molybdopterin cytosine dinucleotide (MCD) form of the cofactor in AutoDock (71,72). The most stable results for both corms of the molybdopterin cofactor were shown to have the pyranopterin bound in the same orientation in a pocket defined by loops composed of residues 274-277, 297-300, 310-311, and 313-114 (Figure 6.11 and 6.12). The cytosine dinucleotide portion of the cofactor binds in a cleft created by residues 24-33. The phosphates of the MCD cofactor

are found adjacent to a number of positive residues (Arg31, Lys, 32, Arg 323). The molybdenum atom of the docked cofactor sits 2.8 Å from the conserved cysteine (Figure 6.13) and is surrounded by residues Ser 28, Ser 29, Cys 92 (the conserved cysteine) and Ser 277. It is to note that the molybdenum cofactor used for docking is the already sulfurated form and in the correct geometry that is observed in crystal structures of xanthine oxidase family of enzymes. Currently, it is not known if the bound molybdenum cofactor is bound in the tri-oxo form, or covalently attached to XdhC via the conserved cysteine residue as in other characterized MOSC proteins which resemble the sulfite oxidase family of enzymes (43). Based upon the present docking model, Cys 92 is close enough to participate in either of these. More on the proposed model of sulfuration of the molybdenum cofactor is discussed in Section 6.4.

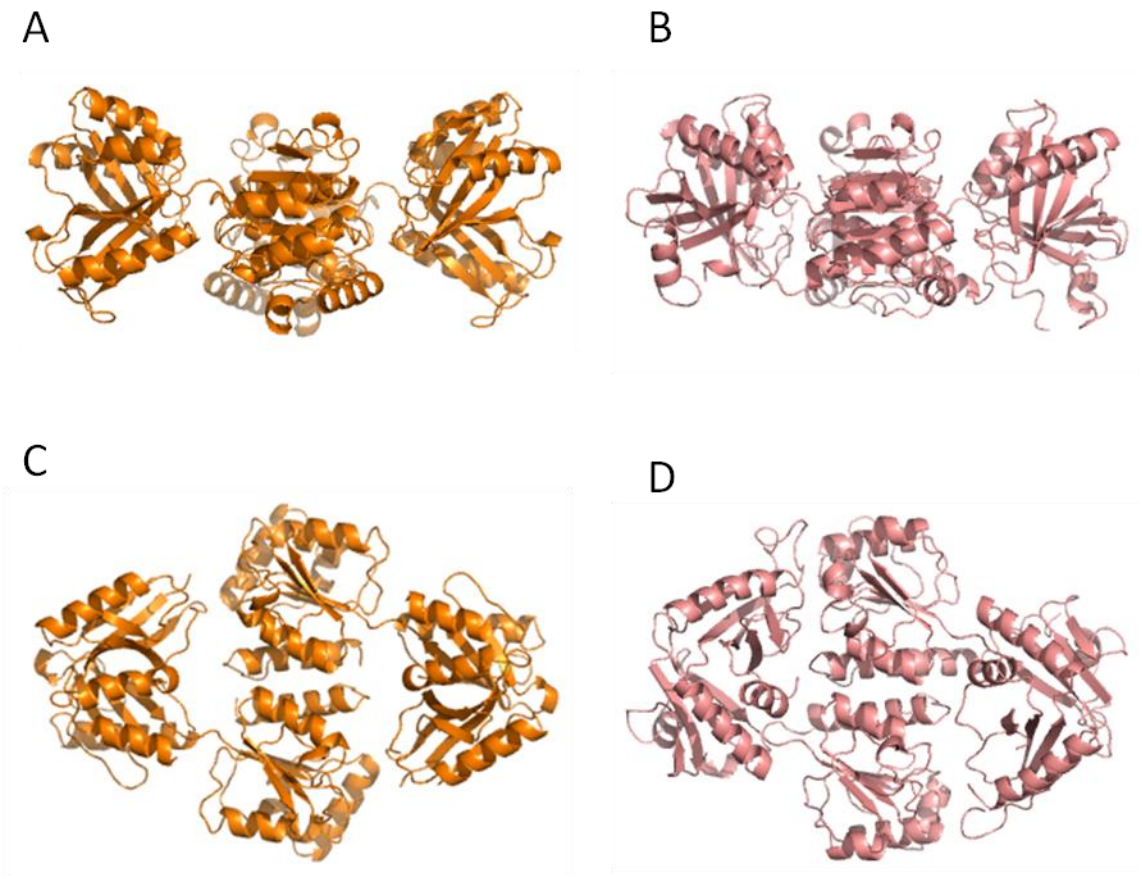

Figure 6.9 *X-ray crystal structures of XdhC homologs from Mycobacterium smegmatis and Bacillus halodurans*. The structures of the biological assembly of the XdhC homologs from *Mycobacterium smegmatis* (A & C; PDB ID: 2WE7) and the other from *Bacillus halodurans* (B & D; PDB ID: 3ON5) are shown in ribbon form. The images of C and D are rotated 90° from the positions seen in A and B, respectively.

Figure 6.10 *Sequence alignments of the XdhC homologs from Mycobacterium smegmatis and Bacillus halodurans and XdhC from Rhodobacter capsulatus.* The PDB chain sequences from the XdhC homologs from *Mycobacterium smegmatis* (2WE7_A) and the other from *Bacillus halodurans* (3ON5_A) were compared to the gene product of *Rhodobacter capsulatus* XdhC (DSAPI3_RHOCB). The conserved cysteine proposed to be involved in molybdenum cofactor sulfuration is marked by a blue arrow.

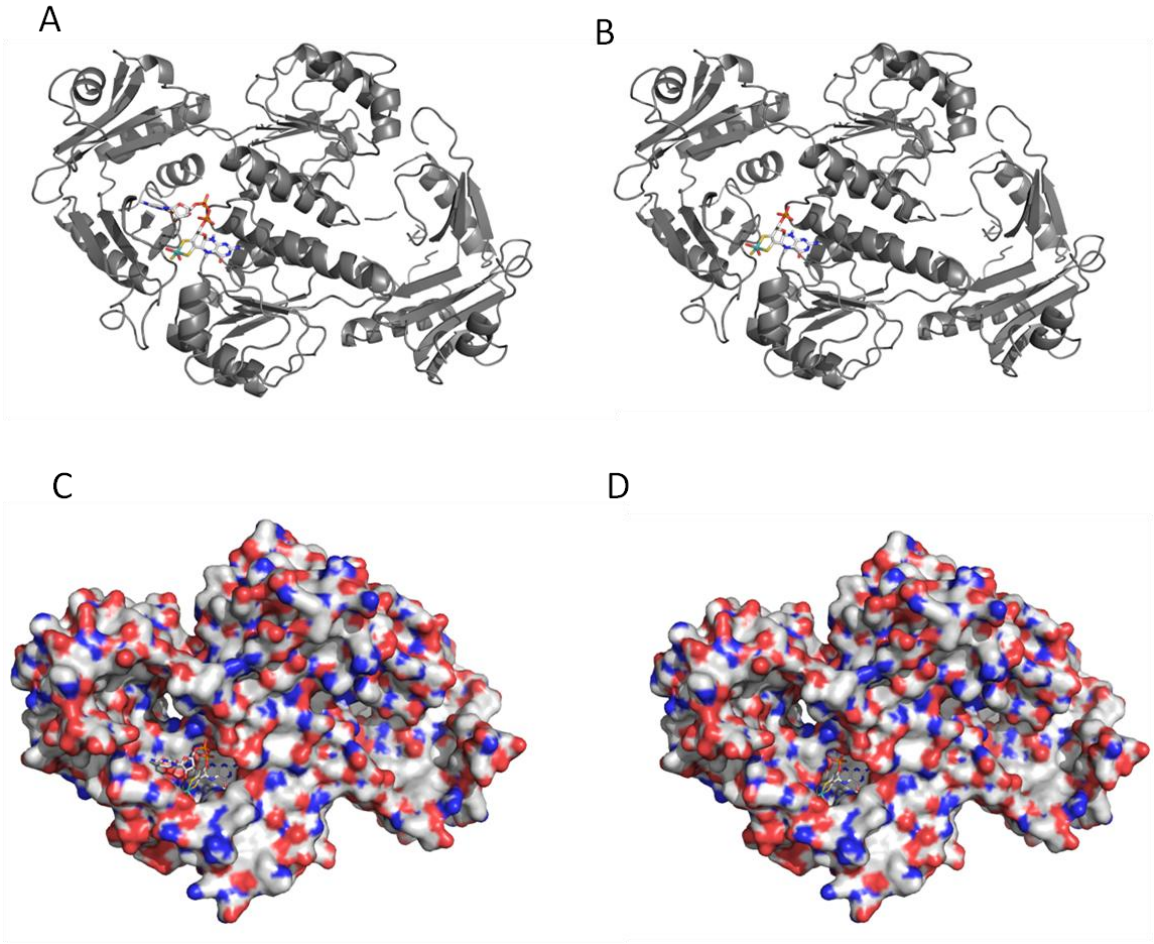

Figure 6.11 *Structures of the XdhC homolog from Bacillus halodurans (PDB ID: 3ON5) docked with the molybdenum cofactor*. (A & C) The crystal structure of the XdhC homolog with the molybdopterin cytosine dinucleotide (MCD) form of the cofactor docked. (B and D) The crystal structure of the XdhC homolog with the molybdopterin (MPT) form of the cofactor docked. The structures in A&B are shown in ribbon representation, with the cofactors shown in stick representation and CPK color scheme. The structures in C&D are shown in surface representation, with the cofactors shown in stick representation and CPK color scheme.

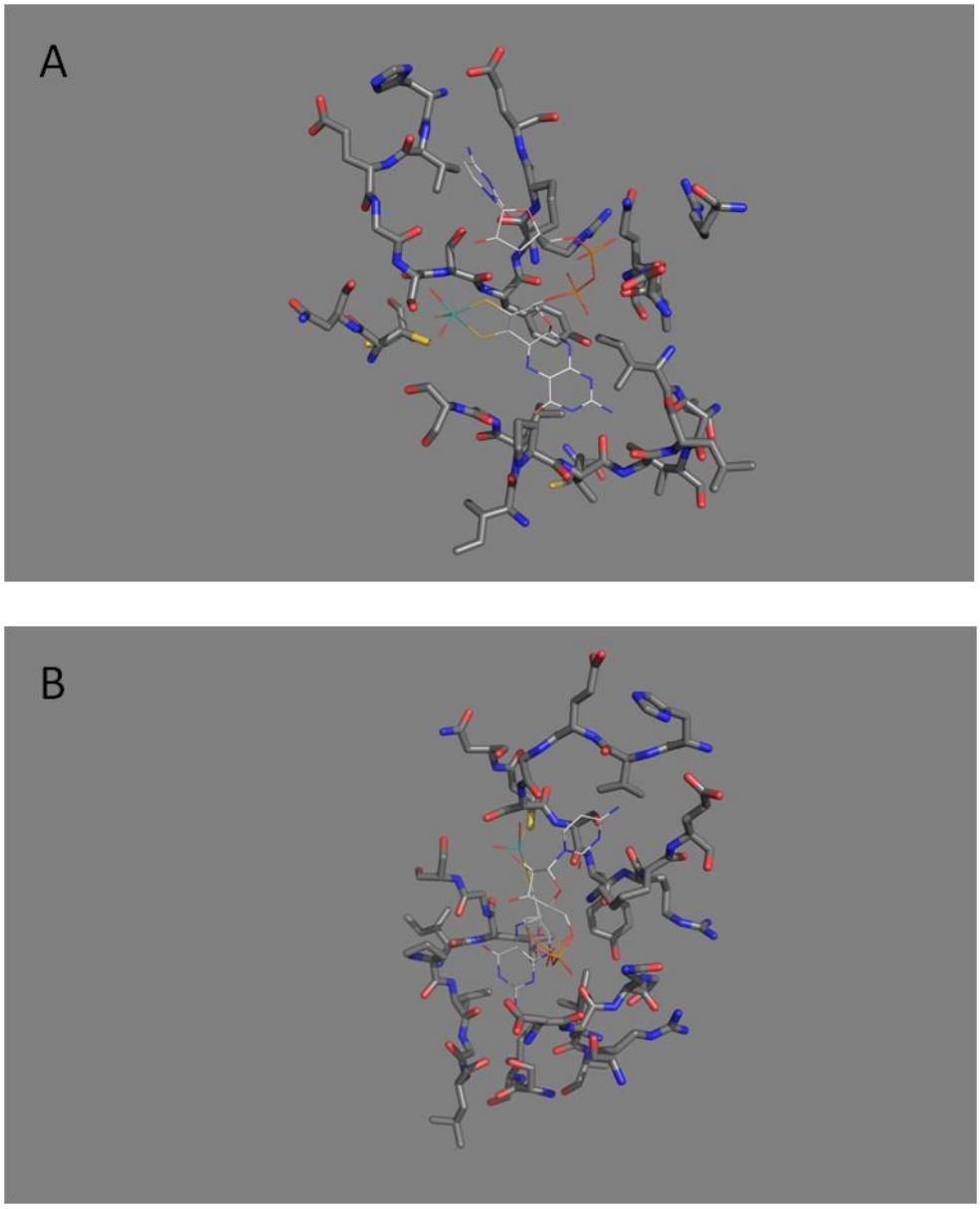

Figure 6.12 *The molybdenum cofactor binding pocket of XdhC.* The MCD form of the molybdenum cofactor is represented in line representation with the CPK color scheme, while the binding site residues are shown in grey stick representation with oxygen atoms in red, carbons in grey, nitrogens in blue and sulfur in yellow. B is rotated roughly 90° horizontally from image A.

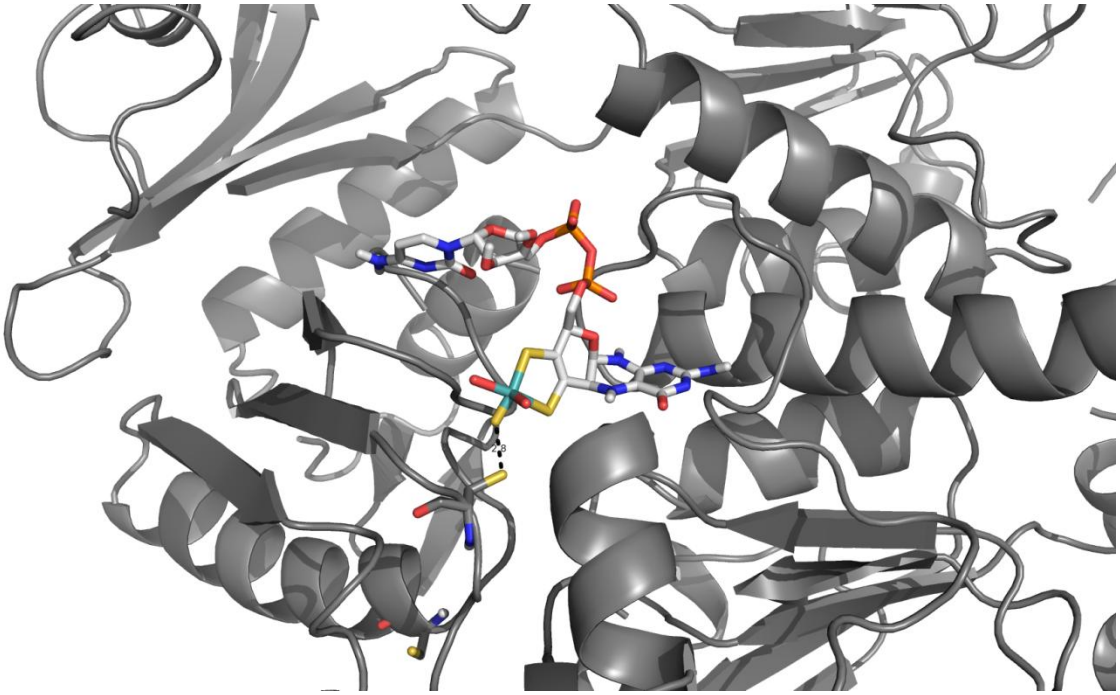

Figure 6.13 *The proximity of the docked molybdenum cofactor to the conserved cysteine residue.* A close up of the docked MCD cofactor with the XdhC homolog (PDB ID: 3ON5) is shown. The position of the Mo=S sulfur atom is found to be within 2.8 Å of the docked molybdenum (MCD) cofactor.

6.3.2 The docking of the XdhC homolog from Bacillus halodurans to xanthine dehydrogenase from R. capsulatus

Docking of the crystal structure of the XdhC homolog from *Bacillus halodurans* to the crystal structure of *Rhodobacter capsulatus* xanthine dehydrogenase has been attempted in PyMol (64). Previously published studies of XdhC and XDH have proposed that the dimeric form of XdhC interacts with the dimeric form of apo-XdhAB and also that XdhC has affinity towards XdhB specifically (94). Given the conserved structure of the hinge region described in section 6.2, it is likely that the hinge would be the site of binding for XdhC. Initially, an attempt to dock the XdhC homolog was to the "open" conformation of the bacterial XDH proposed in Section 6.2 was made. The compact nature of the XdhC homolog, along with the modeled docking site of the molybdenum cofactor in XdhC does not support simultaneous insertion into both active sites via the cavity created by rotation of the hinge region, as proposed in the initial hinge rotation model of section 6.2. The putative "open" conformation of XDH would require two equivalents of the XdhC dimer (one dimer on each side of XDH) to be able to reach both active sites at the same time without radical restructuring of the observed crystallographic structure of the XdhC homolog.

The docking of the XdhC homolog was next attempted to the "closed" conformation (the crystallographically observed) form of *R. capsulatus* XDH and entailed matching patches of complimentarily charged residues as well as complimentary surfaces. The XdhC homologs also contained two sets of clefts bisecting the XdhC homolog, the first being the two-fold axis of symmetry corresponding to the dimerization

face between the two monomers of XdhC and the other being another two-fold axis of symmetry roughly 90° to the first and corresponding to a cleft made between the N- and C-terminal domains of each monomer of XdhC (each monomer contains two domains connected by a linker). The two sets of clefts appeared to fit well with both bacterial inserts described in the section 6.2 (Figure 6.14). The cleft corresponding to the dimerization face sits between the two inserts away from the hinge while the clefts corresponding to the separation of the domains within each monomer of XdhC are complementary to the inserts within the hinge consistent with our suggestion that the hinge inserts are specific targets for specific XdhC-like proteins. In the docked structure, both molybdenum cofactor binding sites on XdhC sit above the hinge region of one protomer, allowing for insertion of the cofactor from the top of both XdhB dimers of XDH simultaneously.

In order to accommodate the known evidence that XdhC binds to apoenzyme which is unique from the holoenzyme, new flexible regions have been identified in addition to the hinge region. The movement of three to four loops (residues 606-623, 713-730, 650-657, and 375-414) located adjacent to the hinge region were identified which, if rearranged (possibly in concert with a hinge motion), would allow access to the deeply buried binding site (Figures 6.15 and 6.16). The new cavity formed in this "top-down" insertion model lies near the cavity described in the hinge rotation model, and still allows for members of the xanthine oxidase family utilizing the cytosine dinucleotide form of the cofactor to bind the cytidine portion extending toward the protein surface within the collapsed walls of the putative cofactor access channel in the "closed"

configuration. As with the hinge rotation model, the phosphate group of the molybdenum center, once inserted, could still play an important role in triggering the closure of the cofactor access channel and that the interaction between the negatively charged phosphate and the positively charged amino terminus of the helix dipole would trigger closure of the protein structure once cofactor has been inserted.

In conclusion, we suggest that the hinge region of *R. capsulatus* xanthine dehydrogenase is involved with the binding of XdhC. The "open" configuration in the "top-down" model would involve the movement of loops adjacent to the hinge (possibly in concert with a hinge motion) to create a channel leading from the binding site of the molybdenum cofactor on XdhC to the binding site in XDH. Cofactor insertion appears to occur from the "top," roughly 90° from the substrate access channel to the active site, rather than the "back" side, opposite the substrate access channel to the active site. As in the hinge rotation model, insertion occurs "molybdenum first", and the side chain phosphate would play a key role in triggering closure of the cofactor access channel once cofactor has bound.

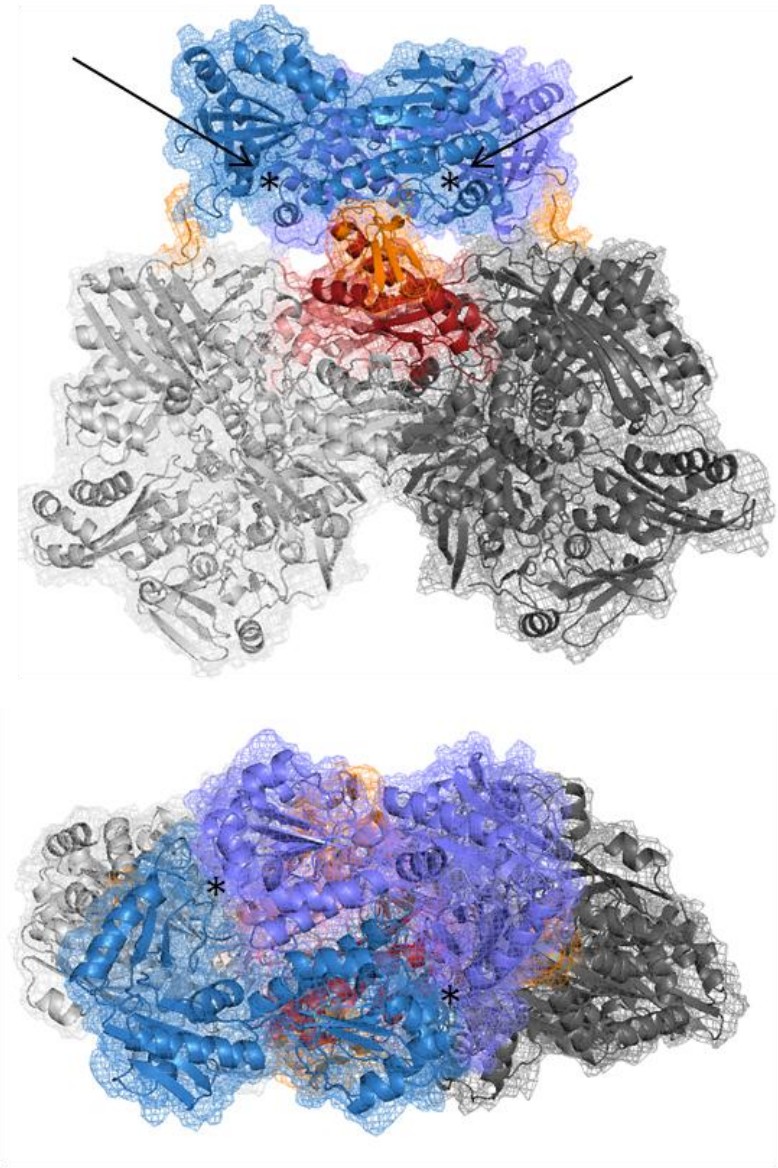

Figure 6.14 *The docking of XdhC homolog to R. Capsulatus XdhAB.* The crystal structure of the XdhC homolog from *Bacillus halodurans* (PDB ID 3ON5) docked to the *R. capsulatus* XDH (PDB ID: 2W3S) is shown. Monomers of the dimer of the XdhC homolog are shown in blue and purple. Monomers of the dimer of the *R. capsulatus* XDH are in shades of grey, with the hinge region, described in section 6.2, in shades of red and the inserts, also described in section 6.2, in orange. The bottom image is rotated roughly 90° vertically from the top image. Arrows and asterisks describe roughly where the binding pocket of the molybdenum cofactor is located in the XdhC dimer.

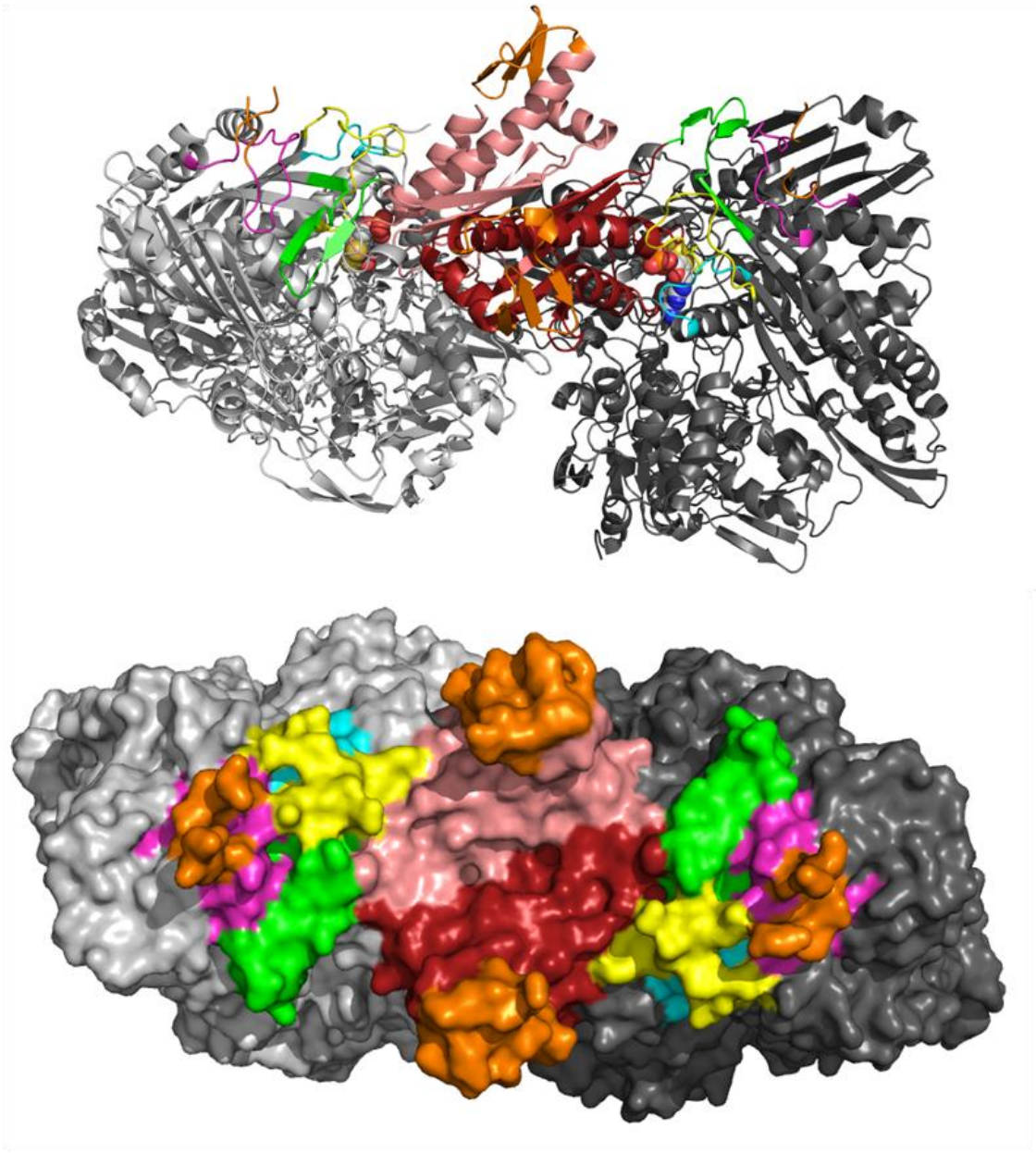

Figure 6.15 *Loops adjacent to the hinge region that block access to the molybdenum cofactor binding site of XDH.* The monomers of the dimer of the *R. capsulatus* XDH shown in cartoon representation (top) and in a surface fill model (bottom). Each monomer of the dimer are in shades of grey, with the hinge region in shades of red and the inserts in orange. Residues 375-414 are in magenta (insert in this loop is colored in orange), residues 606-623 are in green, residues 650-657 in cyan, and residues 713-730 in yellow.

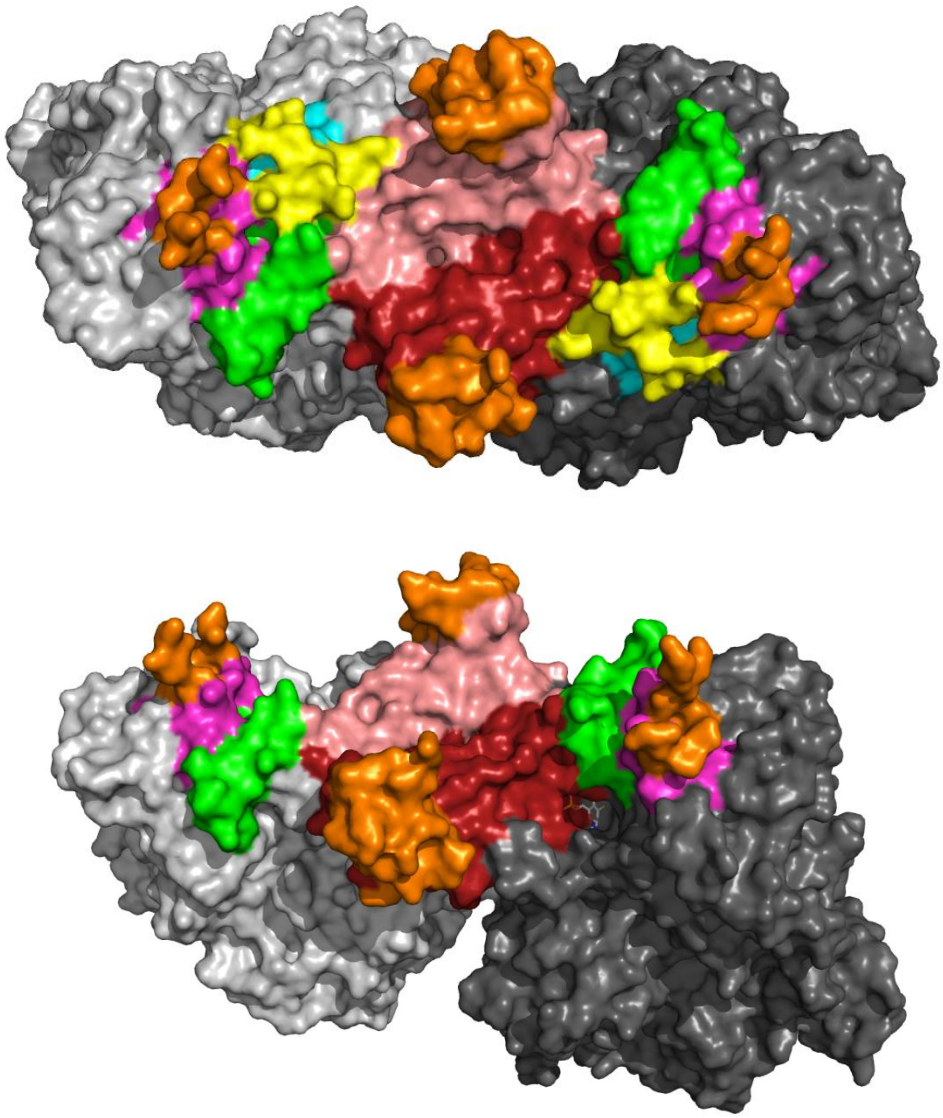

Figure 6.16 *Removal of loops adjacent to the hinge region that block access to the molybdenum cofactor binding site of XDH.* The monomers of the dimer of the *R. capsulatus* XDH shown in a surface fill model. Each monomer of the dimer are in shades of grey, with the hinge region in shades of red and the inserts in orange. Residues 375-414 are in magenta (insert in this loop is colored in orange), residues 606-623 are in green, residues 650-657 in cyan, and residues 713-730 in yellow. The bottom image is slightly rotated vertically and has had residues 650-657 (cyan), and residues 713-730 (yellow) derendered to show the cavity these residues fill leading to the molybdenum cofactor binding site.

6.4 Sulfuration of the molybdenum cofactor

The role of NifS in the sulfuration of the molybdenum cofactor which is bound to XdhC has been known for some time (47), however without structural information for NifS or XdhC, a plausible model for the sulfuration of the molybdenum cofactor could not be assembled. With the existence of homologous structures of the *E. coli* NifS/CsdB protein (PDB ID: 1KMJ, (95)) and the crystal structure of *E. coli* IscS-IscU complex (PDB ID: 3LVL, (96)), the mechanism of how cysteine-derived sulfide is transferred to a cysteine (residue Cys 364) residue on a loop (residues 361-367) in the active site as a persulfide, and subsequently transferred to iron-sulfur cluster assembly proteins via rearrangement of the flexible loop (Figure 6.3) can now be assessed. (95,96).

Due to the highly conserved nature of the NifS, CsdB, and IscS enzymes, similarities in structure between XdhC and IscU were examined to see if similar modes of the binding of NifS to the two physical partners could be accommodated. IscU and XdhC share little significant sequence homology, but surprisingly, a portion of the polypeptide backbone of the molybdenum cofactor binding motif of XdhC is nearly identical to the iron-sulfur cluster assembly motif of IscU. Both contain a set of three anti-parallel β-sheets and contain a cysteine residue three amino residues from the amino terminus of the second β-sheet (Figure 6.17). This cysteine residue corresponds to the conserved cysteine residue in XdhC. Although the backbone trace of this region is very similar, there is little sequence homology other than the conserved cysteine, so NifS may not bind to XdhC in the same manner as IscS binds to IscU. In an alternate model of binding, NifS would bind

adjacent to the molybdenum cofactor binding pocket (Figure 6.18) in a similar position to where the bacterial XDH would bind in the model proposed in section 6.3.2.

Currently, it is not known if NifS sulfurates the molybdenum cofactor directly, or if XdhC is sulfurated and in turn sulfurates the cofactor (43). XdhC has been shown to tightly bind the molybdenum cofactor (94), if NifS binds to XdhC in the same manner as IscS binds to IscU sulfuration of XdhC significant conformational changes would have to occur while the cofactor is bound for NifS to sulfurate the conserved cysteine residue. Alternatively, sulfuration of XdhC could occur before molybdenum cofactor binds to the proposed binding pocket. After the molybdenum cofactor binds, XdhC would then deposit the sulfide onto the molybdenum coordination sphere displacing an oxo group. In both cases, the molybdenum cofactor would be in the tri-oxo form and have a geometry similar to the geometry of the cofactor seen in the xanthine oxidase family enzymes (Figure 9.19 B). The sulfide from the persulfide on the conserved cysteine of XdhC would come in from the "bottom" (see Figure 6.13) to displace an oxo group from the molybdenum coordination sphere similar to how hydroxide displaces product during turnover of xanthine oxidase. Alternatively, NifS could directly sulfurate the bound molybdenum cofactor. In this case, the conserved cysteine would bind the molybdenum cofactor similar to other characterized MOSC domains that have been suggested to covalently link the molybdenum center to the enzyme via a conserved cysteine residue (22). The ligation of the molybdenum center to the enzyme would either stabilize the bound molybdenum cofactor or represent a ligand to generate an electron environment facilitating the sulfur/oxygen exchange reaction (43). The coordination geometry of the

molybdenum center would likely correspond to that seen the sulfite oxidase family (Figure 6.19 A) so that the incoming sulfide from the top would not be blocked by the presence of an axial oxygen. The incoming sulfide from the persulfide would displace the cysteine residue and flip the coordination geometry to that which is seen in the xanthine oxidase family. These models best fit the current information described by Neumann and Leimkühler that XdhC has to dissociate from NifS4 after the sulfuration reaction to interact with XdhB and that the conserved cysteine of XdhC could either act as a sulfur-transferring cysteine on which a persulfide is formed during the reaction or as a ligand to the protein-bound molybdenum cofactor (43).

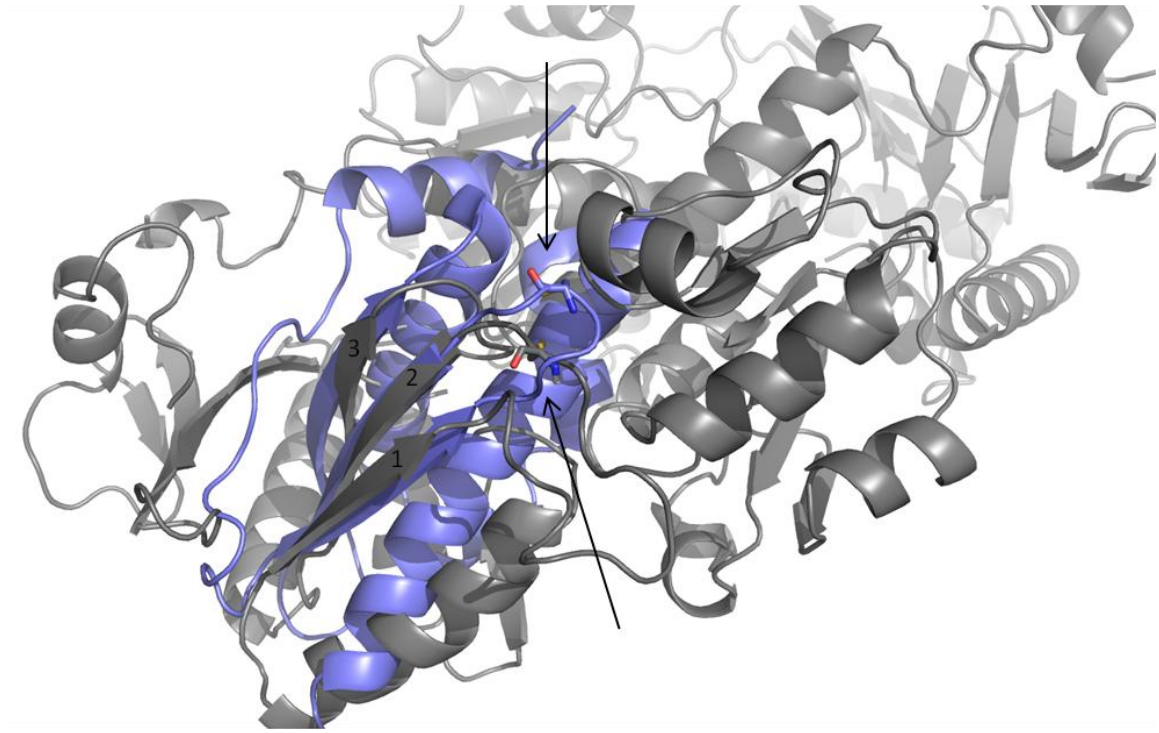

Figure 6.17 *Overlay of the structures of XdhC and IscU.* The structure of IscU (PDB ID: 3LVL), shown in violet ribbons is superimposed upon the structure of the XdhC homolog from *Bacillus halodurans* (PDB ID: 3ON5), shown in grey ribbons. The β sheets that were roughly aligned are numbered 1-3 and the cysteine residues that share the same position in reference to the second β sheet are indicated by the black arrows.

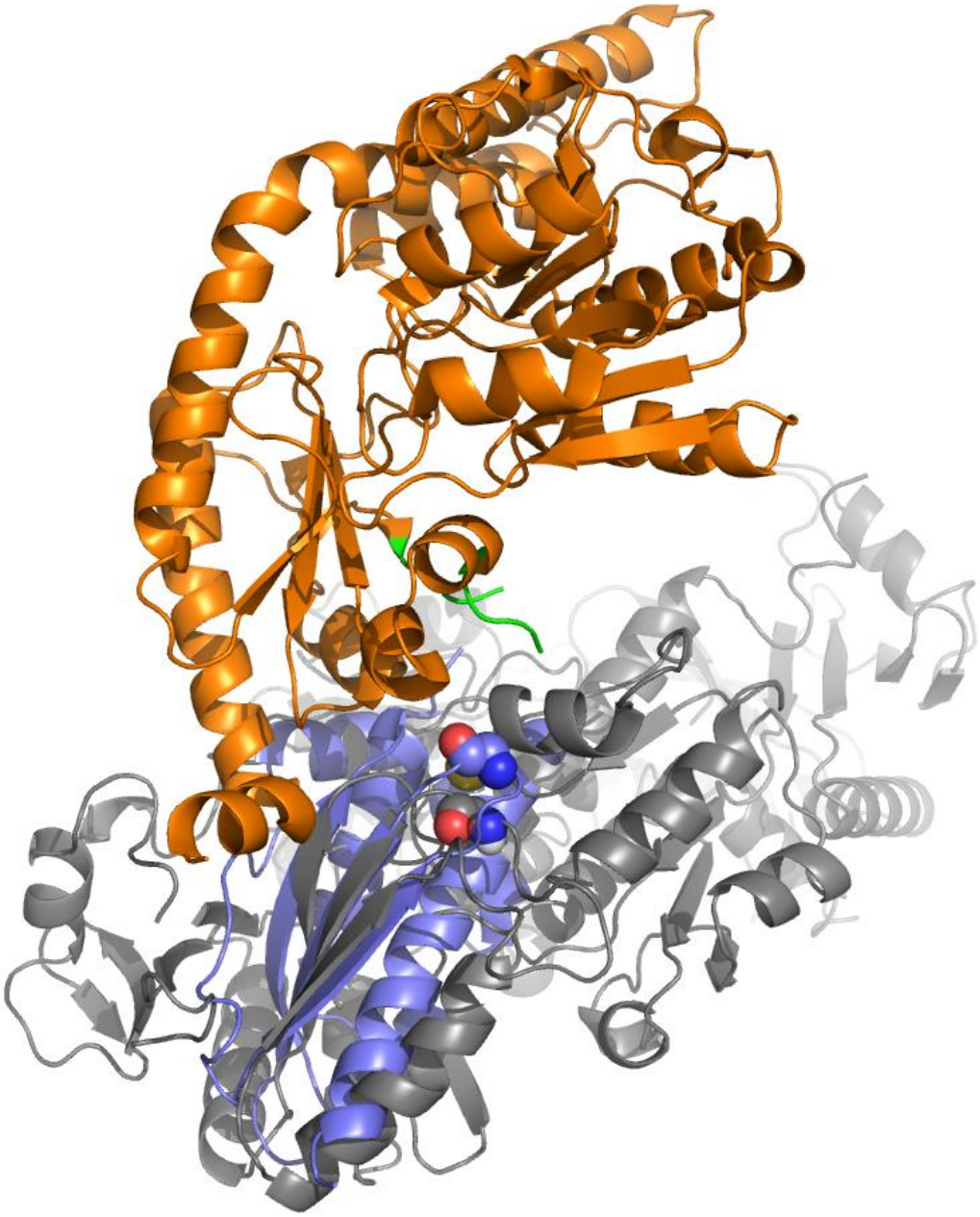

Figure 6.18 *Overlay of the structures of XdhC and IscU (bound to IscS).* The x-ray crystal structure of IscU (violet ribbons) with IscS bound (orange ribbons) (PDB ID: 3LVL), is superimposed upon the structure of the XdhC homolog from *Bacillus halodurans* as shown in Figure 6.17.The loop which is proposed to deliver the persulfide from the active site of IscS to IscU is colored green.

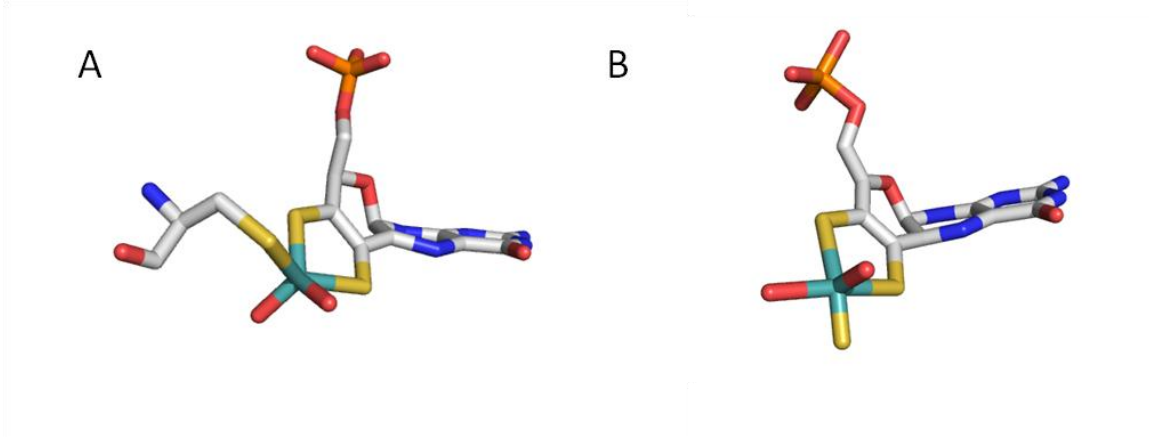

Figure 6.19 *The coordination geometries of the molybdenum center in the sulfite oxidase and xanthine oxidase families.* The coordination geometry of plant sulfite oxidase (A) and *R. capsulatus* xanthine dehydrogenase (B) are shown. It is to note that the coordination geometries are flipped in respect to the dithiolene of the pterin cofactor.

6.5 The insertion complex model

6.5.1 Recombinant expression of the hinge fragment

The highly conserved nature of the overall structure of the hinge region among members of the xanthine oxidase family suggests that it plays an important role in the binding of the cofactor insertion machinery. Recombinant expression of the hinge in *E. coli* has been attempted to determine whether a stable dimer could be formed in the absence of the rest of the protein, and whether it might be recognized by XdhC.

The 142 amino acid hinge fragment along with a 6-His tag connected to the N-terminus via a 4amino acid linker (Figure 2.2, Chapter 2.1) has been expressed in BL21 cells according to the methods outlined in Chapter 2. Initial purification by Ni-NTA and Ni-TED chromatography and subsequent separation by size exclusion shows a few prominent peaks (Figure 6.20, top), but SDS-PAGE results show multiple proteins which all appeared to associate with the hinge (Figure 20, bottom). Subsequent expression efforts also suggest a number of proteins consistently co-purify with the recombinant hinge. Concentration steps and freezing during purification cause the hinge and some of the other proteins to be fairly unstable and precipitate out of solution. The spectral analysis of several purification steps show absorption in the 420nm range, which could correspond to the presence of PLP, flavin, or heme. In one instance, purification yielded a protein with the spectral characteristics and activity of xanthine dehydrogenase. Previously published data has shown that the *E. coli* XdhC homolog can act upon the *R.* capsulatus xanthine dehydrogenase and it has long been known that XdhC is not very stable (43). If the hinge region is involved with interactions with XdhC, native *E. coli*

XdhC homologs could be pulled down during purification and in turn precipitate with the hinge fragment still attached. The estimated molecular weights of several bands from the SDS-PAGE gels have been compared to known molecular weights of characterized *E. coli* proteins homologous to XDH or involved in the final steps of cofactor maturation in the xanthine oxidase family of enzymes in *E. coli.* Several bands in the various SDS-PAGE gels exhibit molecular weights comparable in molecular weight to XdhA, XdhB, XdhC, XdhD, a NifS homolog, and the expressed hinge.

6.5.2 Modeled complexes of NifS, XdhC, and R. capsulatus XDH

Based upon the possibility of several enzymes co-purifying with the hinge fragment, the presence of gel bands corresponding to hinge, a protein of similar molecular weight to XdhC and another band of similar molecular weight to a NifS-like protein raises the possibility of a ternary NifS:XdhC:hinge(XDH) complex (Figure 6.21). While the hinge fragment pulling down an XdhC bound to NifS would suggest such a complex, alternative methods by which a sulfide could be transferred from NifS to the bound molybdenum center in XdhC, followed by subsequent insertion of the sulfurated molybdenum cofactor into XDH without dissociation of the NifS and association of XDH can be envisaged where XdhC, NifS and apo xanthine dehydrogenase would create a ternary complex.

The structure of the XdhC homolog from *Bacillus halodurans* (PDB ID: 3ON5) contains numerous surface indentations and unresolved flexible loops. Only one of the monomers in the asymmetrical unit shows a clearly resolved loop containing the

conserved cysteine residue in its MOSC domain. Using the MOLE 2.0 program (73), we have located several networks of internal cavities of various sizes. With the molybdenum cofactor binding site located along the dimerization face, a tunnel is seen that runs from the conserved cysteine along the dimerization domain roughly 120° from the proposed binding site of XDH in Section 6.2.2 (Figure 6.22). As seen in Figure 6.23, the tunnel is lined by cysteine residue 53, adjacent to two histidines (residues 252 and 253); analogous to what is seen in the active site of NifS (95). Beyond the two histidines is the conserved Cys 92. In this model, the NifS-homolog CsdB has been docked at the end of the tunnel (Figure 6.24 and 6.25) on the basis of structural and charge complementarities. Sulfuration of the molybdenum cofactor would occur through the cleavage of L-cysteine to produce L-alanine and a persulfide on the cysteine of the flexible loop in the active site. The flexible loop of NifS would then be able to deliver the persulfide to cysteine 53. We assume that since the dimerization domain is unresolved in the other half of the asymmetric unit, the sulfide can be transferred from cysteine to cysteine through modest conformational change of the loops and cysteine residues and facilitated through the help of the histidines (as in the active site of CsdB/NifS (95)). Transfer of the sulfide through this tunnel would allow for the sulfide to be effective transfer to the molybdenum cofactor and allow for subsequent insertion of the cofactor into the active site of XDH without having to dissociate from NifS and then bind to the bacterial XDH given the observed instability of XdhC.

After initial docking of the *E. coli* NifS homolog (CsdB) to the XdhC homolog from *Bacillus halodurans*, both have been docked to the wild-type *R. capsulatus* xanthine

dehydrogenase identically to the “top-down” insertion model described in Section 6.3.2. Interestingly, the complex of the NifS homolog: XdhC homolog complex fits with the initial binding of XdhC to the hinge region. The interdomain cleft within each monomer of XdhC is still complementary to the inserts in the hinge of XDH and the clefts corresponding to the dimerization interface remain adjacent to the two inserts away from the XDH hinge. The interface between the NifS homolog and the XdhC homolog is adjacent to the second insert of XDH (residues 381-398) (Figure 6.26) and is roughly rotated 90° clockwise from the orientation modeled after the binding of IscS and IscU. The three-way interface thus identified allows for a strong interaction between apo XDH and XdhC, as well as stabilization of NifS and XdhC via interaction with the unresolved XDH loop. While this model suggests an interaction between XDH and NifS, the interaction need not be as stable as the hinge-XdhC interaction implying that NifS does not bind to XDH alone, consistent with the observation of Neumann et al.(47).

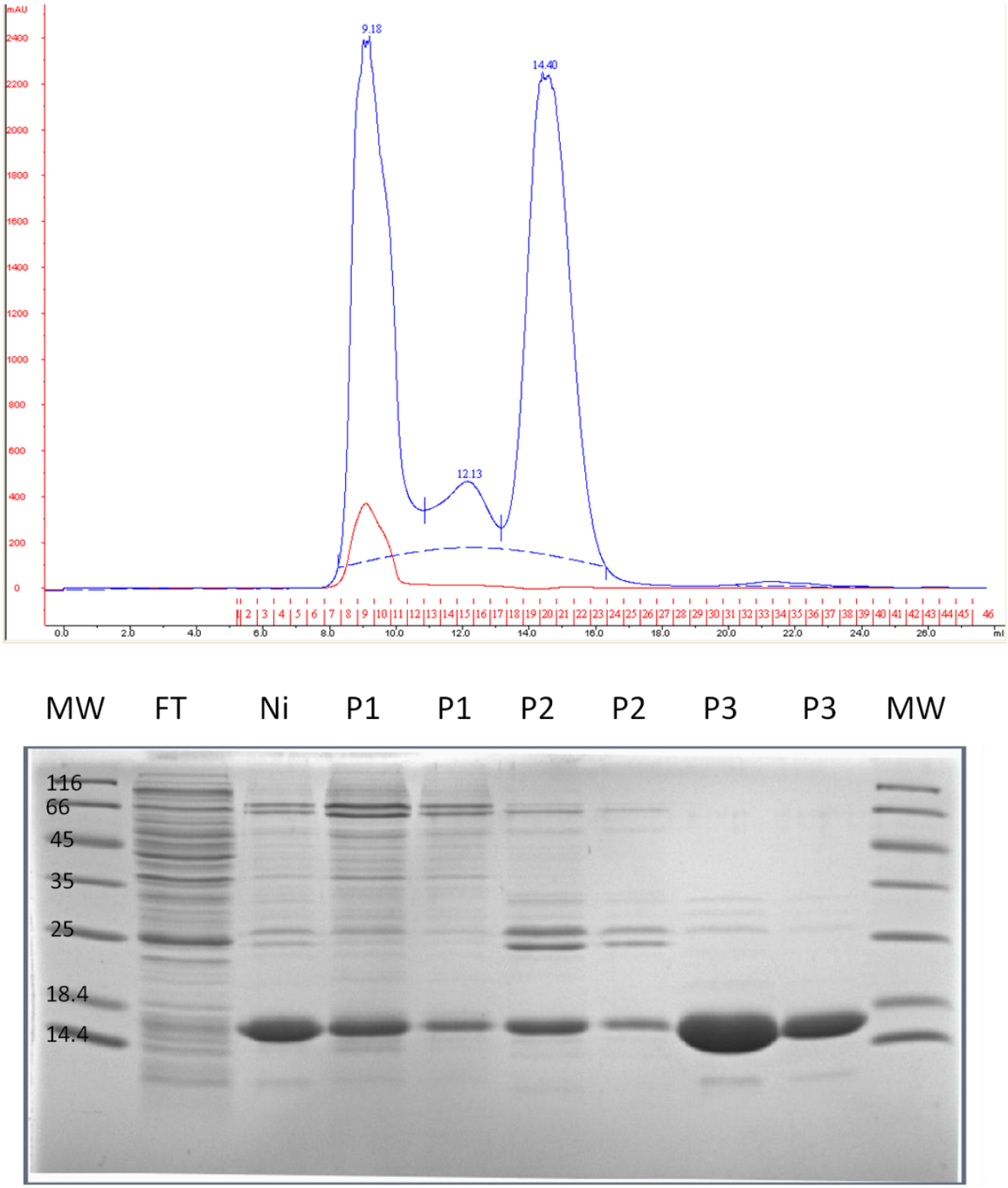

Figure 6.20 *Superdex 75 elution profile and SDS-PAGE analysis of a Ni-NTA elution sample from BL21 cells expressing the his-tagged hinge fragment*. (Top) Absorbance (mAU) versus time (minutes) is plotted. Absorbance at 280nm is in blue while absorbance at 415 is in red. Fraction collection numbers are indicated in red above the x-axis. (Bottom) The SDS-PAGE analysis of the Ni-NTA elution (Ni) and superdex 75 elution peaks 1-3 (P1-P3). Molecular weight markers (MW) are indicated on the left in kDa. The hinge fragment is found at 15kDa.

Figure 6.21 *Modeled complex of Hinge, NifS, and XdhC.* XdhC (PDB 3ON5) is shown in grey, *R. capsulatus* XDH hinge fragment (residues 465-605 from PDB 2W3S) is shown in brown, and the NifS homolog IscS (PDB 3LVL) is shown in orange. The hinge fragment is small enough that NifS could still bind to XdhC, potentially allowing for complexes of these three to be pulled down with the His-tag on the hinge fragment.

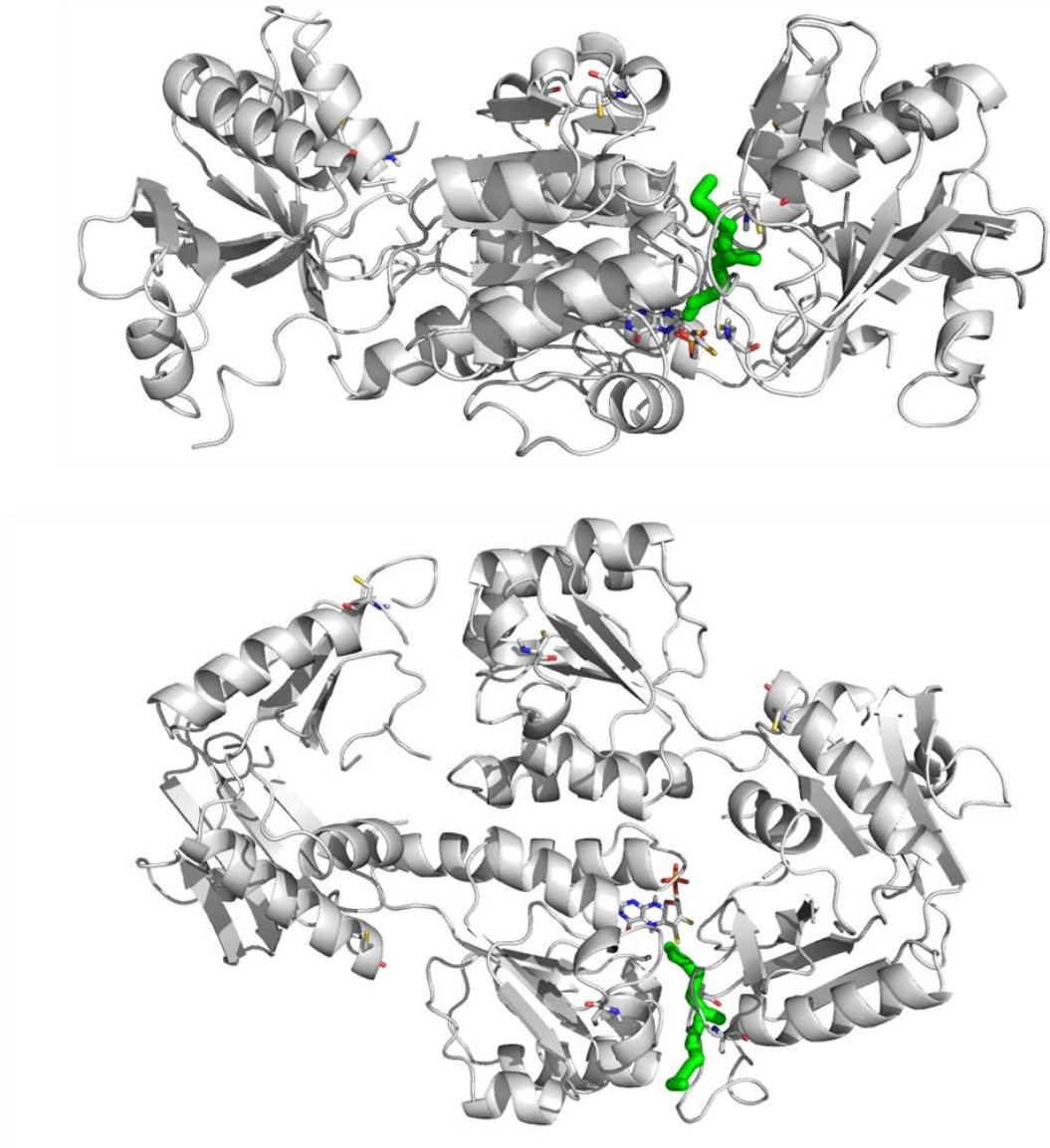

Figure 6.22 *Proposed sulfide transfer channel in XdhC*. The channel is traced by the green tube for the resolved dimer interface in the crystal structure of the XdhC homolog from *Bacillus halodurans* (PDB ID: 3ON5) The docked molybdenum cofactor is shown in stick representation in CPK color scheme.

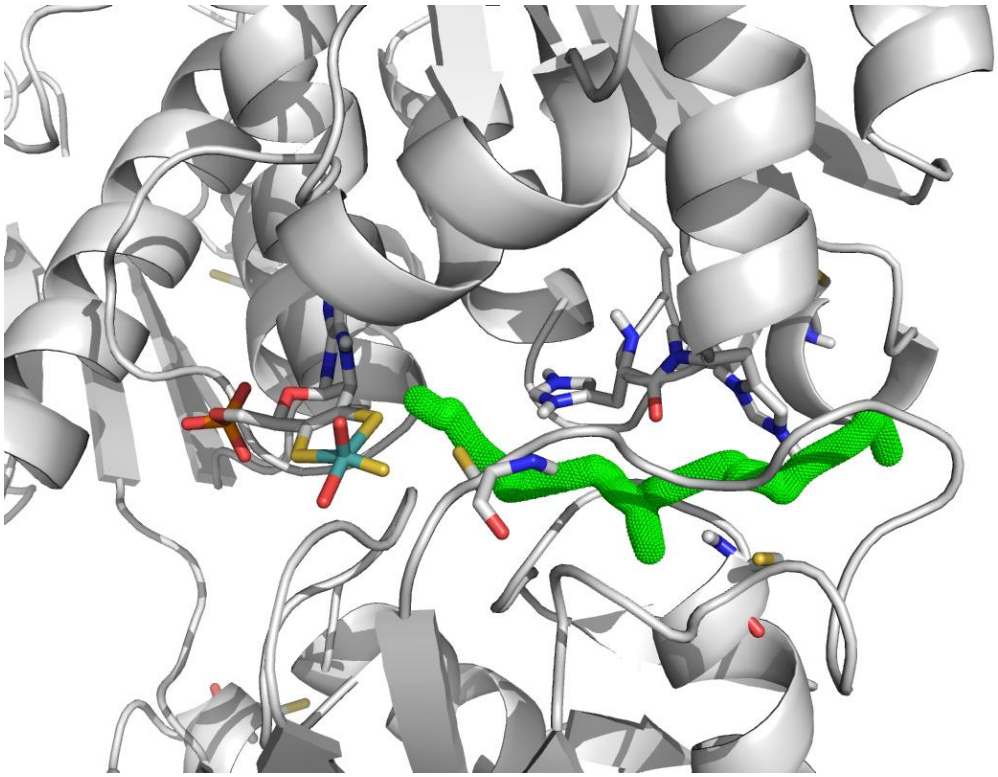

Figure 6.23 *Residues lining the proposed sulfide transfer tunnel.* The proposed tunnel that facilitates sulfide transfer is shown in green. The relevant structures in stick representations from left to right, beginning with the molybdenum center (cyan), Cys 92, His 252 and 253, and last, Cys 53. The Histidines line the "top" of the tunnel, while the cysteine residues line the "bottom."

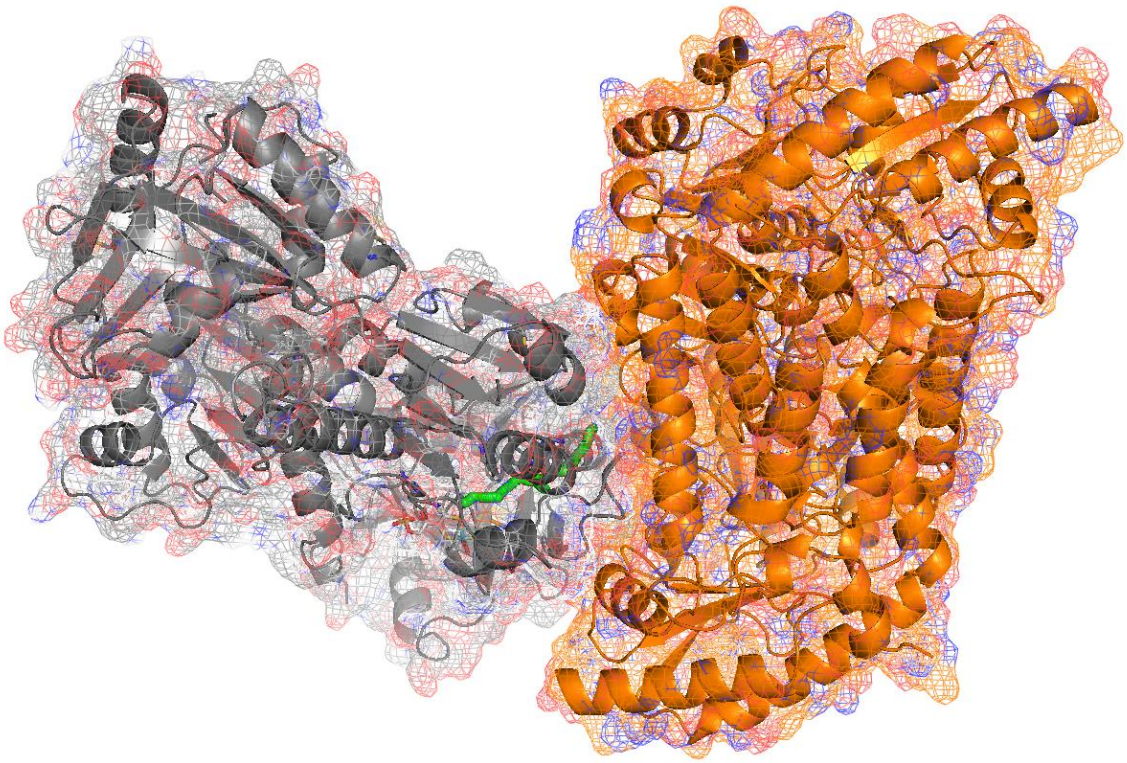

Figure 6.24 *The NifS homolog CsdB docked to the XdhC homolog from Bacillus halodurans.* The biological assemblies from the NifS homolog CsdB is shown in orange (PDB ID: 1KMJ) docked to the XdhC homolog from *Bacillus halodurans* is shown in gray (PDB ID: 3ON5). The proposed tunnel that facilitates sulfide transfer is shown in green.

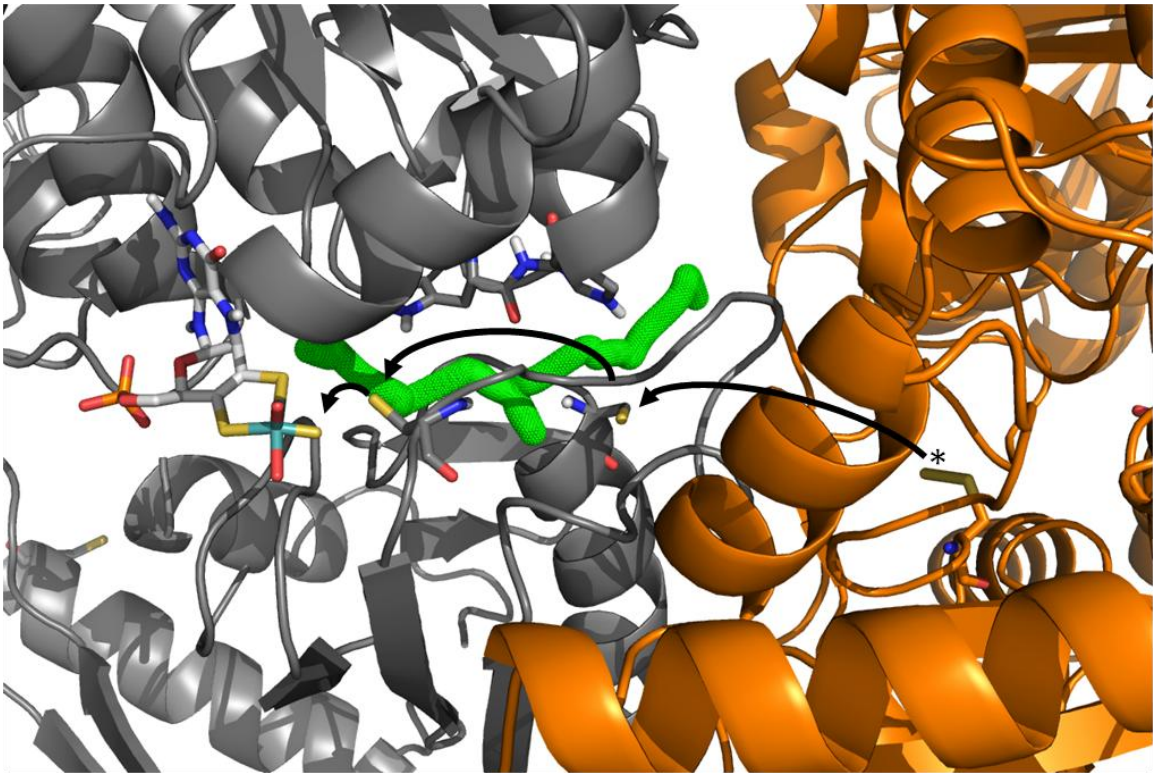

Figure 6.25 *Proposed method of sulfur transfer from the NifS to XdhC.* The biological assemblies from the NifS homolog CsdB is shown in orange (PDB ID: 1KMJ) docked to the XdhC homolog from *Bacillus halodurans* is shown in gray (PDB ID: 3ON5). The proposed tunnel that facilitates sulfide transfer is shown in green. The persulfide on Cys 364 of CsdB would transfer the persulfide to Cys 53, which would then end up on the conserved cysteine 92, and then finally on the molybdenum cofactor.

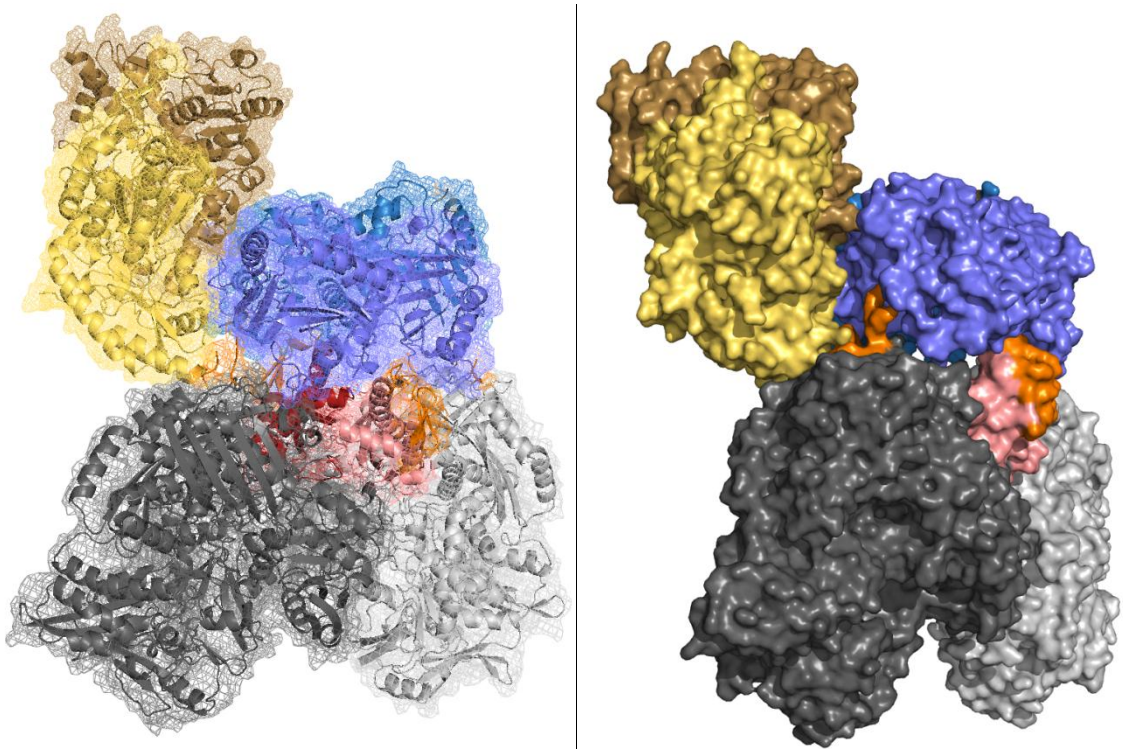

Figure 6.26 *The docking of the NifS homolog CsdB, XdhC homolog, and R. Capsulatus XdhAB.* The crystal structure of CsdB/NifS from *E. coli* is docked to the XdhC homolog from *Bacillus halodurans* (PDB ID 3ON5) and the *R. capsulatus* XDH (PDB ID: 2W3S) is shown. Monomers of the dimer of CsdB/NifS are shown in yellow and gold. Monomers of the dimer of the XdhC homolog are shown in blue and purple. Monomers of the dimer of the *R. capsulatus* XDH are in shades of grey, with the hinge region, described in section 6.2, in shades of red and the inserts, also described in section 6.2, in orange. The image on the left is rendered in cartoon with mesh surface shown, while the image on the right is shown with a solid surface.

6.6 Summary

The current work has identified multiple models for the maturation and insertion of the molybdenum cofactor into the xanthine oxidase family of enzymes. In the xanthine oxidase family of enzymes, a conserved hinge region has been identified that could act as a target for XdhC. The currently known structures of XdhC and NifS homologs have provided a starting point for the modeling of the complex that carries out insertion of the molybdenum cofactor. Docking studies with the molybdenum cofactor and the XdhC homolog from *Bacillus halodurans* show similar binding of both the MPT and MCD forms of the cofactor. Using the models for the docked molybdenum cofactor, docking of the XdhC homolog to *R. capsulatus* xanthine dehydrogenase suggests that a large rotation of the hinge region would be less likely than a more modest rotation/translation of the hinge, in conjunction with movement of several loops adjacent to the hinge region, resulting in a "top-down" insertion (Figure 6.16) rather than a "side-on" insertion (Figure 6.7).

Investigation of molybdenum cofactor sulfuration while bound to XdhC also presents several possible models. The binding of NifS-4 may occur in one of two ways. NifS-4 could bind to XdhC analogously to the crystallographically observed IscS-IscU complex, based upon structural similarities in a motif near the conserved cysteine residue 92 (which also appears in the same place IscU). The binding of NifS-4 to XdhC in a manner similar to the binding of IscS to IscU would result in NifS-4 and XDH not being able to bind to XdhC at the same time. NifS-4 would have to sulfurate XdhC or the cofactor, and then dissociate so that apo-XDH could bind and have the cofactor inserted,

consistent with the current model proposed by Neumann and Leimkühler (43). Investigation of cavities within XdhC illustrate another possible way for sulfur to be transferred from NifS-4 to XdhC, however evidence suggests that XdhC does not insert desulfo-molybdenum cofactor (43), and a model in which a ternary complex of XdhC, NifS-4 and XDH would allow for tight coupling of sulfuration and insertion of the molybdenum cofactor, thereby reducing the chances of oxidative degradation of the molybdenum cofactor. Given the proximity of the conserved cysteine to the bound molybdenum cofactor, this residue could either be sulfurated to give a persulfide which could then donate a sulfide to the molybdenum cofactor, or act as a covalent linkage from the enzyme to the molybdenum center. The models produced in these studies provide a starting point for future studies elucidate to verify the mechanism for which sulfuration and insertion of the molybdenum cofactor occurs.

CHAPTER 7

CONCLUSIONS

7.1 SUMMARY

7.1.1 The roles of the active site residues on substrate specificity, substrate orientation and catalysis

Xanthine oxidase catalyzes the hydroxylation of a broad variety of purines, heterocycles, and aldehydes (39). The reductive half-reaction follows a mechanism where substrate is hydroxylated at specific sp^2-hybridized carbon centers. The reaction begins with Glutamate 1261 (Glu 730 in the *R. capsulatus* xanthine dehydrogenase) abstracting a proton from the equatorial molybdenum hydroxyl group, which allows the $Mo\text{-}O^-$ to undertake nucleophilic attack on the substrate. Simultaneously, a hydride transfer occurs from the carbon to the Mo=S group. At this point, an intermediate is formed where the heterocycle is now coordinated to the molybdenum center by the newly incorporated hydroxyl group. The reaction is completed with the displacement of product from the molybdenum center by solvent hydroxide, thus regenerating the equatorial molybdenum hydroxyl group for a subsequent catalytic cycle.

The active site is highly conserved among the xanthine-hydroxylating enzymes from various species, and Glu 1261/Glu 730 has been shown to be required for activity as mutation studies of this residue to alanine in the *R. capsulatus* XDH resulted in a 10^7-fold decrease in the limiting rate of reduction by xanthine (36). Based upon the crystal structure, substrates intercalate between the phenylalanines 914 and 1009 (Phe 344 and

Phe 459 in the *R. capsulatus* XDH), which together serve to orient the substrate perpendicular to the equatorial plane of the molybdenum center, allowing for simultaneous nucleophilic attack and hydride transfer. Arginine 880 (Arg 310 in the bacterial XDH) is only conserved in enzymes acting upon aromatic heterocycles, and is often a methionine in the otherwise closely related aldehyde-hydroxylating molybdenum-containing enzymes. Arg 880 and Glu 802 (residues 310 and 232 in the bacterial enzyme, respectively), sit below and above the substrate, respectively. Structural and kinetic studies suggest that residues Arg 880 and Glu 802 play a role in substrate binding and orientation, as well as transition state stabilization (36,37,56).

From the work presented in this thesis, the roles of Glu 232 and Arg 310 (Glu 802 and Arg 880 in bovine xanthine oxidase) have been shown to be crucial in the binding of substrate and stabilization of the transition state. In Chapter 3, the properties of the *R. capsulatus* E232Q variant were described. Removal of the ionizable group of Glu 232 was shown to result in a shift in the observed pH profile of k_{red} and a decrease in k_{red}. Given the significant decrease in k_{red}, it is clear that Glu 232 is in fact deprotonated at the onset of catalysis, consistent with it functioning catalytically to facilitate tautomerization of the substrate in the course of catalysis. Furthermore, the decrease in k_{red} as pH increased above pH 7.4 for the E232Q variant (which does not occur in the wild-type enzyme until above pH 8.5) suggests that the negative charge of Glu 232 discriminates against binding of the monoanionic form of xanthine, which is expected to be significantly less susceptible to nucleophilic attack than the neutral form. The negative charge on xanthine resonates between N3 and O2, which in turn does not allow for

xanthine to stably bind in the "right-side up" conformation due to the proximity of negative charges on both xanthine and Glu 232/802. We propose that glutamate 232/802 provides specificity towards the neutral form of the substrate, thereby enhancing the efficiency in catalysis and broadening the pH range for which the enzyme maintains activity.

The positive charge on Arg 310/880 likely interacts with the negative charge on the monoanionic form of xanthine resulting in binding of substrate in the "upside-down" conformation as in the observed crystal structures of demolybdo rat xanthine oxidoreductase complexed with urate and the crystal structure of reduced bovine xanthine oxidoreductase with urate bound (82). In the "upside-down" conformation would also be expected to be significantly less susceptible to nucleophilic attack than the neutral form because the negative charge on xanthine would repel the incoming nucleophilic attack by the Mo-OH (65).

In Chapter 4, we demonstrated a single dominant orientation for binding of both indole-3-aldehyde and guanine in the active site of bovine xanthine oxidase, both of which are expected to be catalytically non-productive on the basis of the distance of the site to be hydroxylated from the catalytically labile equatorial Mo-OH of the enzyme's molybdenum center. In the case of indole-3-aldehyde, while substrate is readily accommodated between Phe 914 and 1009 that define the substrate binding pocket, Arg 880 hydrogen-bonds to the exocyclic aldehyde group that is hydroxylated in such a way that the carbonyl carbon is held approximately 5.4 Å from the Mo-OH oxygen. In order to orient more appropriately for catalysis, substrate must rotate some 30° to bring the

exocyclic carbonyl into catalytic range of the Mo-OH group. This modest motion appears readily allowed sterically in the active site; although it involves disruption of the hydrogen bond with Arg 880, the hydrogen bond with Glu 802 is likely maintained (as are the hydrophobic contacts with Phe 914 and 1009). It is likely that kT is sufficient to populate the catalytically effective orientation at least a portion of the time, in which case the situation is equivalent to the near attack conformation model developed by Hur and Bruice (84-86), in which thermally populated configurations of the Michaelis complex play an important role in facilitating the transition state (and conversely, non-productive orientations can result in a lower observed rate of reaction). Such an interpretation is consistent with the small but finite value seen for k_{red} with indole-3-aldehyde (0.13 s^{-1}). Interestingly, while substitution of Arg 310 (Arg 880 in the bovine enzyme) with methionine resulted in a decrease in observed k_{red} with xanthine as a substrate, it resulted in an increase in the observed k_{red} with indole-3-aldehyde as a substrate. The removal of the positive charge of Arg 310 thus appears to eliminate the unfavorable interaction holding the exocyclic aldehyde in a non-productive orientation, thus allowing an increase in observed limiting rate of reduction. This further supports the conclusion that the exocyclic aldehyde's interaction with Arg 310/880 is the primary cause of the observed low reactivity of the enzyme toward indole-3-aldehyde.

In the case of the complex of enzyme with guanine, a catalytically ineffective orientation is again observed in the crystal structure, with the C8 position that might otherwise become hydroxylated oriented away from the equatorial molybdenum hydroxyl. The principal interactions that hold guanine in this unfavorable orientation are

with Glu 802 (interacting with N1 and the C2 amino group) and Arg 880, hydrogen-bonding to the C6 keto group. A rotation of guanine between the two phenylalanines of ~180° is required to juxtapose its C8 position with the molybdenum center. A rotation of that magnitude would require the network of hydrogen bonds to be broken, and there is also significant steric hindrance with Glu 802 and Arg 880. Guanine would have to dissociate and re-associate with the protein in the correct orientation for C8 to be hydroxylated. The unfavorable binding of guanine is highly advantageous for the cell due to the fact that the product of enzyme action on guanine, 8-hydroxyguanine, is highly mutagenic. It is likely that the enzyme's active site has evolved in such a way to preferentially bind guanine in a dominantly nonproductive manner in order to prevent production of 8-hydroxyguanine.

In Chapter 5, we determined tritium isotope effects and intrinsic deuterium isotope effects on the reductive half reaction of wild-type and Q197A variant of *R. capsulatus* xanthine dehydrogenase and established in each (consistent with earlier work for bovine xanthine oxidase (66)) that the limiting rate of the chemical step ($k_{C\text{-}H}$) was ~62-fold faster than the observed limiting rate of the reaction (k_{cat}), for wild-type XDH that $k_{C\text{-}H}$ is ~11.5-fold faster than k_{cat}, and for the Q197A variant $k_{C\text{-}H}$ is ~2.6-fold faster than k_{cat}. The rate constant for the chemical step of the reaction for each of the enzymes was estimated, yielding values of 930 s^{-1} and 802 s^{-1} for bovine xanthine oxidase and the bacterial xanthine dehydrogenase, respectively. These results indicate that the increased rate of the bacterial enzyme is not due to a faster chemical step of the reaction, but to an increase in the rate of product release. With regard to the Q197A XDH variant, the

increase in k_{cat} as compared to the wild-type is actually accompanied by a decrease in the rate constant for the chemical step, the higher k_{cat} value being due to an increase in the rate of product release. We note that replacing the glutamine with alanine creates a small pocket in the active site above the molybdenum center that could accommodate one or more water molecules, thus increasing the local concentration of water around the molybdenum center which would account for the rate of product displacement from the molybdenum coordination sphere by hydroxide. The change in the rate constant for the chemical step of the reaction for the Q197A variant along with the observed decrease in k_{cat} of the Q197E variant suggests that the hydrogen-bonding interaction of Gln 197 with the axial Mo=O directly modulates the reactivity of the molybdenum center, possibly by electrostatically facilitating its two-electron reduction in the course of electron transfer.

7.1.2 Maturation and Insertion of the Molybdenum Cofactor into the Xanthine Oxidase Family of Molybdenum-Containing Enzymes

The work presented in Chapter 6 described multiple models for the sulfuration and insertion of the molybdenum cofactor into members of the xanthine oxidase family of enzymes. A conserved hinge region was identified that could act as a target for XdhC. The currently known structures of XdhC and NifS homologs provide a starting point for the modeling of the complex that carries out insertion of the molybdenum cofactor. Docking studies with the molybdenum cofactor and the XdhC homolog from *Bacillus halodurans* show similar binding of both the MPT and MCD forms of the cofactor. Docking the molybdenum cofactor bound model of the XdhC homolog to *R. capsulatus*

xanthine dehydrogenase suggests that a large rotation of the hinge region is less likely than a more modest rotation/translation of the hinge, in addition to movement of the several loops adjacent to the hinge region, resulting in a "top-down" insertion (Figure 6.16) rather than a "side-on" insertion, as seen in the hinge rotation model (Figure 6.7).

Investigation of molybdenum cofactor sulfuration while bound to XdhC also resulted in several possible models. The binding of NifS-4 to XdhC may occur in one of two ways. In the first model, NifS-4 could bind to XdhC analogously to the crystallographically observed IscS-IscU complex. This is based upon structural similarities in a motif near the conserved cysteine residue 92 (which also appears in the same place IscU). This would not allow XDH to bind to XdhC at the same time as NifS-4. NifS-4 would have to sulfurate XdhC or the cofactor, and then dissociate so that apo-XDH could bind and have the cofactor inserted, consistent with the current model proposed by Neumann and Leimkühler (43). Alternatively, investigation of cavities within XdhC illustrate another possible way for sulfur to be transferred from NifS-4 to XdhC. Although the evidence suggests that XdhC does not insert desulfo-molybdenum cofactor (43), a model in which a ternary complex of XdhC, NifS-4 and XDH would allow for tight coupling of sulfuration and insertion of the molybdenum cofactor, thereby reducing the chances of oxidative degradation of the molybdenum cofactor. Given the proximity of the conserved cysteine 92 of XdhC to the bound molybdenum cofactor, this residue could either be sulfurated to give a persulfide which could then donate a sulfide to the molybdenum cofactor, or act as a covalent linkage from the enzyme to the molybdenum center. The models produced in these studies provide a starting point for

future studies elucidate to verify the mechanism for which sulfuration and insertion of the molybdenum cofactor occurs.

7.2 FUTURE DIRECTIONS

Xanthine oxidase has been studied for more than a century. Since its discovery, the biological and medical implications of its activity have been described, steady-state and rapid-reaction kinetics have revealed many details of the reaction mechanism and X-ray crystal structures have given insight into its structure. More recently, the development of an expression system for *R. capsulatus* xanthine dehydrogenase in *E. coli* has made possible mutational studies to examine the roles of the active site residues. Even though much has been characterized, there is still much to be investigated.

With the discovery of XanA, a non-molybdenum containing xanthine oxidase in fungi that lacks structural similarity to the molybdenum-containing xanthine oxidase family of enzymes and instead utilizes iron (II) and α-ketoglutarate to hydroxylate xanthine (25), similar experiments to those done on the bovine xanthine oxidase and bacterial xanthine dehydrogenase could be performed. Kinetic studies and mutational studies on the substrate binding site to gain insight into mechanism and substrate specificity in this enzyme system could then be compared to the molybdenum-containing enzymes. One question to be investigated whether the fungal xanthine oxidase is able to discriminate against substrates in a manner similar the molybdenum-containing systems. The ability to discriminate against substrates such as guanine would deter the formation

of harmful products in the cell and would be interesting to see if convergent evolution has led to similar methods of discrimination against unfavorable substrates in XanA.

Many purine substrates of xanthine oxidase exhibit multiple ionic forms as a function of pH. In the case xanthine as a substrate, the neutral form is the only form acted upon by enzyme. Although this has been shown with xanthine and 2-hydroxy-6-methylpurine (53), it has yet to be demonstrated that this is the case with all purine substrates. Investigation of the effect of pH on substrate binding of using X-ray crystallography could explain why the "right-side up" and "upside-down" orientations of purine substrates have been observed. For example uric acid exists as a monoanion at neutral pH. Going to a lower pH for crystallization could result in an inversion of the binding of uric acid as seen crystallographically. Glu 232 variants (such as the E232Q) could be better able to accommodate monoanionic urate resulting in variations in observed rate of the reverse reaction. Implications such studies would provide more knowledge about the functions of the active site residues.

In regard to the mechanism of xanthine dehydrogenase and the roles of the active site residues, re-examination of the kinetic isotope effects for the Q197E, E232Q, E232A and R310M variants of the *R. capsulatus* xanthine dehydrogenase would define the contributions of the amino acid residues towards the chemical step of the reaction or product release. Investigation of the Q197E variant would be particularly interesting. If a significant decrease in the rate of chemical step of the reaction was observed it would support that the role of Gln 197 (being within hydrogen bonding distance of the axial

Mo=O) is to stabilize the charge accumulation on the molybdenum center during catalysis.

Computational substrate docking and X-ray crystallography remain key tools for drug design targeting xanthine oxidase. Xanthine oxidase has been known to metabolize the chemotherapeutic agent 6-mercaptopurine (100) and can generate reactive oxygen species causing oxidative stress or production of uric acid which in high levels can result in the painful condition gout (101). In the case of thiopurine anti-inflammatories and chemotherapeutic agents, inhibition of the enzyme allows for more efficient treatment with smaller doses (102). Although several xanthine oxidase inhibitors are on the market (103), the design of stable compounds with fewer side-effects, higher affinity, higher specificity towards xanthine oxidase and efficient cellular incorporation are always being sought. The roles of the active site residues and influence of pH on substrate binding and orientation could play a large role in future drug design.

Another group of studies to be an examination of the method of sulfuration and incorporation of the molybdenum cofactor in the xanthine oxidase family of enzymes. While many of the involved proteins are known, it is not clear how the proteins physically interact to facilitate the final two steps of cofactor maturation and insertion in the xanthine oxidase family. Removal of the hinge inserts described in Chapter 6 would be a method to determine if the inserts are required for recognition and binding of XdhC. Surface Plasmon resonance or isothermal titration calorimetry could be used to probe the binding affinity of the hinge fragment (or a modified hinge fragment, lacking the inserts not found in the bovine enzyme) to XdhC, which then could be compared to the currently

published values for the bacterial xanthine dehydrogenase towards XdhC. Similar affinities would suggest that the hinge is the site where XdhC binds.

Crystallization of the bacterial hinge alone could provide evidence for the folding and dimerization of the hinge region in absence of the rest of xanthine dehydrogenase, supporting the hinge model proposed in Section 6.2. Crystallization of the hinge fragment in complex with XdhC and/or NifS-4 would provide important structural information on how the cofactor machinery could interact with the apo-enzyme to facilitate the maturation of the cofactor. If x-ray crystallography is not feasible, NMR could be used to look at the hinge fragment structure and flexibility in solution. In Chapter 6, evidence of the formation of a complex containing hinge and protein with similar molecular weight to *E. coli* NifS and XdhC was presented. Small-angle X-ray scattering (SAXS) could be used for investigation of the structure of the complex presumed to be pulled down with the hinge fragment. Even though the structure would be of low resolution, the currently described crystal structures of XdhC, NifS-4 and bacterial XDH could be used as models for fitting the electron density obtained. All of these experiments could also be attempted with the eukaryotic xanthine dehydrogenases or aldehyde oxidases to describe interactions with their cofactor maturation and insertion machinery (ABA3 or HMCS).

Lastly, characterization and comparison of XdhC- like enzymes, iron-sulfur cluster assembly proteins (like IscU (96)) and radical S-adenylmethionine enzymes (like QueE from *Burkholderia multivorans* (104)) could reveal conserved structural motifs characteristic of sulfur chemistry. Many enzymes involved with sulfur chemistry in the cell tend to be highly conserved, so similarities in motifs would suggest evolutionary

adaption of ancient iron-sulfur assembly proteins to carry out diverse enzymatic reactions or convergent evolution of various proteins to resemble a similar structural motif allowing for sulfuration. Confirmation of a similarity between the binding and action of NifS-4 to XdhC and IscS to IscU would imply that motifs involved in sulfur chemistry in the cell are conserved between iron-sulfur assembly enzymes, and enzymes involved in the sulfuration of molybdenum centers. The study of the similarities and differences in the prokaryotic and eukaryotic systems involved with sulfur trafficking will likely be an interesting direction for future studies providing insight into the evolution of the systems and the complex mechanisms they facilitate.

Portions of this dissertation are adapted from the following publications:

Cao, H., Hall, J. and Hille, R. (2014) Substrate Orientation and Specificity in Xanthine Oxidase: Crystal Structures of the Enzyme in Complex with Indole-3-acetaldehyde and Guanine *Biochemistry 53* (3), 533-541.

Hille, R., Hall, J., Basu, P. (2014) The Mononuclear Molybdenum Enzymes. *Chemical Reviews* **Article ASAP.**

References

1. Kletzin, A., and Adams, M. W. W. (1996) Tungsten in biological systems. *FEMS Microbiology Reviews* **18**, 5-63

2. Schwarz, G., Hagedoorn, P.-L., and Fischer, K. (2007) Molybdate and Tungstate: Uptake, Homeostasis, Cofactors, and Enzymes. in *Molecular Microbiology of Heavy Metals* (Nies, D., and Silver, S. eds.), Springer, Berlin Heidelberg. pp 421-451

3. Hille, R. (2002) Molybdenum and tungsten in biology. *Trends in Biochemical Sciences* **27**, 360-367

4. Magalon, A., Fedor, J. G., Walburger, A., and Weiner, J. H. (2011) Molybdenum enzymes in bacteria and their maturation. *Coordination Chemistry Reviews* **255**, 1159-1178

5. Silberberg, M. S. (2003) *Chemistry: The Molecular Nature of Matter and Change* Kent A. Peterson, New York, NY

6. Mitchell, P. C. H. (2003) *Molybdenum*, American Chemical Society, Washington, DC, ETATS-UNIS

7. Emsley, J. E. (1991) *The elements* 2nd ed. ed., Oxford University Press. , New York

8. Kim, H. J., Ricardo, A., Illangkoon, H. I., Kim, M. J., Carrigan, M. A., Frye, F., and Benner, S. A. (2011) Synthesis of carbohydrates in mineral-guided prebiotic cycles. *Journal of the American Chemical Society* **133**, 9457-9468

9. Hille, R. (1996) The Mononuclear Molybdenum Enzymes. *Chemical reviews* **96**, 2757-2816

10. Raaijmakers, H., Macieira, S., Dias, J. M., Teixeira, S., Bursakov, S., Huber, R., Moura, J. J. G., Moura, I., and Romão, M. J. (2002) Gene Sequence and the 1.8 Å Crystal Structure of the Tungsten-Containing Formate Dehydrogenase from Desulfovibrio gigas. *Structure* **10**, 1261-1272

11. Chan, M., Mukund, S., Kletzin, A., Adams, M., and Rees, D. (1995) Structure of a hyperthermophilic tungstopterin enzyme, aldehyde ferredoxin oxidoreductase. *Science* **267**, 1463-1469

12. Hagedoorn, P.-L., Hagen, W. R., Stewart, L. J., Docrat, A., Bailey, S., and Garner, C. D. (2003) Redox characteristics of the tungsten DMSO reductase of Rhodobacter capsulatus. *FEBS Letters* **555**, 606-610

13. Johnson, J. L., and Rajagopalan, K. V. (1976) Electron paramagnetic resonance of the tungsten derivative of rat liver sulfite oxidase. *The Journal of biological chemistry* **251**, 5505-5511

14. Lancaster, K. M., Roemelt, M., Ettenhuber, P., Hu, Y., Ribbe, M. W., Neese, F., Bergmann, U., and DeBeer, S. (2011) X-ray emission spectroscopy evidences a central carbon in the nitrogenase iron-molybdenum cofactor. *Science* **334**, 974-977

15. Yang, Z. Y., Dean, D. R., and Seefeldt, L. C. (2011) Molybdenum nitrogenase catalyzes the reduction and coupling of CO to form hydrocarbons. *The Journal of biological chemistry* **286**, 19417-19421

16. Hille, R. (2013) The molybdenum oxotransferases and related enzymes. *Dalton transactions* **42**, 3029-3042

17. Romao, M. J., Archer, M., Moura, I., Moura, J. J., LeGall, J., Engh, R., Schneider, M., Hof, P., and Huber, R. (1995) Crystal structure of the xanthine oxidase-related aldehyde oxido-reductase from D. gigas. *Science* **270**, 1170-1176

18. Hille, R. (2005) Molybdenum-containing hydroxylases. *Archives of Biochemistry and Biophysics* **433**, 107-116

19. Solomonson, L. P., and Barber, M. J. (1990) Assimilatory Nitrate Reductase: Functional Properties and Regulation. *Annual Review of Plant Physiology and Plant Molecular Biology* **41**, 225-253

20. Kisker, C., Schindelin, H., Pacheco, A., Wehbi, W. A., Garrett, R. M., Rajagopalan, K. V., Enemark, J. H., and Rees, D. C. (1997) Molecular Basis of Sulfite Oxidase Deficiency from the Structure of Sulfite Oxidase. *Cell* **91**, 973-983

21. Krompholz, N., Krischkowski, C., Reichmann, D., Garbe-Schonberg, D., Mendel, R. R., Bittner, F., Clement, B., and Havemeyer, A. (2012) The mitochondrial Amidoxime Reducing Component (mARC) is involved in detoxification of N-hydroxylated base analogues. *Chemical research in toxicology* **25**, 2443-2450

22. Anantharaman, V., and Aravind, L. (2002) MOSC domains: ancient, predicted sulfur-carrier domains, present in diverse metal–sulfur cluster biosynthesis proteins including Molybdenum cofactor sulfurases. *FEMS microbiology letters* **207**, 55-61

23. Morgan, Stewart, and Hopkins. (1922). *Proc. Roy. Soc. London, B* **94**, 109

24. Dixon, M., and Thurlow, S. (1924) STUDIES ON XANTHINE OXIDASE. *The Biochemical journal* **18**, 971

25. Simmons, J. M., Muller, T. A., and Hausinger, R. P. (2008) Fe(II)/alpha-ketoglutarate hydroxylases involved in nucleobase, nucleoside, nucleotide, and chromatin metabolism. *Dalton transactions*, 5132-5142

26. Coelho, C., Mahro, M., Trincao, J., Carvalho, A. T., Ramos, M. J., Terao, M., Garattini, E., Leimkuhler, S., and Romao, M. J. (2012) The first mammalian aldehyde oxidase crystal structure: insights into substrate specificity. *The Journal of biological chemistry* **287**, 40690-40702

27. Enroth, C., Eger, B. T., Okamoto, K., Nishino, T., and Pai, E. F. (2000) Crystal structures of bovine milk xanthine dehydrogenase and xanthine oxidase: Structure-based mechanism of conversion. *Proceedings of the National Academy of Sciences of the United States of America* **97**, 10723-10728

28. Dobbek, H., Gremer, L., Meyer, O., and Huber, R. (1999) Crystal structure and mechanism of CO dehydrogenase, a molybdo iron-sulfur flavoprotein containing S-selanylcysteine. *Proceedings of the National Academy of Sciences* **96**, 8884-8889

29. Dobbek, H., Gremer, L., Kiefersauer, R., Huber, R., and Meyer, O. (2002) Catalysis at a dinuclear [CuSMo(==O)OH] cluster in a CO dehydrogenase resolved at 1.1-A resolution. *Proceedings of the National Academy of Sciences of the United States of America* **99**, 15971-15976

30. Truglio, J. J., Theis, K., Leimkühler, S., Rappa, R., Rajagopalan, K. V., and Kisker, C. (2002) Crystal Structures of the Active and Alloxanthine-Inhibited Forms of Xanthine Dehydrogenase from Rhodobacter capsulatus. *Structure* **10**, 115-125

31. Bonin, I., Martins, B. M., Purvanov, V., Fetzner, S., Huber, R., and Dobbek, H. (2004) Active site geometry and substrate recognition of the molybdenum hydroxylase quinoline 2-oxidoreductase. *Structure* **12**, 1425-1435

32. Unciuleac, M., Warkentin, E., Page, C. C., Boll, M., and Ermler, U. (2004) Structure of a xanthine oxidase-related 4-hydroxybenzoyl-CoA reductase with an additional [4Fe-4S] cluster and an inverted electron flow. *Structure* **12**, 2249-2256

33. Unciuleac, M., Boll, M., Warkentin, E., and Ermler, U. (2004) Crystallization of 4-hydroxybenzoyl-CoA reductase and the structure of its electron donor ferredoxin. *Acta crystallographica. Section D, Biological crystallography* **60**, 388-391

34. Wagener, N., Pierik, A. J., Ibdah, A., Hille, R., and Dobbek, H. (2009) The Mo-Se active site of nicotinate dehydrogenase. *Proceedings of the National Academy of Sciences of the United States of America* **106**, 11055-11060

35. Huber, R., Hof, P., Duarte, R. O., Moura, J. J. G., Moura, I., Liu, M. Y., LeGall, J., Hille, R., Archer, M., and Romao, M. J. (1996) A structure-based catalytic mechanism for the xanthine oxidase family of molybdenum enzymes. *Proceedings of the National Academy of Sciences of the United States of America* **93**, 8846-8851

36. Leimkuhler, S., Stockert, A. L., Igarashi, K., Nishino, T., and Hille, R. (2004) The role of active site glutamate residues in catalysis of Rhodobacter capsulatus xanthine dehydrogenase. *The Journal of biological chemistry* **279**, 40437-40444

37. Pauff, J. M., Hemann, C. F., Junemann, N., Leimkuhler, S., and Hille, R. (2007) The role of arginine 310 in catalysis and substrate specificity in xanthine dehydrogenase from Rhodobacter capsulatus. *Journal of Biological Chemistry* **282**, 12785-12790

38. Lehninger, A. L., Nelson, D. L., Cox, M. M., and Nelson, D. L. (2004) *Lehninger Principles of Biochemistry Fourth Edition*, W H Freeman & Co

39. Hille, R., Hall, J., and Basu, P. (2014) The Mononuclear Molybdenum Enzymes. *Chemical reviews* **In Press**

40. Schwarz, G., and Mendel, R. R. (2006) Molybdenum Cofactor Biosynthesis and Mo Enzymes. *Annu. Rev. Plant Biol.* **57**, 623-647

41. Morrison, M. S., Cobine, P., and Hegg, E. (2007) Probing the role of copper in the biosynthesis of the molybdenum cofactor in Escherichia coli and Rhodobacter sphaeroides. *JBIC Journal of Biological Inorganic Chemistry* **12**, 1129-1139

42. Amy, N. K., and Rajagopalan, K. V. (1979) Characterization of molybdenum cofactor from Escherichia coli. *Journal of bacteriology* **140**, 114-124

43. Neumann, M., and Leimkuhler, S. (2011) The role of system-specific molecular chaperones in the maturation of molybdoenzymes in bacteria. *Biochemistry research international* **2011**, 850924

44. Leimkühler, S., and Klipp, W. (1999) Role of XDHC in Molybdenum Cofactor Insertion into xanthine Dehydrogenase of Rhodobacter capsulatus. *Journal of bacteriology* **181**, 2745–2751

45. Schumann, S., Saggu, M., Moller, N., Anker, S. D., Lendzian, F., Hildebrandt, P., and Leimkuhler, S. (2008) The mechanism of assembly and cofactor insertion into Rhodobacter capsulatus xanthine dehydrogenase. *The Journal of biological chemistry* **283**, 16602-16611

46. Neumann, M., Stocklein, W., and Leimkuhler, S. (2007) Transfer of the molybdenum cofactor synthesized by Rhodobacter capsulatus MoeA to XdhC and MobA. *The Journal of biological chemistry* **282**, 28493-28500

47. Neumann, M., Stocklein, W., Walburger, A., Magalon, A., and Leimkuhler, S. (2007) Identification of a Rhodobacter capsulatus L-cysteine desulfurase that sulfurates the molybdenum cofactor when bound to XdhC and before its insertion into xanthine dehydrogenase. *Biochemistry* **46**, 9586-9595

48. Wollers, S., Heidenreich, T., Zarepour, M., Zachmann, D., Kraft, C., Zhao, Y., Mendel, R. R., and Bittner, F. (2008) Binding of sulfurated molybdenum cofactor to the C-terminal domain of ABA3 from Arabidopsis thaliana provides insight into the mechanism of molybdenum cofactor sulfuration. *The Journal of biological chemistry* **283**, 9642-9650

49. Massey, V., Brumby, P. E., and Komai, H. (1969) STUDIES ON MILK XANTHINE OXIDASE - SOME SPECTRAL AND KINETIC PROPERTIES. *Journal of Biological Chemistry* **244**, 1682-&

50. Edmondso.D, Ballou, D., Vanheuve.A, Palmer, G., and Massey, V. (1973) KINETIC STUDIES ON SUBSTRATE REDUCTION OF XANTHINE-OXIDASE. *Journal of Biological Chemistry* **248**, 6135-6144

51. Leimkuhler, S., Hodson, R., George, G. N., and Rajagopalan, K. V. (2003) Recombinant Rhodobacter capsulatus xanthine dehydrogenase, a useful model system for the characterization of protein variants leading to xanthinuria I in humans. *The Journal of biological chemistry* **278**, 20802-20811

52. Nishino, T., and Tsushima, K. (1981) PURIFICATION OF HIGHLY-ACTIVE MILK XANTHINE-OXIDASE BY AFFINITY-CHROMATOGRAPHY ON SEPHAROSE 4B-FOLATE GEL. *Febs Letters* **131**, 369-372

53. Pauff, J. M., Zhang, J. J., Bell, C. E., and Hille, R. (2008) Substrate orientation in xanthine oxidase - Crystal structure of enzyme in reaction with 2-hydroxy-6-methylpurine. *Journal of Biological Chemistry* **283**, 4818-4824

54. Cao, H., Pauff, J. M., and Hille, R. (2010) Substrate Orientation and Catalytic Specificity in the Action of Xanthine Oxidase THE SEQUENTIAL HYDROXYLATION OF HYPOXANTHINE TO URIC ACID. *Journal of Biological Chemistry* **285**, 28044-28053

55. Cao, H., Hall, J., and Hille, R. (2011) X-ray crystal structure of arsenite-inhibited xanthine oxidase: mu-sulfido,mu-oxo double bridge between molybdenum and arsenic in the active site. *Journal of the American Chemical Society* **133**, 12414-12417

56. Cao, H., Hall, J., and Hille, R. (2014) Substrate Orientation and Specificity in Xanthine Oxidase: Crystal Structures of the Enzyme in Complex with Indole-3-acetaldehyde and Guanine. *Biochemistry*

57. Winn, M. D., Ballard, C. C., Cowtan, K. D., Dodson, E. J., Emsley, P., Evans, P. R., Keegan, R. M., Krissinel, E. B., Leslie, A. G. W., McCoy, A., McNicholas, S. J., Murshudov, G. N., Pannu, N. S., Potterton, E. A., Powell, H. R., Read, R. J., Vagin, A., and Wilson, K. S. (2011) Overview of the CCP4 suite and current developments. *Acta Crystallographica Section D-Biological Crystallography* **67**, 235-242

58. Turkenburg, J. P., and Dodson, E. J. (1996) Modern developments in molecular replacement. *Current Opinion in Structural Biology* **6**, 604-610

59. Murshudov, G. N., Vagin, A. A., and Dodson, E. J. (1997) Refinement of macromolecular structures by the maximum-likelihood method. *Acta Crystallographica Section D-Biological Crystallography* **53**, 240-255

60. Pannu, N. S., Murshudov, G. N., Dodson, E. J., and Read, R. J. (1998) Incorporation of prior phase information strengthens maximum-likelihood structure refinement. *Acta Crystallographica Section D-Biological Crystallography* **54**, 1285-1294

61. Murshudov, G. N., Vagin, A. A., Lebedev, A., Wilson, K. S., and Dodson, E. J. (1999) Efficient anisotropic refinement of macromolecular structures using FFT. *Acta Crystallographica Section D-Biological Crystallography* **55**, 247-255

62. Schuttelkopf, A. W., and van Aalten, D. M. F. (2004) PRODRG: a tool for high-throughput crystallography of protein-ligand complexes. *Acta Crystallographica Section D-Biological Crystallography* **60**, 1355-1363

63. Emsley, P., and Cowtan, K. (2004) Coot: model-building tools for molecular graphics. *Acta Crystallographica Section D-Biological Crystallography* **60**, 2126-2132

64. DeLano, W. L. (2004) *The PyMol Molecular Graphics System*, DeLaon Scientific LLC, San Carlos, CA

65. Kim, J. H., Ryan, M. G., Knaut, H., and Hille, R. (1996) The reductive half-reaction of xanthine oxidase. The involvement of prototropic equilibria in the course of the catalytic sequence. *The Journal of biological chemistry* **271**, 6771-6780

66. D'Ardenne, S. C., and Edmondson, D. E. (1990) Kinetic isotope effect studies on milk xanthine oxidase and on chicken liver xanthine dehydrogenase. *Biochemistry* **29**, 9046-9052

67. SIMON, H., and PALM, D. (1966) Isotope Effects in Organic Chemistry and Biochemistry. *Angew. Chem. internat. Edit.* **5**, 920-933

68. Phillips, J. C., Braun, R., Wang, W., Gumbart, J., Tajkhorshid, E., Villa, E., Chipot, C., Skeel, R. D., Kale, L., and Schulten, K. (2005) Scalable molecular dynamics with NAMD. *Journal of computational chemistry* **26**, 1781-1802

69. MacKerell, A. D., Bashford, D., Bellott, Dunbrack, R. L., Evanseck, J. D., Field, M. J., Fischer, S., Gao, J., Guo, H., Ha, S., Joseph-McCarthy, D., Kuchnir, L., Kuczera, K., Lau, F. T. K., Mattos, C., Michnick, S., Ngo, T., Nguyen, D. T., Prodhom, B., Reiher, W. E., Roux, B., Schlenkrich, M., Smith, J. C., Stote, R., Straub, J., Watanabe, M., Wiórkiewicz-Kuczera, J., Yin, D., and Karplus, M. (1998) All-Atom Empirical Potential for Molecular Modeling and Dynamics Studies of Proteins†. *The Journal of Physical Chemistry B* **102**, 3586-3616

70. Humphrey, W., Dalke, A., and Schulten, K. (1996) VMD: Visual molecular dynamics. *Journal of Molecular Graphics* **14**, 33-38

71. Morris, G. M., Goodsell, D. S., Halliday, R. S., Huey, R., Hart, W. E., Belew, R. K., and Olson, A. J. (1998) Automated docking using a Lamarckian genetic algorithm and an empirical binding free energy function. *Journal of computational chemistry* **19**, 1639-1662

72. Morris, G. M., Huey, R., Lindstrom, W., Sanner, M. F., Belew, R. K., Goodsell, D. S., and Olson, A. J. (2009) AutoDock4 and AutoDockTools4: Automated docking with selective receptor flexibility. *Journal of computational chemistry* **30**, 2785-2791

73. Sehnal, D., Svobodova Varekova, R., Berka, K., Pravda, L., Navratilova, V., Banas, P., Ionescu, C. M., Otyepka, M., and Koca, J. (2013) MOLE 2.0: advanced approach for analysis of biomacromolecular channels. *Journal of cheminformatics* **5**, 39

74. Yamaguchi, Y., Matsumura, T., Ichida, K., Okamoto, K., and Nishino, T. (2007) Human xanthine oxidase changes its substrate specificity to aldehyde oxidase type upon mutation of amino acid residues in the active site: Roles of active site residues in binding and activation of purine substrate. *Journal of Biochemistry* **141**, 513-524

75. Ilich, P., and Hille, R. (1997) Tautomerization of the substrate heterocycle in the course of the reaction of xanthine oxidase. *Inorganica Chimica Acta* **263**, 87-93

76. Choi, E.-Y., Stockert, A. L., Leimkühler, S., and Hille, R. (2004) Studies on the mechanism of action of xanthine oxidase. *Journal of Inorganic Biochemistry* **98**, 841-848

77. Okamoto, K., Matsumoto, K., Hille, R., Eger, B. T., Pai, E. F., and Nishino, T. (2004) The crystal structure of xanthine oxidoreductase during catalysis: Implications for reaction mechanism and enzyme inhibition. *Proceedings of the National Academy of Sciences of the United States of America* **101**, 7931-7936

78. Xia, M., Dempski, R., and Hille, R. (1999) The reductive half-reaction of xanthine oxidase - Reaction with aldehyde substrates and identification of the catalytically labile oxygen. *Journal of Biological Chemistry* **274**, 3323-3330

79. Aguey-Zinsou, K. F., Bernhardt, P. V., and Leimkühler, S. (2003) Protein Film Voltammetry of Rhodobacter Capsulatus Xanthine Dehydrogenase. *Journal of the American Chemical Society* **125**, 15352-15358

80. Kulikowska, E., Kierdaszuk, B., and Shugar, D. (2004) Xanthine, xanthosine and its nucleotides: solution structuresof neutral and ionic forms, and relevance to substrate properties in various enzyme systems and metabolic pathways. *Acta Biochem Pol.* **51**, 493-531

81. Pauff, J. M., Cao, H., and Hille, R. (2009) Substrate Orientation and Catalysis at the Molybdenum Site in Xanthine Oxidase CRYSTAL STRUCTURES IN COMPLEX WITH XANTHINE AND LUMAZINE. *Journal of Biological Chemistry* **284**, 8751-8758

82. Okamoto, K., Kawaguchi, Y., Eger, B. T., Pai, E. F., and Nishino, T. (2010) Crystal structures of urate bound form of xanthine oxidoreductase: substrate orientation and structure of the key reaction intermediate. *Journal of the American Chemical Society* **132**, 17080-17083

83. McCrudden, F. H. (1905) *Uric Acid*, Samuel Usher

84. Hur, S., and Bruice, T. C. (2002) The mechanism of catalysis of the chorismate to prephenate reaction by the Escherichia coli mutase enzyme. *Proceedings of the National Academy of Sciences of the United States of America* **99**, 1176-1181

85. Hur, S., and Bruice, T. C. (2003) Comparison of formation of reactive conformers (NACs) for the Claisen rearrangement of chorismate to prephenate in water and in the E-coli mutase: The efficiency of the enzyme catalysis. *Journal of the American Chemical Society* **125**, 5964-5972

86. Hur, S., and Bruice, T. C. (2003) Enzymes do what is expected (chalcone isomerase versus chorismate mutase). *Journal of the American Chemical Society* **125**, 1472-1473

87. Cao, H. (2011) *Crystallographic, Kinetic and Computational Studies on the Reaction Mechanism of Xanthine Oxidoreductase*. Ph.D., University of California, Riverside

88. Perutz, M. F., Watson, H. C., Muirhead, H., Diamond, R., and Bolton, W. (1964) STRUCTURE OF HAEMOGLOBIN - X-RAY EXAMINATION OF REDUCED HORSE HAEMOGLOBIN. *Nature* **203**, 687-&

89. Kendrew, J. C. (1950) THE CRYSTAL STRUCTURE OF HORSE MET-MYOGLOBIN .1. GENERAL FEATURES - THE ARRANGEMENT OF THE POLYPEPTIDE CHAINS. *Proceedings of the Royal Society of London Series a-Mathematical and Physical Sciences* **201**, 62-&

90. Carr, H. S., and Winge, D. R. (2003) Assembly of Cytochrome c Oxidase within the Mitochondrion. *Accounts of Chemical Research* **36**, 309-316

91. Leach, M. R., and Zamble, D. B. (2007) Metallocenter assembly of the hydrogenase enzymes. *Current opinion in chemical biology* **11**, 159-165

92. Lill, R. (2009) Function and biogenesis of iron–sulphur proteins. *Nature* **460**, 831-838

93. Schwarz, G., Mendel, R. R., and Ribbe, M. W. (2009) Molybdenum cofactors, enzymes and pathways. *Nature* **460**, 839-847

94. Neumann, M., Schulte, M., Junemann, N., Stocklein, W., and Leimkuhler, S. (2006) Rhodobacter capsulatus XdhC is involved in molybdenum cofactor binding and insertion into xanthine dehydrogenase. *The Journal of biological chemistry* **281**, 15701-15708

95. Lima, C. D. (2002) Analysis of the E. coli NifS CsdB protein at 2.0 A reveals the structural basis for perselenide and persulfide intermediate formation. *Journal of molecular biology* **315**, 1199-1208

96. Shi, R., Proteau, A., Villarroya, M., Moukadiri, I., Zhang, L., Trempe, J.-F., Matte, A., Armengod, M. E., and Cygler, M. (2010) Structural Basis for Fe–S Cluster Assembly and tRNA Thiolation Mediated by IscS Protein–Protein Interactions. *PLoS Biol* **8**, e1000354

97. Schwartz, S. H., Leon-Kloosterziel, K. M., Koornneef, M., and Zeevaart, J. (1997) Biochemical Characterization of the aba2 and aba3 Mutants in Arabidopsis thaliana. *Plant Physiology* **114**, 161-166

98. Bittner, F., Oreb, M., and Mendel, R. R. (2001) ABA3 is a molybdenum cofactor sulfurase required for activation of aldehyde oxidase and xanthine dehydrogenase in Arabidopsis thaliana. *The Journal of biological chemistry* **276**, 40381-40384

99. Dobbek, H., Gremer, L., Kiefersauer, R., Huber, R., and Meyer, O. (2002) Catalysis at a dinuclear CuSMo(==O)OH cluster in a CO dehydrogenase resolved at 1.1-angstrom resolution. *Proceedings of the National Academy of Sciences of the United States of America* **99**, 15971-15976

100. Lennard, L. (1992) The clinical pharmacology of 6-mercaptopurine. *Eur J Clin Pharmacol* **43**, 329-339

101. Aucamp, J., Gaspar, A., Hara, Y., and Apostolides, Z. (1997) Inhibition of xanthine oxidase by catechins from tea (Camellia sinensis). *Anticancer research* **17**, 4381-4385

102. Sparrow, M. P. (2008) Use of Allopurinol to Optimize Thiopurine Immunomodulator Efficacy in Inflammatory Bowel Disease. *Gastroenterol Hepatol* **4**, 505–511

103. Okamoto, K., and Nishino, T. (2008) Crystal Structures of Mammalian Xanthine Oxidoreductase Bound with Various Inhibitors: Allopurinol, Febuxostat, and FYX-051. *Journal of Nippon Medical School* **75**, 2-3

104. Dowling, D. P., Bruender, N. A., Young, A. P., McCarty, R. M., Bandarian, V., and Drennan, C. L. (2014) Radical SAM enzyme QueE defines a new minimal core fold and metal-dependent mechanism. *Nat Chem Biol* **10**, 106-112